

Combustion of Zero Carbon Fuels

A thesis submitted for the degree of Masters of Science in

Engineering with Finance

by

Weerawickramage Mahima Dilshan Gunewardena BEng (Hons)

Department of Mechanical Engineering

University College London

I, Mahima, confirm that the work presented in this thesis is my own. Where information has been derived from other sources, I confirm that this has been specified in the thesis.

September 2023

Student number: 22193065

Total number of words: 11,990

I give permission to UCL to make this report public after the end of my studies, so UCL students and staff can access it.

YES

NO

Abstract

The present study examines the viability of utilising ethanol-ammonia fuel blends in internal combustion engines. This study focuses on the development and analysis of concepts that facilitate the swift implementation of sustainable fuels. The objective is to address the escalating carbon reduction targets. The primary focus of this study is to examine the combustion characteristics of blended fuels when used in naturally aspirated engines equipped with spark ignition and port fuel injection systems.

The blended fuel samples were produced through the introduction of gaseous ammonia into ethanol, with the objective of attaining the maximum solubility of ammonia in the solvent. Subsequently, the blended samples underwent analysis and validation to determine the extent of ammonia retention within the samples using acid-base titrations, calorimetry, and gas chromatography mass spectroscopy. Despite the samples failing to attain solubility limits, engine testing was carried out to investigate the impact of ammonia addition to reference ethanol samples.

The blended samples displayed expected combustion characteristics, including decreased power output and in-cylinder pressure. However, these observations were only made during most recent timed runs during engine testing, suggesting the presence of fuel stratification. Fuel stratification refers to the separation of fuel components based on density differences, which is not desirable for implementation in current internal combustion engines. Therefore, additional research is needed to comprehend and address the issue of fuel stratification. Visual discrepancies were also noted in the fuel samples over a one-month period, potentially indicating fuel degradation. This could pose a concern if the fuels are unable to be stored and transported over extended periods of time. Notwithstanding these concerns, the blended samples exhibit a stable combustion cycle and demonstrate viable power outputs.

From an economic standpoint, the competitiveness of fuels is remarkably inadequate. Consequently, it is necessary to introduce a range of incentives and policy changes to enhance the appeal of fuel blends to end consumers. The utilisation of autoregressive integrated moving average (ARIMA) models and Monte Carlo simulations has yielded projections indicating a forthcoming surge in demand. Consequently, this implies the existence of investment prospects for ammonia blended samples in the future.

The fuels exhibit promising prospects for integration into existing infrastructure and internal combustion engines, thereby holding significant potential for future utilisation in mitigating global carbon emissions. Further investigation is necessary to examine the characteristics of emissions released from the samples under different equivalence ratios. Additionally, it is imperative to develop chemical reaction mechanisms that can accurately simulate combustion performance under high temperatures and pressures.

Acknowledgements

I would like to express my profound appreciation to my supervisor **Professor Paul Hellier**, whose consistent support and invaluable guidance have played a crucial role in the successful completion of this project. His enthusiasm and unwavering commitment to the realm of research not only served as a source of inspiration for me, but also cultivated an environment that was extremely beneficial to the development of novel ideas and advancements.

I dedicate this thesis to my loving parents, whose constant encouragement and unrelenting trust in me throughout my academic journey have inspired me to push myself and persevere through difficult times.

Table of Contents

| | |
|--|-----------|
| Abstract | 1 |
| Acknowledgements | 2 |
| List of Figures | 5 |
| List of Tables | 9 |
| Nomenclature..... | 10 |
| Introduction | 11 |
| Overview..... | 16 |
| Literature Review | 16 |
| Principles of Combustion..... | 16 |
| Combustion Characteristics of Ammonia | 18 |
| Combustion Characteristics of Oxygenated Fuels | 20 |
| Current Studies on Ammonia Alcohol Fuel Blends | 21 |
| Advanced Combustion Modes | 26 |
| Effects of Water on Combustion | 29 |
| Research Gap | 30 |
| Methodology and Experimental Techniques | 31 |
| Fuel Preparation | 31 |
| Fuel Sample Analysis and Quantification | 36 |
| Energy Content Analysis..... | 38 |
| Combustion Characteristic Analysis | 39 |
| Economic Feasibility | 40 |
| Aspen Simulation..... | 40 |
| Time Series Forecasting..... | 42 |

| | |
|--|-----------|
| Monte Carlo Simulations..... | 44 |
| <i>Experimental Results and Discussion.....</i> | 46 |
| Calorimetry..... | 46 |
| Acid-Base Titrations | 47 |
| Gas Chromatography Mass Spectroscopy Results and Discussion | 49 |
| Engine Testing..... | 50 |
| <i>Economic Analysis Results and Discussion</i> | 58 |
| Aspen Simulation..... | 58 |
| ARIMA model forecast | 59 |
| ARIMA model discussion | 64 |
| Monte Carlo Results..... | 65 |
| Monte Carlo Simulation Discussion..... | 66 |
| <i>Conclusion</i> | 67 |
| <i>Bibliography.....</i> | 68 |
| <i>Appendix.....</i> | 78 |
| Section A - Air Fuel Ratio Calculation | 78 |
| Section B – Titration Curves..... | 79 |
| Section C – Arima Model Code..... | 80 |
| Section D – In cylinder Volume Engine | 85 |

List of Figures

| | |
|--|----|
| Figure 1 Global transport sector CO ₂ emissions by transportation type [1]..... | 11 |
| Figure 2 Scenario-based global CO ₂ emissions [3] | 11 |
| Figure 3 Life cycle emissions by vehicle [6] | 12 |
| Figure 4 Contribution to transport greenhouse-gas intensity reduction in 2030 [6] | 13 |
| Figure 5 Ammonia production, energy efficiency improvement [11] | |
| Figure 6 Ammonia production, emissions improvements [11] | 13 |
| Figure 7 Ammonia production supply chain and uses [12] | 14 |
| Figure 8 Ethanol production energy saving potential [17] | 15 |
| Figure 9 Bio Ethanol Production Pathways [18] | 15 |
| Figure 10 Different combustion modes in internal combustion engine. [19] | 17 |
| Figure 11 Flame propagation types [20] | 17 |
| Figure 12 Detonation Characteristics of stoichiometric mixtures of conventional fuels [34] | 19 |
| Figure 13 Flame speeds in ammonia/oxygen mixtures at various equivalence ratios with respect to the distance of propagation [34]..... | 20 |
| Figure 14 Indicated diagram for petrol and methanol [38] | 20 |
| Figure 15 Comparison of the measured LBVs with combustion enhancers to ammonia [42].... | 21 |
| Figure 16 Laminar burning velocity of ammonia- methanol (Left), and ammonia-ethanol (Right), at 298 K and 1 atm [43]..... | 21 |
| Figure 17 Experimental Ignition delay times of ammonia-ethanol stoichiometric mixtures at 20 and 40 bars [44] (Left)..... | 22 |
| Figure 18 Experimental ignition delay times of various ammonia/fuel blends [43] (Right) | 22 |
| Figure 19 Comparison of combustion performance (Left) and pollutant emissions (Right) between the homogeneous and stratified fuel injection strategies for varying ammonia fractions. [46] | 23 |
| Figure 20 Heat release rates (Left) and burned mass fractions (Right) at 1 bar of intake pressure with homogeneous injection strategy for varying ammonia fractions [46] | 23 |
| Figure 21 Ammonia dissolution in various classes of organic solvents at 1.013 bar and 25 °C [47] | 24 |

| | |
|--|----|
| Figure 22 Polar Nature of OH group and its interaction with ammonia [48] | 24 |
| Figure 23 Fuel stability of the ammonia solubility in selected solvent at varying temperatures. [47] | 25 |
| Figure 24 Theoretical lower heating values for different ammonia-solvent mixtures (Left), Theoretical CO ₂ emissions for different ammonia-solvent mixtures (Right) [47] | 25 |
| Figure 25 The operating zones of different combustion modes [19] | 26 |
| Figure 26 Comparison of HCCI with conventional combustion modes [54]..... | 27 |
| Figure 27 Nature of heat release rates of HCCI combustion [54] | 27 |
| Figure 28 The cumulative heat release | |
| Figure 29 Effect of cetane number on CO emissions [56] for different blends of aqueous ethanol [17] | 28 |
| Figure 30 Nature of combustion with water [57] | 29 |
| Figure 31 Concept 1 Block Diagram..... | 31 |
| Figure 32 Concept 1's Key Reaction [61] | 32 |
| Figure 33 Concept 2 Block Diagram..... | 32 |
| Figure 34 Concept 3 Block Diagram..... | 33 |
| Figure 35 Lab Scale Fuel Production Setup..... | 35 |
| Figure 36 The liquid flow pattern, gas–liquid interfacial area, and gas streamlines for column packing [63]..... | 35 |
| Figure 37 Methyl Orange operating pH range [64] | 36 |
| Figure 38 Computed Titration Curve for Ethanol / Ammonia | 37 |
| Figure 39 Equivalence point for Ethanol / Ammonia..... | 37 |
| Figure 40 Engine Setup - Adopted from [65] | 39 |
| Figure 41 Simulation Flowsheet..... | 40 |
| Figure 42 Distillation species profile..... | 41 |
| Figure 43 Distillation temperature, and pressure profiles | 41 |
| Figure 44 ARIMA model breakdown and terms | 42 |
| Figure 45 ARIMA model flowchart [74] | 42 |

| | |
|---|----|
| Figure 46 Time Series Decomposition, Historical data (Left), Time series characteristics (Right) [76] | 43 |
| Figure 47 Supply of Ethanol in the United States and Goldman Sachs Chicago Ethanol Price Index [78] [79] | 45 |
| Figure 48 Theoretical ammonia solubility in solvents [81] | 48 |
| Figure 49 Simulated concentration of ammonia - effect of alkali addition (Left), experimental measurements of ammonia concentration from aqueous ammonia evaporation at 50 °C and 101 kPa (Right) [82] | 49 |
| Figure 50 Initial Chromatogram for pure sample | 49 |
| Figure 51 NIST library search | 49 |
| Figure 52 In-cylinder pressure of ethanol pure and blend samples | 50 |
| Figure 53 Filtered Heat Release Rates of ethanol pure and blend samples | 50 |
| Figure 54 Mass Fraction Burnt of one sample | 51 |
| Figure 55 Planar Laser Induced Fluorescence images of turbulent flames at 0.5 MPa and mixture temperature of 298 K (a) methane - air flame; (b) methane-ammonia-air, same parameters, and conditions [85] | 52 |
| Figure 56 Pure Methanol NIMEP | 53 |
| Figure 57 Methanol Blend NIMEP reduction | 54 |
| Figure 59 Proposed fuel stratification mechanism | 55 |
| Figure 60 Methanol samples in cylinder pressures | 56 |
| Figure 61 Methanol samples heat release rates | 56 |
| Figure 62 Ethanol / Ammonia Samples - Left - 1 month, Right - 1 day | 57 |
| Figure 63 Methanol / Ammonia Samples - Left - 1 month, Right - 1 day | 57 |
| Figure 64 Fuel manufacturing costs £/L – Aspen Plus Simulation | |
| Figure 65 Cost Breakdown of petrol [88] | 58 |
| Figure 66 Ethanol differencing results | 59 |
| Figure 67 First iteration of parameter selection, PACF plots | 60 |
| Figure 68 Seasonal Plot of Ethanol Cost | 60 |
| Figure 69 Effects of seasonal and normal differencing on Ethanol dataset | 61 |

| | |
|--|----|
| Figure 70 Residual Plots of ARIMA model. A - residual errors. B - Density plot, C- Quantile - Quantile Distribution D - ACF plot | 62 |
| Figure 71 ARIMA model ethanol forecast..... | 64 |
| Figure 72 Monte Carlo simulation | 65 |
| Figure 73 Statistical analysis of Monte Carlo simulation..... | 65 |
| Figure 74 Convergence plot for Monte Carlo simulation | 66 |
| Figure 75 Titration Curve for fuel mixture / H ₂ SO ₄ - Methanol..... | 79 |
| Figure 76 Titration Curve Equivalence point – Methanol..... | 79 |
| Figure 77 ARIMA Code 1/13 [67] [68] [69] [70] [71] [72] | 80 |
| Figure 78 ARIMA Code 2/13 [67] [68] [69] [70] [71] [72] | 80 |
| Figure 79 ARIMA Code 3/13 [67] [68] [69] [70] [71] [72] | 80 |
| Figure 80 ARIMA Code 4/13 [67] [68] [69] [70] [71] [72] | 81 |
| Figure 81 ARIMA Code 5/13 [67] [68] [69] [70] [71] [72] | 81 |
| Figure 82 ARIMA Code 6/13 [67] [68] [69] [70] [71] [72] | 82 |
| Figure 83 ARIMA Code 7/13 [67] [68] [69] [70] [71] [72] | 82 |
| Figure 84 ARIMA Code 8/13 [67] [68] [69] [70] [71] [72] | 82 |
| Figure 85 ARIMA Code 9/13 [67] [68] [69] [70] [71] [72] | 83 |
| Figure 86 ARIMA Code 10/13 [67] [68] [69] [70] [71] [72] | 83 |
| Figure 87 ARIMA Code 11/13 [67] [68] [69] [70] [71] [72] | 83 |
| Figure 88 ARIMA Code 12/13 [67] [68] [69] [70] [71] [72] | 84 |
| Figure 89 ARIMA Code 13/13 [67] [68] [69] [70] [71] [72] | 84 |
| Figure 90 In cylinder volume of test engine | 85 |

List of Tables

| | |
|---|----|
| Table 1 Fuel properties of various fuels [22], [23], [24], [25], [18], [26], [27], [28], [29]..... | 18 |
| Table 2 Design Selection Criteria | 33 |
| Table 3 Experimental Setup Equipment | 35 |
| Table 4 Calorimetry Results | 46 |
| Table 5 Average Titres and corresponding ammonia content | 47 |
| Table 6 Burnt Mass Fraction Trends [46] | 52 |
| Table 7 Net Indicated Mean Effective Pressure and Combustion Stability for the last timed run of each sample | 53 |
| Table 8 Simulated Price in comparison to conventional fuels spot price [87] | 58 |
| Table 9 Initial Statistical Test for Ethanol (pre-differencing) | 61 |
| Table 10 Ethanol Statistical Results | 63 |
| Table 11 Ethanol Coefficient Selection Statistical Analysis | 63 |
| Table 12 Ethanol Residuals Analysis | 63 |

Nomenclature

ARIMA – Autoregressive Integrated Moving Average
BEV – Battery Electric Vehicle
BTC - Bottom Dead Centre
CFD – Computational Fluid Dynamics
CH₄ – Methane
CI – Compression Ignition
CO – Carbon Monoxide
CO₂ – Carbon Dioxide
COSMO-RS – Conductor-like screening model for Real Solvents
COV – Coefficient of Variation
DDT – Deflagration to Detonation Transition
DI – Direct Injection
GCMS – Gas Chromatography Mass Spectroscopy
GWP – Global Warming Potential
H₂ – Hydrogen
H₂O – Water
H₂SO₄ – Sulphuric Acid
HC – Hydrocarbon
HCCI – Homogenous Charged Compression Ignition
HHV – Higher Heating Value
ICE – Internal Combustion Engine
IDT – Ignition Delay Time
LBV – Laminar Burning Velocity
LHV – Lower Heating Value
mol% - mole percent
NH₃ – Ammonia
NIMEP – Net indicated mean effective pressure
NO_x – Nitrogen Oxide
NTC – Negative Temperature Coefficient
PFI – Port Fuel Injection
PLIF – Planar laser induced fluorescence
SI – Spark Ignition
SOI – Start of Injection
TDC – Top Dead Centre
THC – Total hydrocarbons
wt% - weight percent

Introduction

Global warming has devastating social, environmental, and economic impacts. Achieving net-zero targets has been widely adopted throughout the world after the Paris Agreement. The transport sector emits 24% of the global carbon dioxide (CO₂) emissions expedited from energy production and use [1] of which road passenger and freight produce most of the emissions as seen in Figure 1. Current temperature rise predictions have been shown to exceed the 1.5°C limit, even with the most stringent scenarios where leading countries meet their emissions targets; the lowest temperature rise is 1.7 °C as seen in Figure 2. An artificial intelligence model has also predicted that between 2033 and 2035 global temperatures will cross the 1.5 °C threshold in all scenarios [2]. This highlights the importance of the rapid need to decarbonise the transport sector.



Figure 1 Global transport sector CO₂ emissions by transportation type [1]

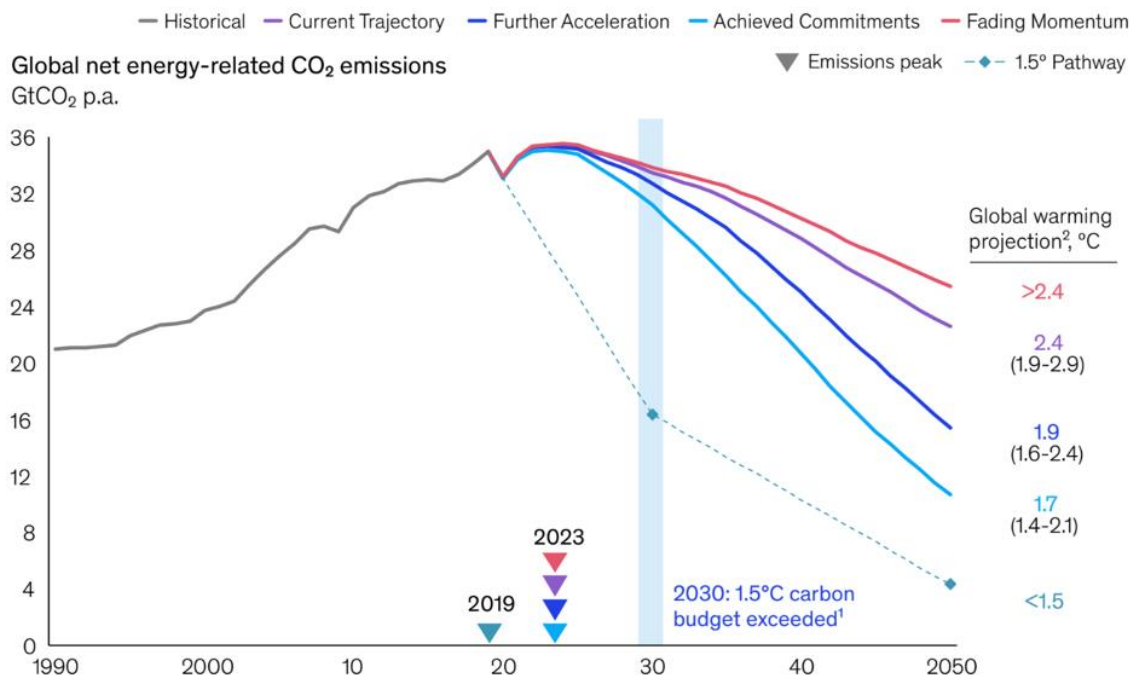


Figure 2 Scenario-based global CO₂ emissions [3]

Battery electric vehicles (BEV) are the target mode of transportation if emissions targets are to be achieved, but there are several technical and economical constraints such as infrastructure requirements and supply chain constraints which will delay their mass adoption. Only 36.7% of electricity is produced from low-carbon sources globally [4] which means great efforts must be made to decarbonize the electricity mix to make BEVs sustainable. Transitioning to net zero quickly will require the use of alternative fuels. It is anticipated that the demand for alternative fuels will triple over the next two decades [3], and that by 2050, alternative fuels will account for 37% of the energy share within the transport sector [5]. The slower than anticipated deployment of battery electric vehicles (BEVs) necessitates the use of alternative fuels to meet the demanding carbon reduction goals depicted in Figure 3. This will aid in closing the gap in decarbonization efforts. Adopting drop-in technology, which allows existing infrastructure and internal combustion engines (ICE) to be utilised with little to no changes, is the greatest choice for having the quickest and most effective impact possible and should be prioritized as a result. Furthermore, when looking at the lifecycle emissions (Figure 4) of BEVs compared to ICEs, the largest difference is expectedly in the tailpipe emissions. When compared to BEVs, ICEs would produce the same amount of pollution if tailpipe emissions could be reduced by 50%.

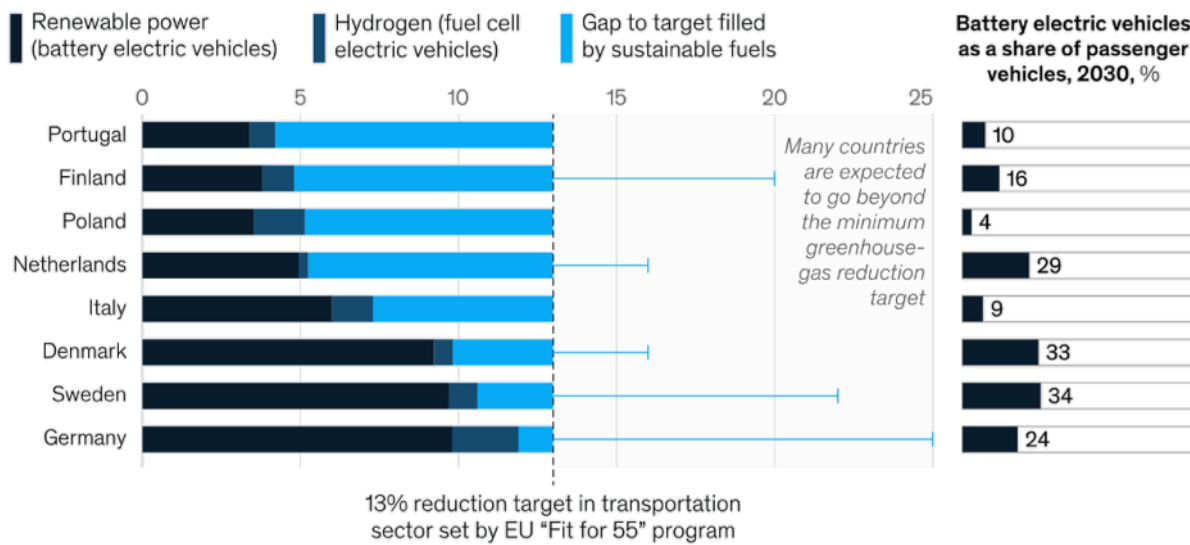


Figure 3 Life cycle emissions by vehicle [6]

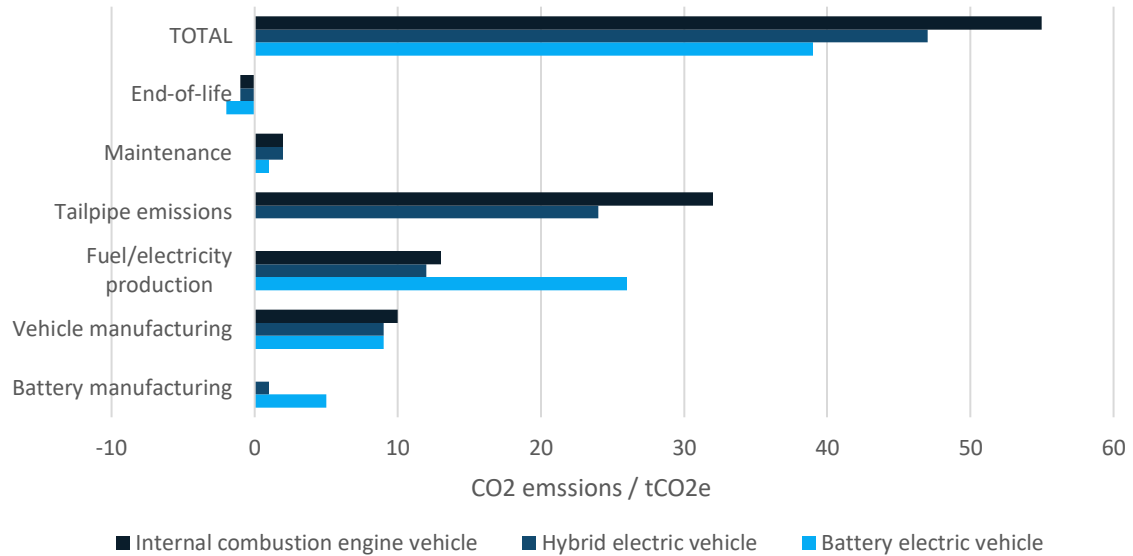


Figure 4 Contribution to transport greenhouse-gas intensity reduction in 2030 [6]

Nitrogen oxide (NOx) emissions are more significant than CO2 emissions because NOx has a global warming potential (GWP) of 298 [7] compared to CO2's 1 GWP over a 100-year time horizon and they both have similar half-lives in the atmosphere. This means that even relatively lesser amounts of NOx emissions can have two orders of magnitude worse effects than CO2. Nitrogen oxides have significant health implications, leading to disability, reduced life expectancy, and increased risks of cardiovascular and pulmonary diseases, ultimately resulting in premature mortality [8]. A research study was conducted to examine the levels of NOx emissions in 11 different diesel vehicle markets. The findings of the study indicate that if more stringent emission regulations and cleaner combustion modes are implemented, it is projected that by the year 2040, approximately 183,600 premature deaths could be prevented [9] [10].

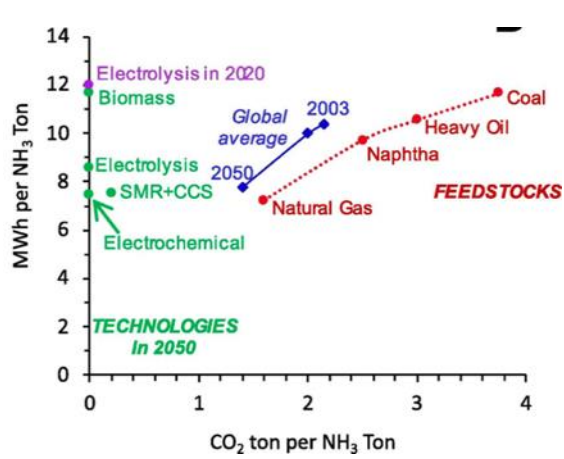
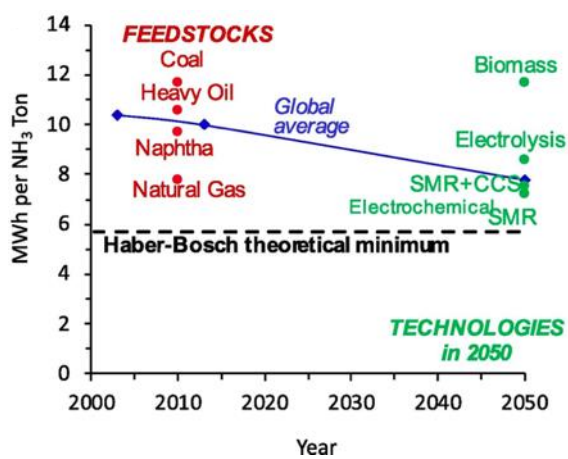


Figure 5 Ammonia production, energy efficiency improvement [11] Figure 6 Ammonia production, emissions improvements [11]

Zero-carbon fuels are fuels which don't contain carbon atoms such as hydrogen (H₂) and ammonia (NH₃). Ammonia is typically manufactured through the Haber Bosch process, which is a mature process to make a plethora of products (Figure 7), mostly fertilizer but has increasing adoption in internal combustion engines. Ammonia can be made renewably, Figure 5 depicts the efficiency in production methods of ammonia and shows higher efficiency is likely to occur by 2050, these production methods (Figure 7) will, in turn, decrease the CO₂ emissions in future as shown by Figure 6 which is beneficial since ammonia production solely produces 1.2% of the global CO₂ emissions [11].

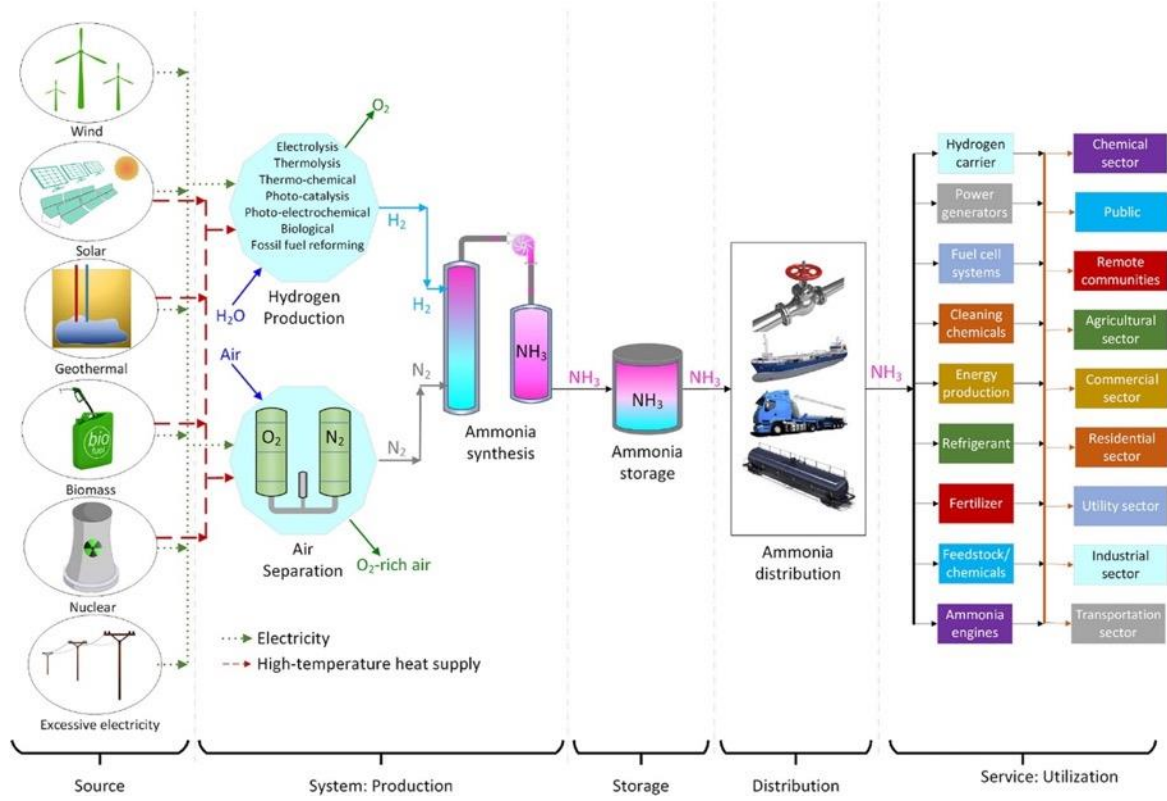


Figure 7 Ammonia production supply chain and uses [12]

Ammonia is a gas at ambient conditions, which makes its transportation difficult. There are numerous ways to transport ammonia; compressed gas, liquified at -33°C at ambient pressure, liquified via pressurization to 9 bar and finally in solid forms such as ammonia borane. However, all these methods require energy input to contain the ammonia and have an inherent hazardous element if the ammonia does leak.

Ammonia is a polar molecule and thus is soluble in polar solvents. Water has an extremely high affinity to ammonia since it can easily create hydrogen bonds with ammonia, this allows for ammonia transportation through solvent dissolution. Ammonia is less dense than air and has a narrow flammability range which means the chances of a fire or explosion are reduced [11] and spills can be neutralized quickly with water. Furthermore, it is easily detectable due to its distinct odour. Alcohol's can also be polar solvents, in which ammonia can dissolve. Additionally, alcohols can be made via renewable pathways such as the fermentation of organic crops and thus they can be deemed to be carbon-neutral fuels since they absorb the emissions from the combustion process during the feedstock growth phase via photosynthesis.

Bioethanol can be renewably produced through the fermentation of crops containing fermentable sugars as seen in Figure 9 [13]. A large proportion of the cost of bioethanol is the dehydration process [14], generally accounting for 37% [15] of the energy expedited for fuel production since water and ethanol create an azeotrope and thus require energy-intensive processes. It would be beneficial to keep the bioethanol with a small fraction of water to decrease dehydration energy and costs (Figure 8) [16] and thus decrease overall fuel costs for the end consumer.

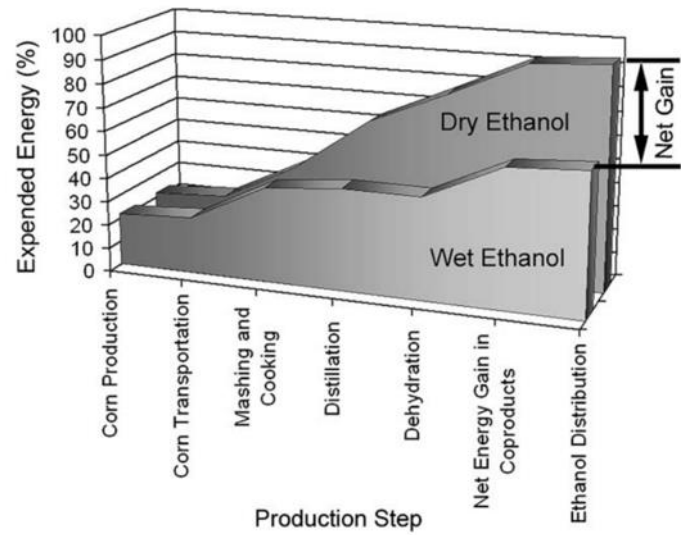


Figure 8 Ethanol production energy saving potential [17]

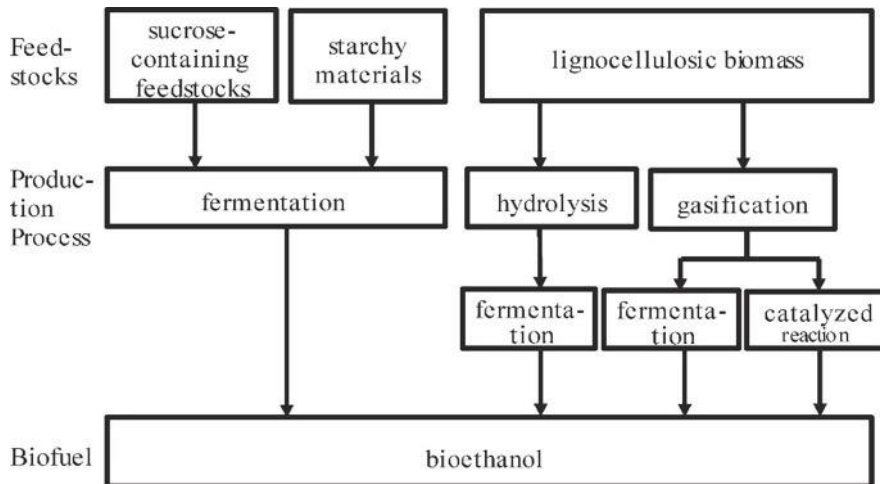


Figure 9 Bio Ethanol Production Pathways [18]

Overview

This thesis will investigate the technical and economic feasibility of a mixture of ammonia and alcohol to aid in the decarbonization of the transportation sector. The thesis will begin with a review of the main research surrounding the topic to determine what areas of research still need to be investigated. Following this, a detailed methodology will be laid out so that any future research can be replicated and investigated further if needed. The experimental results will be thoroughly discussed to fully understand the combustion characteristics of the alternative fuels.

The literature review will begin with an overview of combustion principles and introduce the concepts and nomenclature used throughout. The combustion characteristics of each individual component of the fuels will be discussed separately, followed by a discussion of current research that blends the two components together. Finally, advanced combustion modes and parameters that can improve combustion or reduce emissions will be discussed.

Literature Review

Principles of Combustion

There is a plethora of combustion modes (Figure 10), which vary by fuel injection methods, ignition type, the number of fuels used and the level of fuel-air mixing before introduction into the combustion chamber. Engines typically work on a 4-stroke principle. The piston moves up and down in the 4 strokes and the end of a stroke is indicated by the maximum distance the piston travels before changing direction, these maximum points are called top dead centre (TDC) and bottom dead centre (BDC). The first stroke is where the intake valve opens and air enters the combustion chamber, the piston is also moving downwards “sucking” air into the chamber until BDC. This air is compressed by the piston moving upwards decreasing the volume of air until TDC, it is at this stage where the fuel is introduced into the chamber via a fuel injector as liquid which would atomize or as a vapour via the air intake. The fuel is ignited via a spark plug or the temperature within the chamber combusts the fuel due to the high temperature created from the compression leading to autoignition. The expansion stroke follows, and this is where chemical energy is converted to mechanical power by pushing the piston downwards until BDC by the energy transfer occurring from the combustion of the fuel. The final phase is the exhaust stroke where the contents in the combustion chamber are emptied via the exhaust valve due to a pressure difference until TDC. A plot of in-cylinder volume against crank angle degree is presented in the appendix section D to help visualise this process. The equivalence ratio is the ratio of the actual fuel/air ratio to the stoichiometric fuel/air ratio and can show whether the combustion occurs in excess air (lean) or excess fuel (rich) conditions.

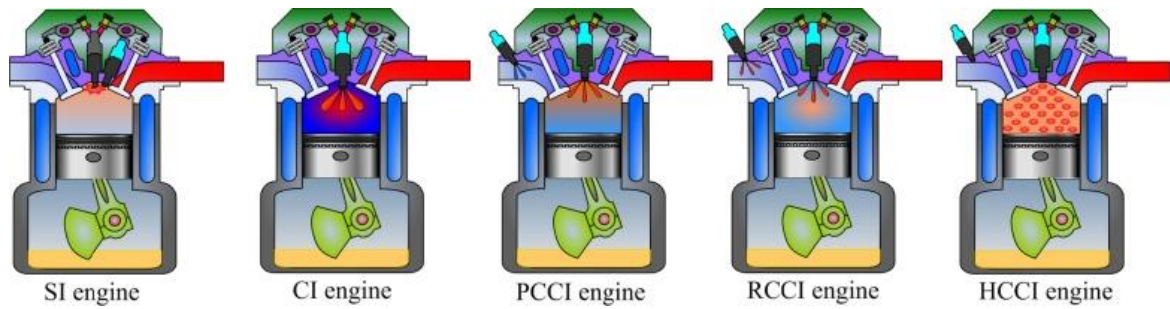


Figure 10 Different combustion modes in internal combustion engine. [19]

Laminar burning velocity (LBV) is how quickly the flame front of a combustion process moves with respect to an unburned mixture of fuel and air that has been pre-mixed. The flame front can also be turbulent (as shown in Figure 11), this is dependent on the nature of the air induction and subsequent swirl generation, engine geometry or compression ratios [20]. LBVs are a fundamental aspect of combustion research since they give insights into combustion efficiency and controllability. The speed of the flame directly affects the proportion of emissions produced due to its influence on chemical kinetics. A closely related combustion characteristic is the ignition delay time (IDT). IDT is the time between the injection of fuel into the combustion chamber and the initiation of the combustion process. The delay gives useful insights into the chemical kinetics rate, the degree of fuel-air mixing, pressure rise rates and consequently, the prevalence of knocking or the smoothness of the engine [21].

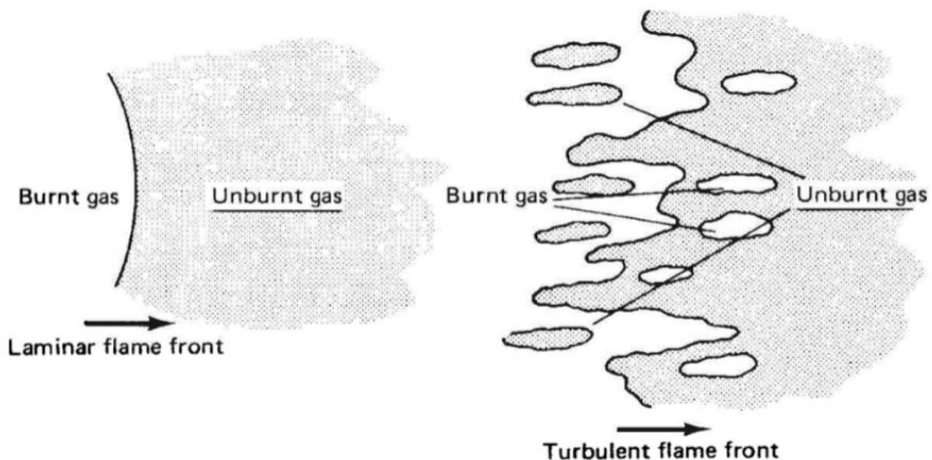


Figure 11 Flame propagation types [20]

Combustion Characteristics of Ammonia

Table 1 Fuel properties of various fuels [22], [23], [24], [25], [18], [26], [27], [28], [29]

| Properties | Units | Gasoline | Diesel | Ammonia | Ethanol | Methanol |
|------------------------------------|---------------------|----------|---------|---------|-------------|----------|
| Energy Density | MJ / m ³ | 31,074 | 36,403 | 11,333 | 21,070 | 15,650 |
| Octane Number | - | 90-98 | N/A | 130 | 108 | 108 |
| Cetane Number | - | N/A | 48 - 55 | 0 | 5 - 8 | 3 |
| Lower Heating Value | MJ / kg | 44.5 | 43.5 | 18.80 | 21.4 – 26.9 | 19.90 |
| Laminar Burning Velocity | m / s | 0.58 | 0.87 | 0.07 | 0.58 | 0.56 |
| Autoignition Temperature | °C | 300 | 230 | 630 | 423-434 | 464 |
| Latent heat of vaporization | kJ / kg | 71.78 | 47.86 | 1369 | 900 | 1160 |
| Minimum ignition energy | MJ | 0.14 | 0.23 | 680 | 0.14 | 0.6 |

Ammonia has a very slow LBV and has an extremely high minimum ignition energy requirement which means in its pure form it may not be suitable for spark ignition. Additionally, it exhibits a high autoignition temperature as seen in Table 1 which would also make it unsuitable for use in a compression ignition engine; very high compression ratios are required of 35:1 – 100:1 [30] to cause autoignition, this is because of an increase in flame propagation with increasing compression ratio [31]. However, this is not ideal since the most feasible compression ratios range from 12:1 to 24:1 [30]. It is also reported that engine modifications would be required if ICEs were to run on pure ammonia [31]. Ammonia is best combusted with another fuel with a low ignition temperature, creating a high-temperature atmosphere inside the combustion chamber [22], thus acting as a combustion promoter.

The combustion reaction chemical kinetics of ammonia are also very slow and in conjunction with its high latent heat of vaporization, incomplete combustion is more prevalent at the end of the combustion cycle and thus unburned ammonia could be emitted [22] as a pollutant. Most studies state that an ammonia content above 60-70% should not be used since there is a large increase in NOx from unburnt ammonia [30]. The high latent heat of vaporization also means combustion temperatures would be reduced, further exacerbating incomplete combustion if liquid ammonia is directly injected into an ICE [32], undermining pure ammonia's use in spark ignition modes. Alternatively, the use of gaseous fuel-air premixing may circumvent the significant temperature reduction seen during combustion using port fuel injection (PFI). However, the introduction of fuel through the intake manifold results in the displacement of an equivalent volume of air by the ammonia vapour, thus leading to a reduction in volumetric efficiency [31].

Attempts have previously been made to run ICEs on pure ammonia, using pilot injection with methanol to start the engines and transitioning to pure ammonia at a compression ratio of 15:1, 2000 rpm and an equivalence ratio of 0.88-1.15. The engine could only run for 90 mins, the combustion cycle was deemed to be "erratic" and unburned ammonia emissions ranged from 11.8% to 23.2% [33] [31].

An experimental study has looked at ammonia's detonation characteristics the deflagration to detonation transition (DDT) and compared it to other conventional fuels through testing in a large-scale horizontal tube. DDTs are interesting properties to investigate since they help in understanding how engine knocking and rapid increases in pressure occur in ICEs. The findings indicate that stoichiometric ammonia mixtures have the highest detonation overpressure and demonstrate favorable propagation velocities compared to other conventional combustible gases [34] [35] (Figure 12), this collectively means high combustion efficiency is possible using ammonia as a fuel. The study also shows that the detonation characteristics change by a large degree through changing the equivalence ratio (Figure 13) which is beneficial for operating under different load conditions in ICEs.

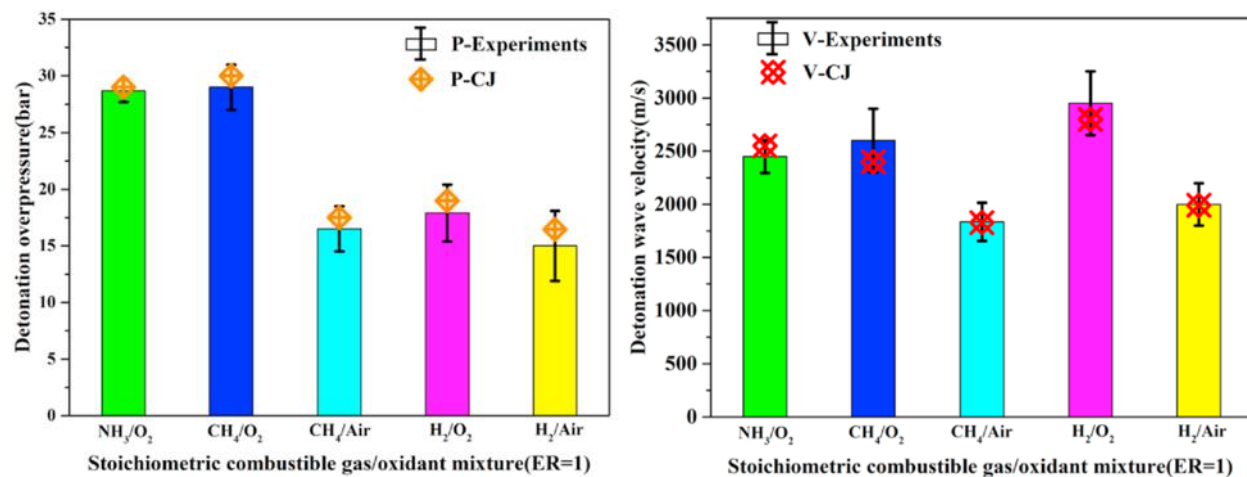


Figure 12 Detonation Characteristics of stoichiometric mixtures of conventional fuels [34]

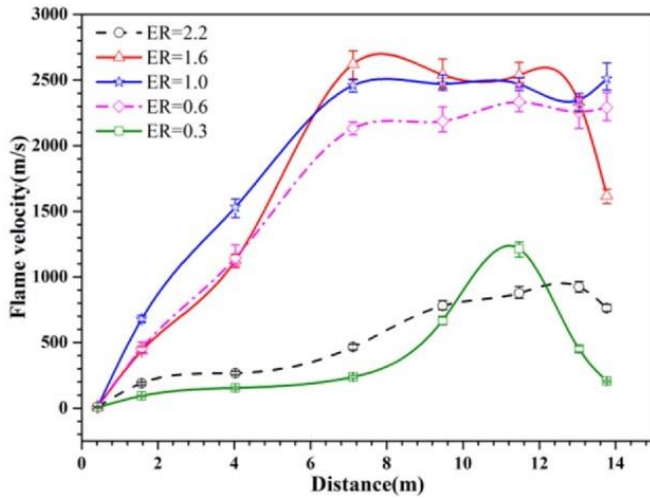


Figure 13 Flame speeds in ammonia/oxygen mixtures at various equivalence ratios with respect to the distance of propagation [34]

Combustion Characteristics of Oxygenated Fuels

The combustion of alcohols has the “alcohol bonus” advantage; more products are formed from the same quantity of reactants relative to other fuels, this results in a larger volumetric expansion [36] (Figure 14) which can be used to produce more work during the expansion stroke thus being more efficient, this is purely due to alcohols having oxygen molecules within their chemical structures. Experimental studies have shown that 10% water content [37] is optimal for maintaining desirable combustion characteristics via the highest observed LBVs and lowest

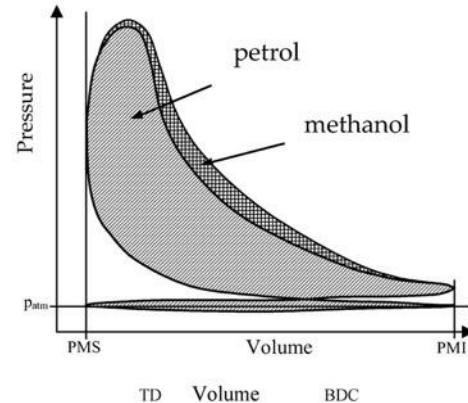


Figure 14 Indicated diagram for petrol and methanol [38]

IDTs. Low water content ethanol resulted in low NOx emissions from low temperatures but at higher water contents incomplete combustion occurred. Hydrous ethanol has a high oxygen content at 36.6% [37] and is shown to promote combustion and reduce carbon monoxide (CO), hydrocarbon (HC) and particulate emissions. Increasing water content showed a reduction in hydrodynamic instability but also an increase in diffusion-thermal stability, resulting in a net decrease in flame stability [37].

Combustion of hydrous ethanol can corrode metallic parts of the engine and react with rubber components [39]. Bioethanol typically also contains impurities such as chlorides and halides which can further exacerbate corrosion and thus corrosion inhibitors may be beneficial to add [39]. Bioethanol has a low lower heating value (LHV), which means you'd need large amounts to

match a conventional fuel this can be mitigated by mixing it with another fuel.

Current Studies on Ammonia Alcohol Fuel Blends

Dual fuel operations were researched which aim to utilize fuel properties to start a combustion chain reaction which will consequently ignite pure ammonia. An experimental study conducted at 1 atm and 298K – 448K used the heat flux method to measure the LBV of ammonia and alcohol-premixed flames; the study concluded that the addition of alcohol has similar improvements to the addition of H₂ or methane (CH₄) as combustion promotores [40], this is due to the increase in reactive radicals which in turn increases the adiabatic flame temperature [40]. Additionally, ethanol was shown to better improve the LBV [41] across a larger range of alcohol mole fractions in the mixture as shown by Figure 16 at low and high temperatures. Figure 15 shows the LBVs of a few more combustion promotores into NH₃; ethanol is still the best solvent across most of the equivalence ratio range.

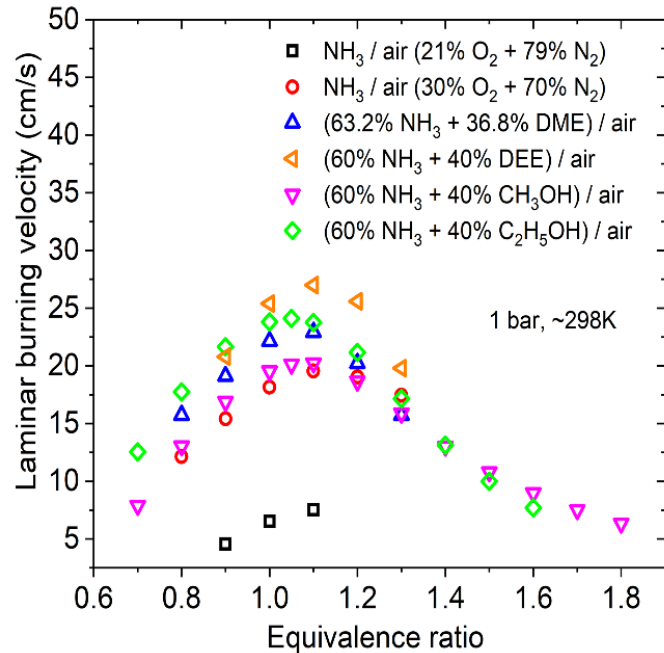


Figure 15 Comparison of the measured LBVs with combustion enhancers to ammonia [42]

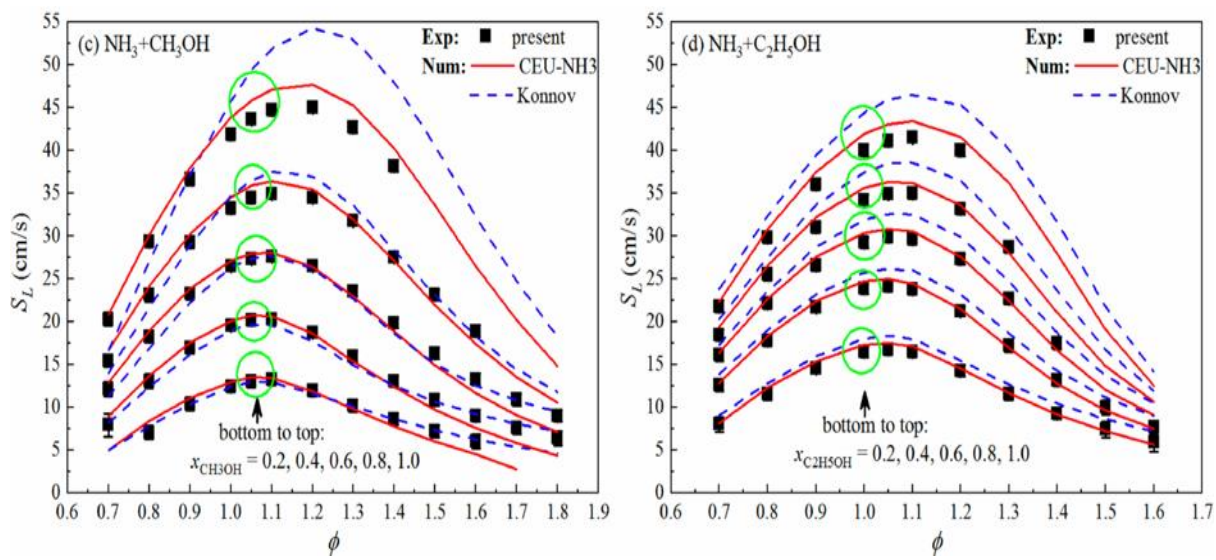


Figure 16 Laminar burning velocity of ammonia-methanol (Left), and ammonia-ethanol (Right), at 298 K and 1 atm [43]

An experimental study used rapid compression machines to study IDTs at elevated pressures of 20 and 40 bars and temperatures of 820K and 1120 K, their findings are presented in Figures 17 and 18. The addition of 1% ethanol to the mixture at 40 bars (Figure 17 - left) has drastically decreased the autoignition temperature, in turn, this would also decrease NOx emissions. Ethanol's reactivity is further highlighted in Figure 18 which shows the largest shift in autoignition temperature out of all the combustion promoters. This study could be improved by seeing the effect of ethanol addition at smaller fraction ranging from 0 – 5% in 0.5% intervals and how drastically the ignition delay time changes at 0% ethanol with 40 bars.

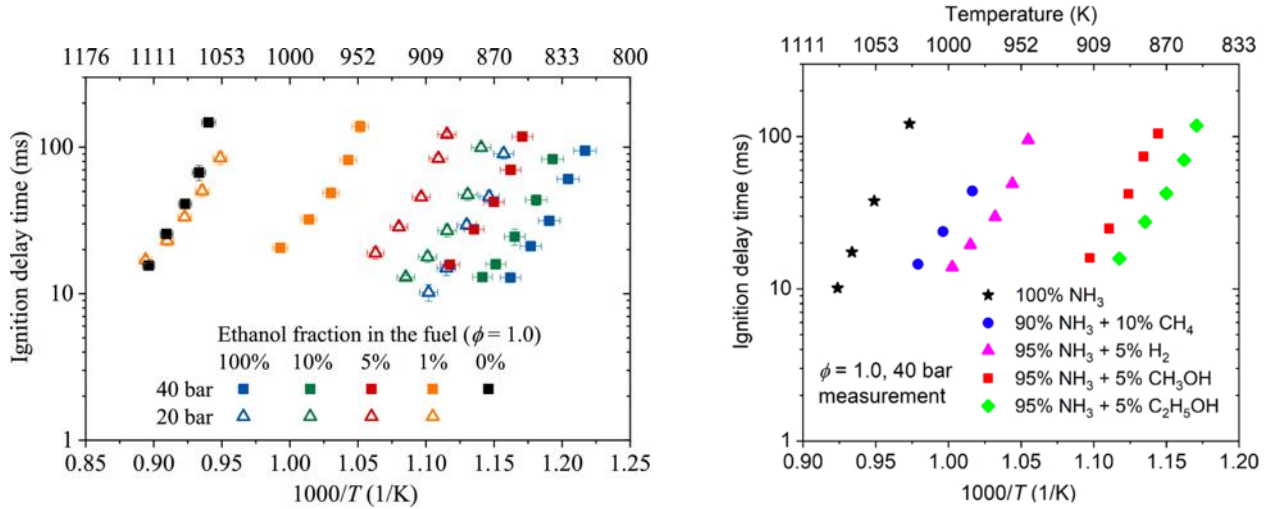


Figure 17 Experimental Ignition delay times of ammonia-ethanol stoichiometric mixtures at 20 and 40 bars [44] (Left)

Figure 18 Experimental ignition delay times of various ammonia/fuel blends [43] (Right)

Engine testing on ethanol-ammonia fuels has recently been conducted on a spark ignition (SI) engine through direct injection (DI) of the blended liquid fuel under different fuel injection strategies: homogenous (Start of Injection – SOI 175) and stratified modes (SOI 90) [45] corresponding to differing levels of fuel-air mixing as a result of differing fuel injection times with respect to crank angle degrees before TDC. Ammonia and ethanol fuels were contained under a pressure of 120 bar to keep them in liquid phase and thus the engine tests were also conducted at an injection pressure of 120 bars in conjunction with an intake temperature of 80 °C at 1000 rpm.

The combustion performance and emissions differences between both modes of combustion are presented in Figure 19, X100 represents pure ammonia and X0 represents pure ethanol. A drastic difference in the maximum heat release rate is observed between both injection modes. In homogenous mode the maximum heat release rate was observed to decrease with increasing ammonia content, a difference of 40% [45] between pure ethanol and pure ammonia. As expected, the combustion duration was observed to increase with increasing ammonia fraction which can be seen by the wider heat release rate (Figure 20) and the larger spread of burned mass fraction to reach complete fuel combustion (Figure 20). The highest combustion efficiencies were observed near a 0.25-mole fraction of ammonia in the fuel blends. Analysis of exhaust

emissions shows drastic increases in emissions in the stratified injection mode, but an improvement is in NOx emission, albeit a very small decrease from the homogenous injection. Thermal and combustion efficiencies are also observed to be lower in stratified mode. Overall, the study concludes homogenous injection has more benefits and that a fuel mix of 20% ammonia and 80% ethanol on a molar basis is optimal [45].

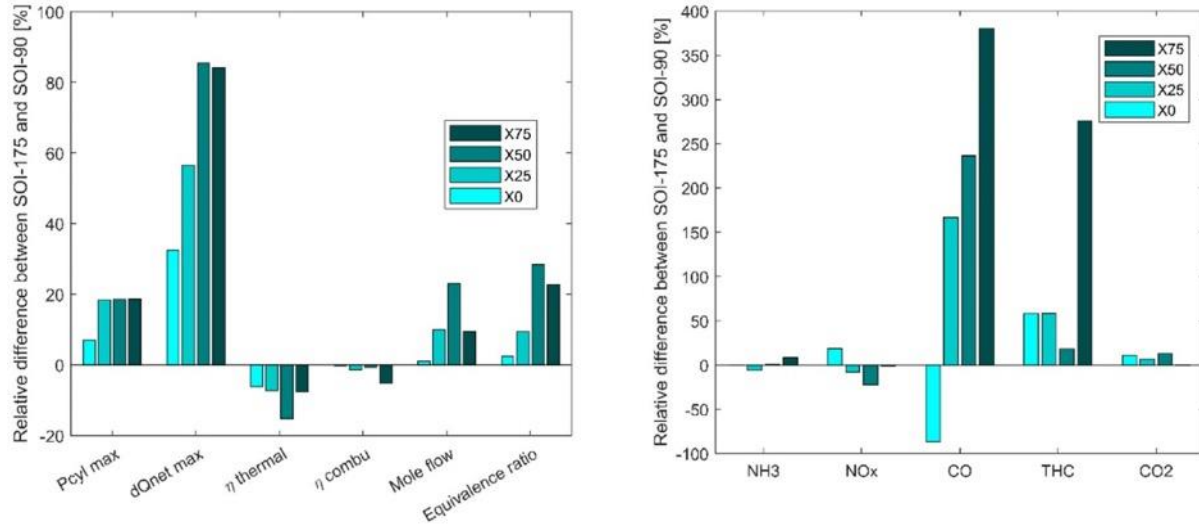


Figure 19 Comparison of combustion performance (Left) and pollutant emissions (Right) between the homogeneous and stratified fuel injection strategies for varying ammonia fractions. [46]

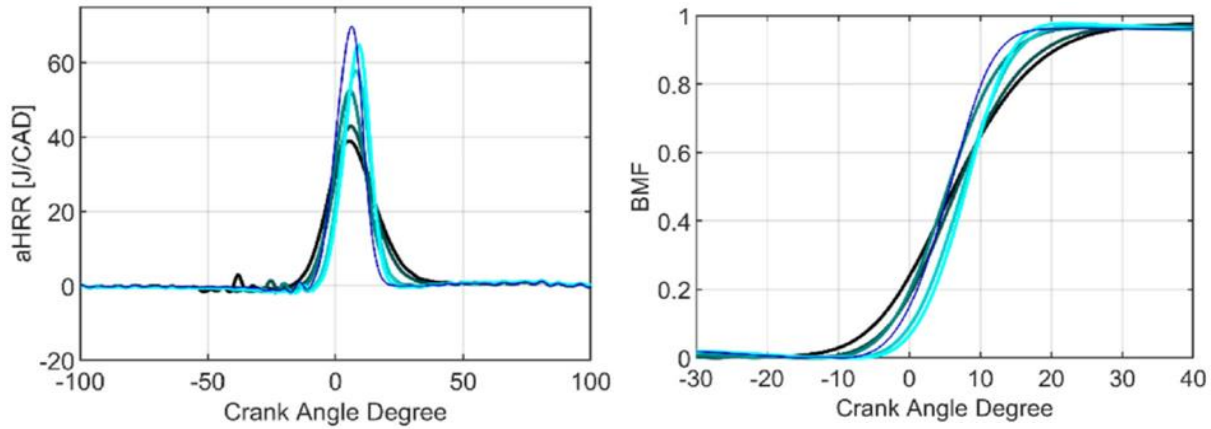


Figure 20 Heat release rates (Left) and burned mass fractions (Right) at 1 bar of intake pressure with homogeneous injection strategy for varying ammonia fractions [46]

A simulation study [47] has used the conductor-like screening model for real solvents (COSMO-RS) which is based on quantum chemistry and statistical thermodynamics to research the physicochemical properties of solvents. Figure 21 shows the solvents which have been analysed for solubility with ammonia. The trend in solubility between the solvents reflects the bond's polarity and the solvent's capacity to form hydrogen bonds with ammonia, the smaller the molecule the better it acts as a solvent. Despite carboxylic acids exhibiting the best solubility,

they can react to create an ammonium salt as Figure 22 shows both of which don't exhibit great combustion characteristics.

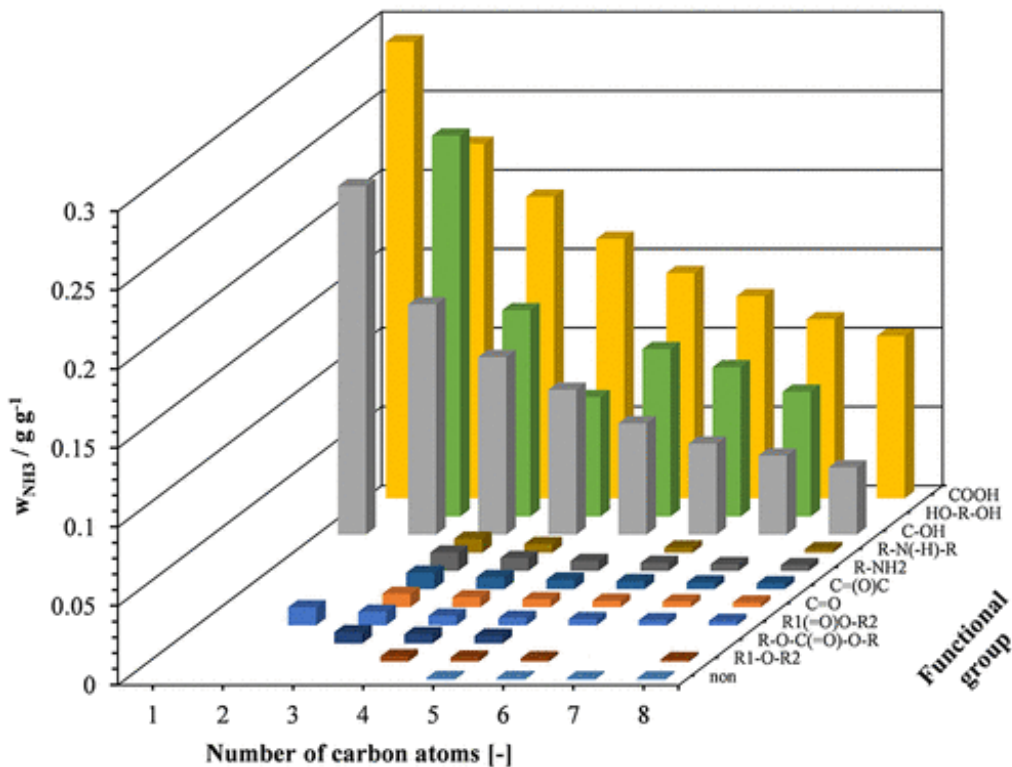


Figure 21 Ammonia dissolution in various classes of organic solvents at 1.013 bar and 25 °C [47]

Figure 23 shows the solubility of ammonia in the solvents with respect to temperature. Firstly, the COMSO-RS data follows experimental data. The figure highlights the difficulty of ethanol in creating a stable mixture in A10 (weight percent of ammonia) and A20 blends, whilst methanol can create blends of any configuration, which relates to the improved solubility of methanol due to its increased polarity. A5 blends are the most stable for the other solvents in the study.

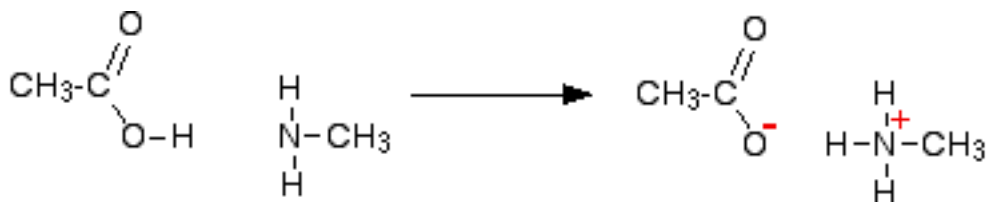


Figure 22 Polar Nature of OH group and its interaction with ammonia [48]

Figure 24 shows the LHV for all the solvents. The energy density is shown to reach a maximum of 70 – 50% relative to gasoline [49]. Despite propanol exhibiting similar LHV to E85 its poor ammonia solubility means it cannot be used as a fuel blend at ambient conditions.

Figure 24 also shows the carbon emissions, and it is evident there is a decreasing emissions savings the higher the ammonia content since ammonia doesn't contain any carbon atoms itself. The difference in CO₂ emissions between the blends is marginal, however, the NO_x and THC emissions can be expected to vary and be one of the deciding factors in the selection of an appropriate solvent. This study concluded that an A10 blend of methanol would be suitable, however, it didn't compute other emissions which may be a deciding factor in the suitability of a solvent.

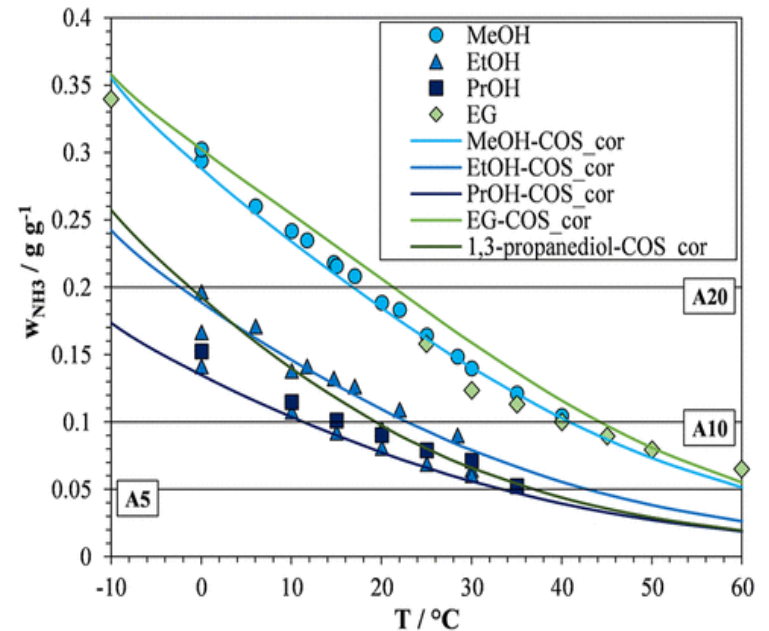


Figure 23 Fuel stability of the ammonia solubility in selected solvent at varying temperatures. [47]

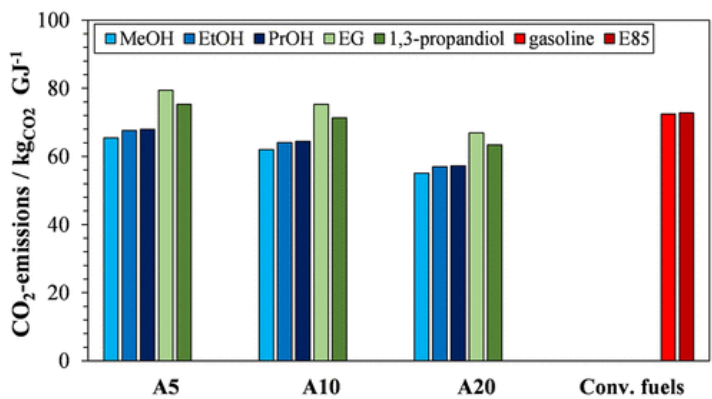
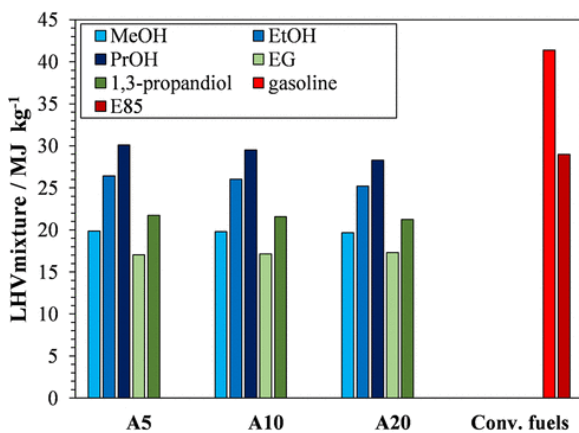


Figure 24 Theoretical lower heating values for different ammonia-solvent mixtures (Left), Theoretical CO₂ emissions for different ammonia-solvent mixtures (Right) [47]

Advanced Combustion Modes

Homogenous charged compression ignition (HCCI) premixes the fuel with air before being introduced into the combustion chamber through PFI introducing the fuel as a vaporised mixture through the air intake. The piston increases compression and causes autoignition of the mixture simultaneously throughout the combustion chamber. The key characteristic is the mixture is homogenous which means there are no fuel-rich zones and thus no thermal hotspots offering the lowest in-cylinder temperatures [50], this all leads to the highest combustion efficiency and lowest NOx and soot levels compared to all the combustion modes, as depicted in Figure 25.

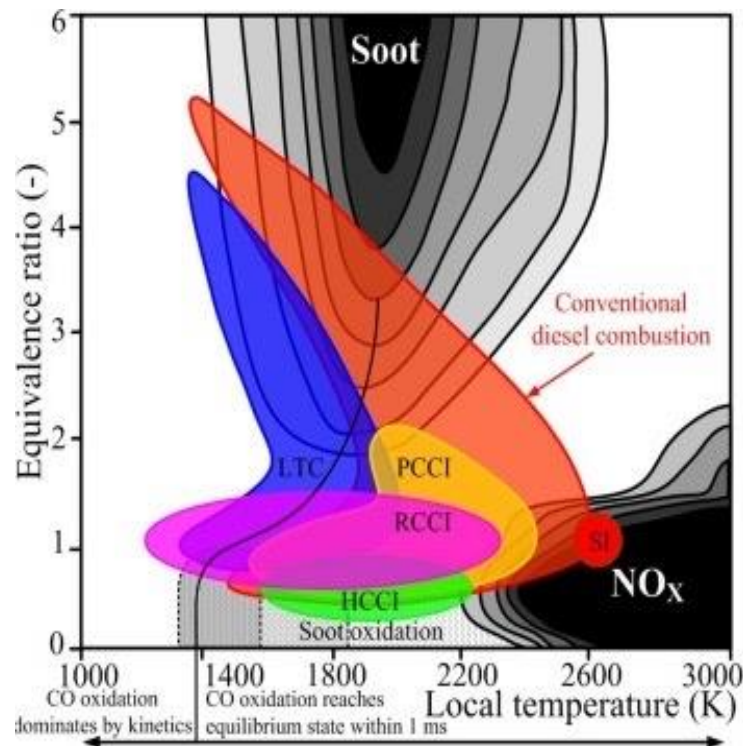


Figure 25 The operating zones of different combustion modes [19]

HCCI would be the best option to decarbonise the transport sector but currently, literature has stated limitations of its use in ICEs and thus is yet to be implemented on a large scale. The lack of ignition control leads to difficulty in controlling the combustion process. The low-temperature conditions can also lead to increased unburnt HC levels due to incomplete combustion relative to SI and compression ignition (CI) [51].

HCCI also tends to knock at high engine loads due to high peak pressures and has cold start and misfiring issues at low engine loads, limiting its operating load range [52]. HCCI combustion tends to occur in two stages which produce differing power levels. The negative temperature coefficient (NTC) zone is the region where temperature and rate of combustion are indirectly proportional. Controlling the duration of the NTC region allows for the control of the main combustion event, the NTC can be controlled by charge reactivity by using fuels like ethanol [53].

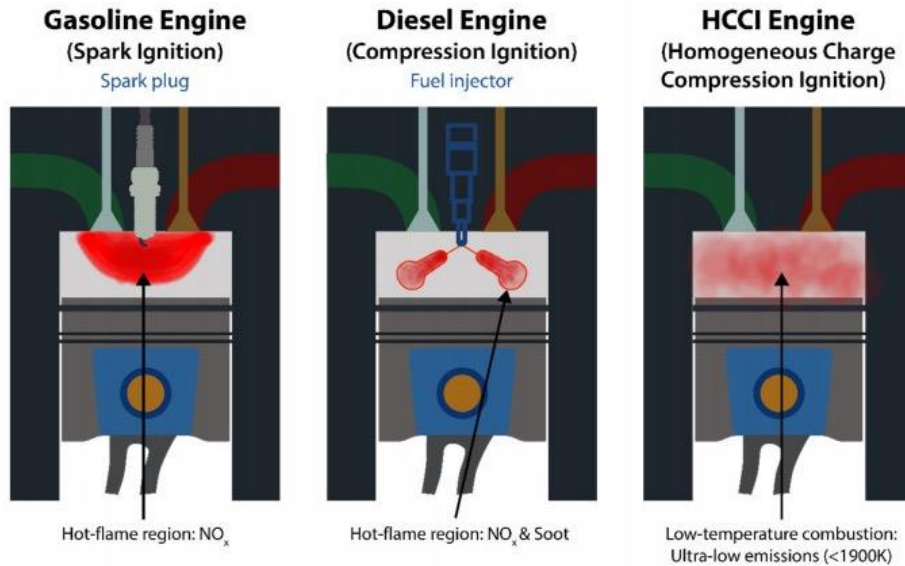


Figure 26 Comparison of HCCI with conventional combustion modes [54]

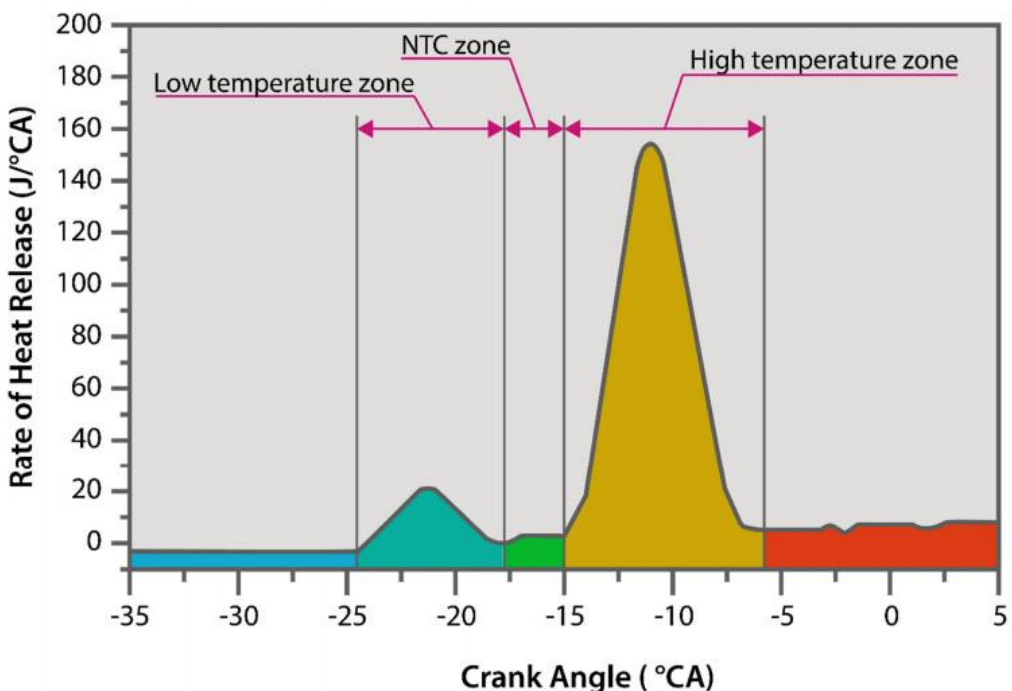


Figure 27 Nature of heat release rates of HCCI combustion [54]

Variable compression engines (VCE) allow HCCI engines to operate over a wide range of loads. VCEs change the volume of the combustion chamber by changing the travelling distance of the piston [20] and thus the compression ratio depending on the intended driving conditions. Alcohols tend to inhibit low-temperature oxidation under HCCI mode, which allows for better control over the combustion timing [52]. A study has reported that two fuels with differing octane numbers are suitable for HCCI since this allows for the combustion phasing to be controlled [51]. Research has shown hydrous ethanol can run efficiently in HCCI mode but there are increases in HC and CO emissions as the water content increases [55]. Hydrous ethanol is deemed to be better than anhydrous ethanol in most modes of combustion due to the high latent heat of vaporization of water (H_2O) which decreases the in-cylinder temperatures and thus decreases NOx emissions. A slight drawback is the heat release rate does drastically decrease with increasing water content as seen in Figure 28.

Fuels possessing a low cetane number are deemed advantageous for combustion within HCCI systems. Figure 29 depicts a decline in carbon monoxide emissions generated by an engine employing HCCI and running on fuels with diverse cetane values.

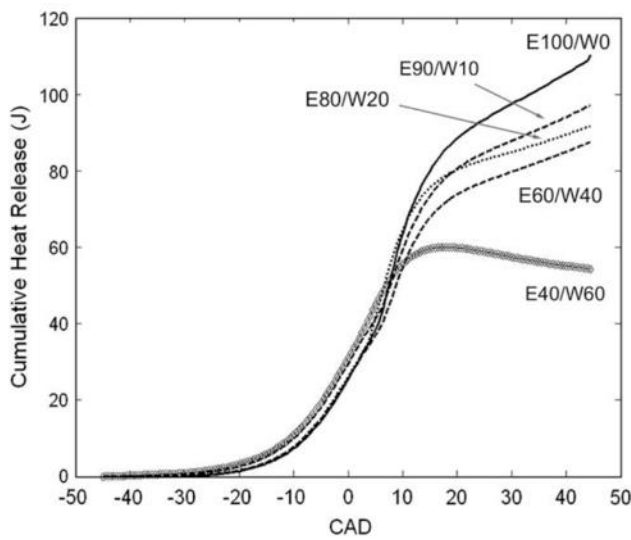


Figure 28 The cumulative heat release for different blends of aqueous ethanol [17]

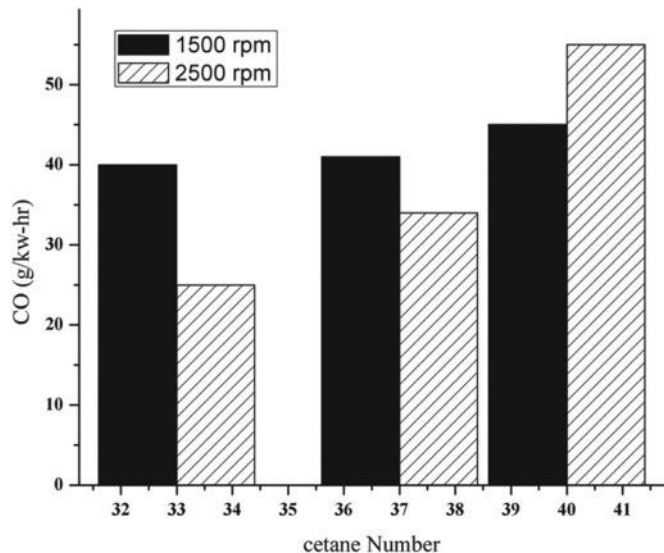


Figure 29 Effect of cetane number on CO emissions [56]

Effects of Water on Combustion

The addition of water to combustion processes can decrease in-cylinder temperatures and thus decrease NOx emissions and PM emissions [14]. Water can be added in three main ways; blended with fuels (mixture or an emulsion), direct injection or through the intake manifold.

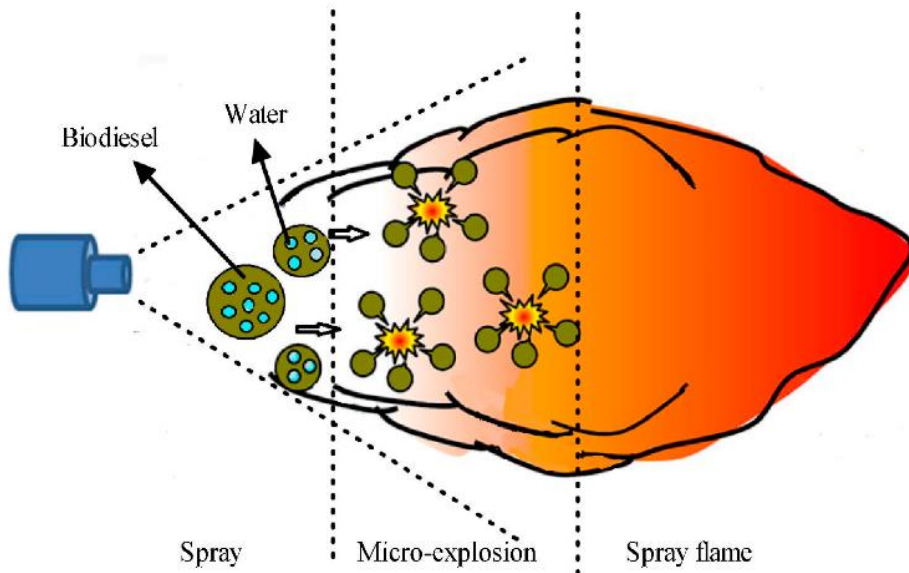


Figure 30 Nature of combustion with water [57]

Combusting blends of fuels and water causes the water to reach a supercritical state and leads to micro-explosions [58] and results in enhanced fuel-air mixing due to increased atomization (Figure 30) which is suitable for HCCI applications. Molecular dynamic simulations conducted through ReaxFF-MD have shown that H₂O addition increases OH radicals and the conversion of NO_x to hydrogen atom-containing species [59] [14]. Another numerical study concluded low quantities of water (<20%) improved ethanol oxidation [60] improving flame propagation characteristics and thus decreasing ignition delay times.

Literature Review Summary: The implementation of an ammonia-fuel blend has two benefits, ease of transportation and as a combustion promoter to mitigate the slow laminar burning velocity, slow chemical kinetics, and high ignition temperature requirements. The disadvantages of ammonia and alcohol individually are counteracted when they are combined. The presence of water in low concentrations is beneficial but can lead to engine damage at high concentrations. Primary and secondary alcohols have the best solubility for ammonia and thus their combustion characteristics should be further investigated. Current spark ignition research on ammonia/alcohol blends shows homogenous injection of the blends are suitable for use in internal combustion engines, with power decreases as the ammonia content is increased. Homogenous charged compression ignition would be the best mode of combustion, but there some challenges that need to be further investigated.

Research Gap

Analysis of existing literature reveals a substantial number of studies using simulations, but the amount of actual research conducted on homogeneous ammonia-solvent fuel blends at ambient conditions is notably limited. Specifically, this thesis will focus on the analysis of the combustion characteristics of alcohol-ammonia fuel blends in spark ignition modes. The objective of this study is to address the research gap by investigating the efficacy of ammonia blended fuel mixtures via engine testing. The obtained results will be corroborated with findings from extensively referenced simulations.

Aims and Objectives

This report aims to answer the following questions which will be investigated via the following objectives:

- 1. How will the fuel be made?**
 - a. Experimental work to investigate solubility limits
 - b. Experimental work to determine the simplest route to make fuels
- 2. What are the chemical characteristics of the fuel blend?**
 - a. Conducting calorimetric analysis to identify the presence of ammonia
 - b. Gas chromatography-mass spectroscopy and titrations for concentration analysis
- 3. Is the combustion cycle controllable, reliable, and appropriate for a wide load range?**
 - a. Engine testing to investigate cyclic variations and power outputs
 - b. Engine testing to determine the heat release rates, in cylinder pressures and burnt mass fractions
- 4. Are the fuels financially viable?**
 - a. Aspen simulations to determine cost drivers in production of the fuel
 - b. Time series forecasting to see the future viability of fuel
 - c. Statistical modelling to see plausible fuel prices

Methodology and Experimental Techniques

Fuel Preparation

Concepts that allowed the fuel to be made inside a vehicle or via industrial production processes were considered, and the criteria that were evaluated are presented in Table 2 (weightings and scores out of 10). The emphasis was on ensuring that the concepts consider safety, the environment, society, and commercial applications. To reduce costs and increase the potential for in-vehicle fuel production, operating conditions were assumed to be obtained through inbuilt systems such as exhaust gas recirculation cooling loops and hot waste exhaust gases sent to catalytic converters or forced induction systems. As explained below, the following design concepts were shortlisted.

Concept 1: Aqueous ammonia shows great promise as a means of transporting ammonia in bulk. But once the ammonia has been released from the solution, large amounts of water would be left over, and should ideally be sent for water treatment before discharging due to the possibility of trace amounts of ammonia. From this, the idea (Figure 31) of using a reactant which uses up the “wastewater” was investigated. Ethanol: one of the required solvents can be produced from the reaction of ethene and water via a direct hydration reaction at 300 C, 1-10 bars and a phosphoric acid catalyst, as shown by the reaction in Figure 32. Although the large amounts of water utilized make the method very sustainable, the presence of the high pressures makes it very unlikely to be implemented inside vehicles or fuel stations but does have great potential for industrialisation.

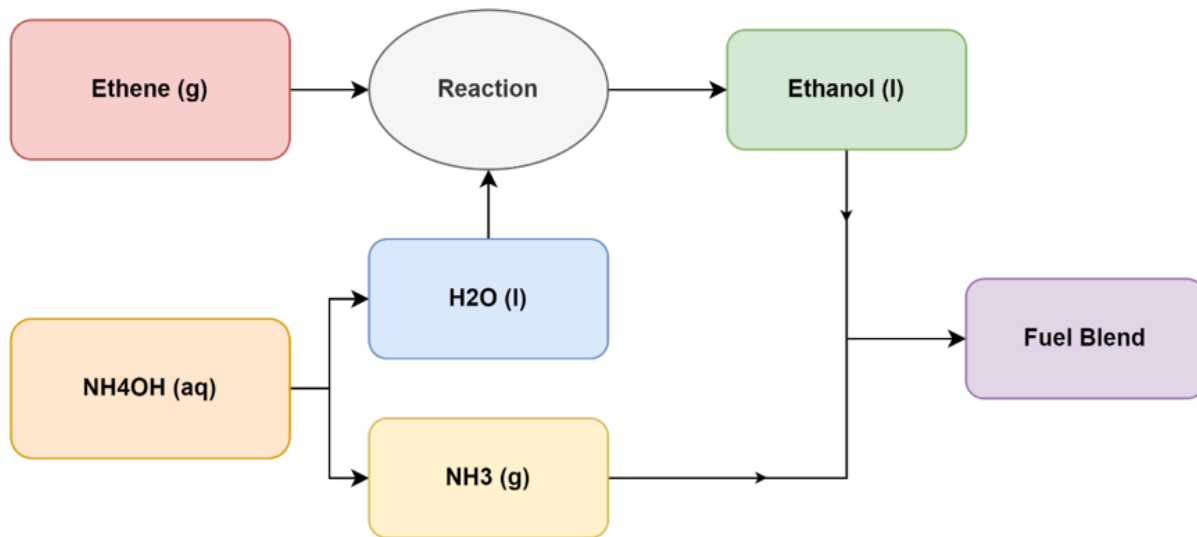


Figure 31 Concept 1 Block Diagram

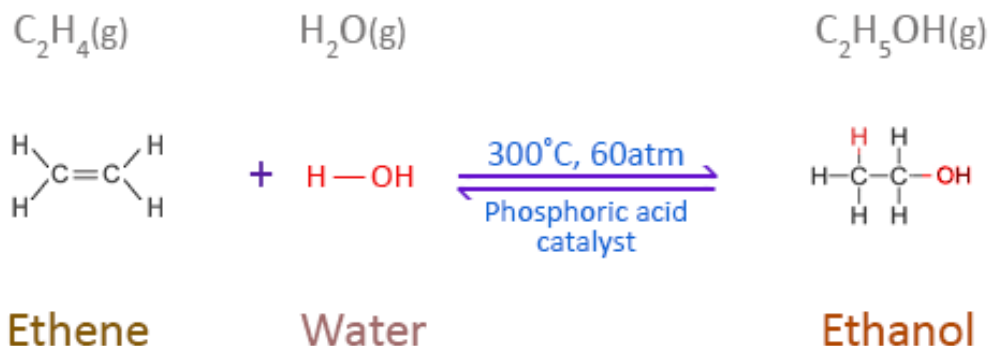


Figure 32 Concept 1's Key Reaction [61]

Concept 2: Simple distillation of ethanol and water results in 95% purity of ethanol due to the presence of an azeotrope. To ensure 95% is achieved distillation columns with multiple stages would be desirable to enhance separation, this can be achieved via a fractional distillation column. This concept was based on the idea of transporting all the required reagents in one vessel allowing for easier transportation and storage of the reagents. Figure 33 shows the ternary distillation setup, with one mixture of ammonia, water and ethanol being separated based on their boiling points, ammonia would evaporate first leaving the ethanol and water to undergo vapour liquid equilibrium on the column's stages. Although the purity level of the ethanol is reduced, fractional distillation is still a very energy-intensive process thus ranking it low on the design matrix.

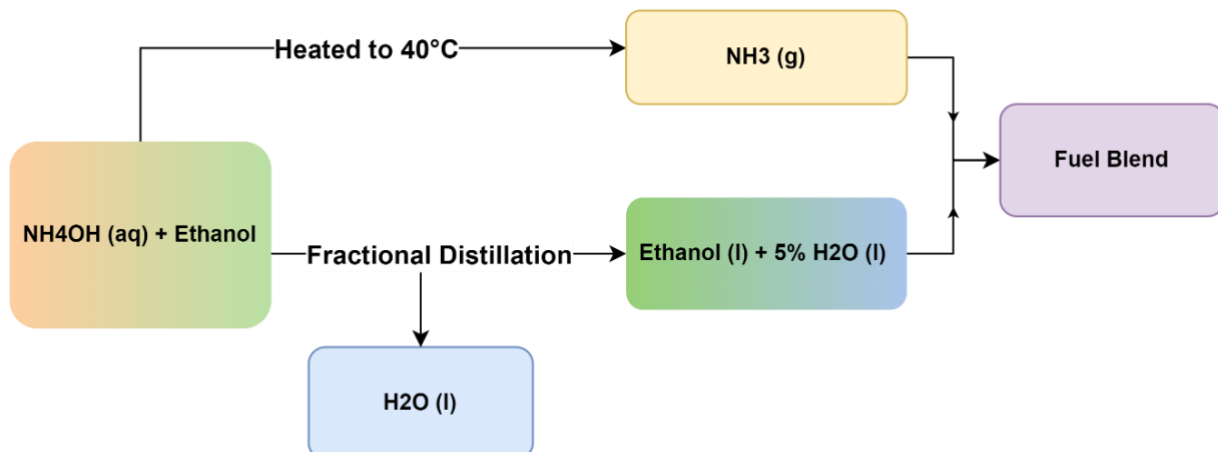


Figure 33 Concept 2 Block Diagram

Concept 3: Ammonia can be very easily released from a mixture of aqueous ammonia with gentle heating. The introduction of gaseous ammonia can be done at a fast rate by introducing the ammonia as fine gas bubbles. This concept (Figure 34) allows for very rapid fuel mixture formation; the rate of reaction is only dependent on the rate of reactant introduced thus making it mass transport limited, it is also the most energy efficient out of the three concepts. This concept is also the simplest and thus the easiest to implement into current fuel infrastructure from a technical and economic perspective.

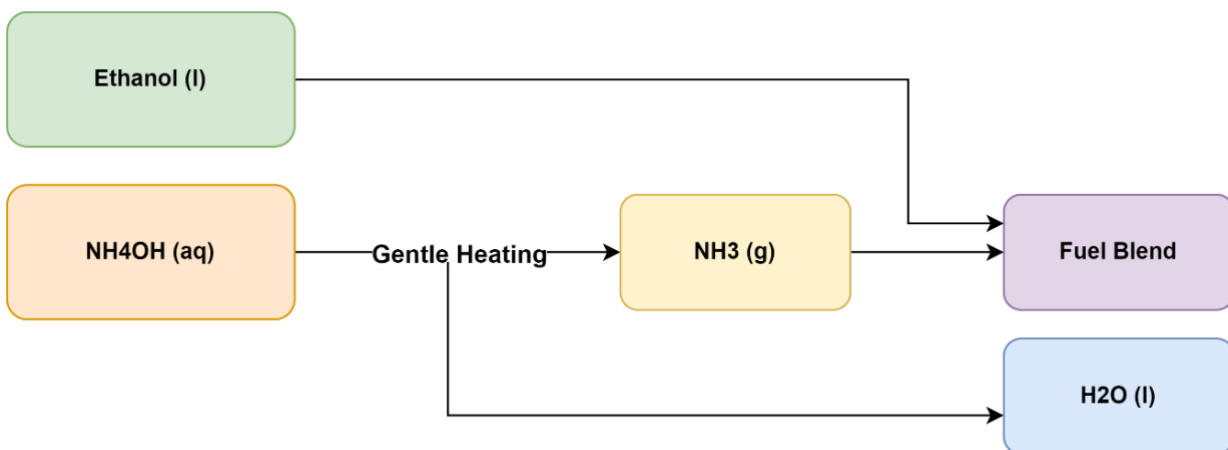


Figure 34 Concept 3 Block Diagram

Table 2 Design Selection Criteria

| Criteria | Weighting | Concept 1 | Concept 2 | Concept 3 |
|--|-----------|-----------|-----------|-----------|
| Sustainability | 10 | 8 | 7 | 6 |
| Ease of Implementation | 7 | 2 | 7 | 8 |
| Ease of Storage and transport | 5 | 2 | 6 | 9 |
| Material Costs | 3 | 1 | 6 | 6 |
| Potential for industrialisation | 4 | 10 | 8 | 8 |
| Potential for in-vehicle production | 6 | 1 | 3 | 8 |
| Safety | 8 | 5 | 6 | 7 |
| Energy Efficiency | 6 | 7 | 5 | 8 |
| Fuel Quality and Reproducibility | 7 | 8 | 4 | 8 |
| Total | - | 291 | 323 | 419 |

An experimental method (Figure 35) to prepare the fuels was developed to investigate Aim 1b following the selection of Concept 3 since it had the best score from the design matrix. The below method allowed for precise control over the proportion of ammonia in the fuel blends.

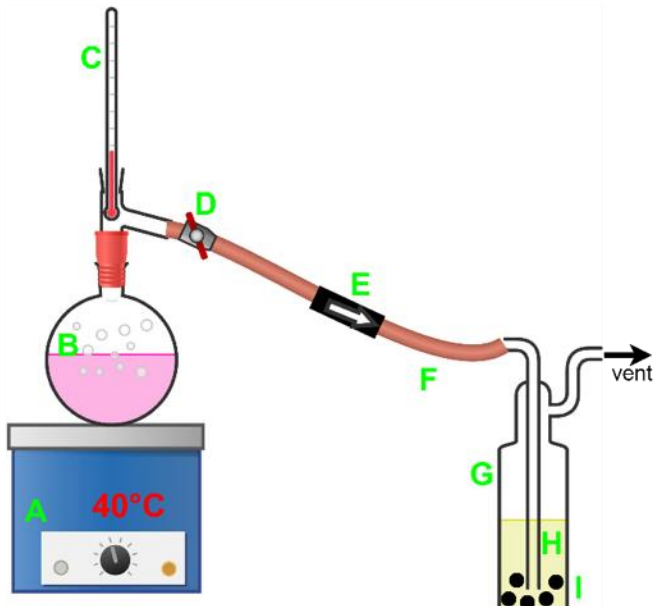
The boiling point of ammonium hydroxide 35% was raised above 37°C in a heating flask with a heating mantle to create a positive pressure gradient between both flasks. At the end of the reaction, the phenolphthalein pH indicator in the heating flask turned from vibrant pink to colourless, indicating that all the ammonia had been released. To improve mass transfer, the heating vessel was connected to a stopcock that controlled ammonia gas flow to the gas washing bottle. Reverse flow was a common issue and was stopped with a stop cock and one-way valve. Ammonia gas was transferred to the gas washing bottle via the one-way valve and rubber NBR fuel hose pipe. Gas washing bottle inlet connects to a 20µm pore sparger, generating fine bubbles. Equation 1 shows that increasing the interfacial area ensures ammonia gas dissolves into solvents, allowing us to determine the equilibrium rate and whether the process is feasible for in-vehicle production. Ceramic rasching rings and stainless-steel saddles in the gas washing bottle increased gas–liquid mass transfer by increasing the interfacial area, as shown in Figure 36 from a CFD study. Further evidence of completion is a colour change (colourless to yellow) in the fuel mixture and a decrease in sparger gas bubbles. At the end of the reaction, reverse flow was likely due to a lack of a pressure gradient between flasks. Ammonia condensing in the heating flask decreases the pressure gradient, mixing ethanol with the aqueous ammonia to create an azeotrope.

$$\frac{dC}{dt} = k_l a (C_{sat} - C) \quad \text{Equation (1) [62]}$$

where: $\frac{dC}{dt}$ = gas dissolution rate, k_l = Mass Transfer Coefficient

a = Gas – Liquid interface area, $C_{sat} - C$ = concentration gradient

Table 3 Experimental Setup Equipment



| ID | Item |
|----|------------------------------------|
| A | Heating Mantle |
| B | Heating Flask with Aqueous Ammonia |
| C | Thermometer |
| D | Stopcock |
| E | One way valve |
| F | Rubber Tubing |
| G | Gas Washing Bottle with Sparger |
| H | Ethanol |
| I | Column Packing |

Figure 35 Lab Scale Fuel Production Setup

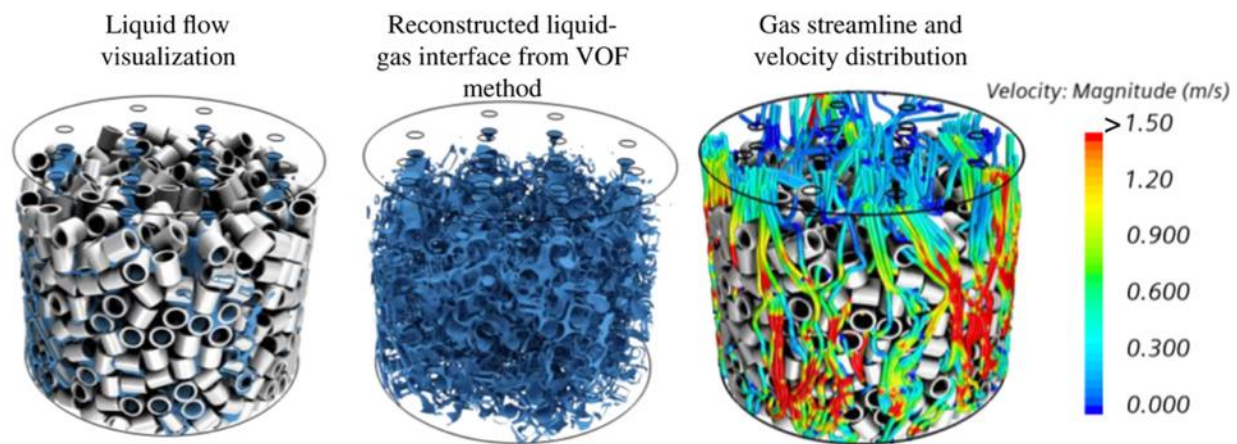


Figure 36 The liquid flow pattern, gas–liquid interfacial area, and gas streamlines for column packing [63]

Fuel Sample Analysis and Quantification

To understand the solubility limits and the contents of the fuel mixture, titrations were carried out. The alcohols, although they act as a weak acid are assumed to not have major effects on the titration's stoichiometric equation (equation 2). Ammonia is a weak base and thus should ideally be titrated with a strong acid, as a result, 0.1M sulphuric acid (H_2SO_4) was chosen. The pH indicator was chosen based on the estimated equivalence point. The equivalence point was estimated by looking at the characteristics of the titration curve with H_2SO_4 and the fuel sample and measuring the pH at intervals of 5ml of acid added, the titration curve computed is seen in Figure 38 and Figure 39 illustrates the equivalence better. The pH range of the equivalence point is 6 – 3, as a result, Methyl Orange was selected since it has a pH colour change range of 3.1 – 4.4. The titrations were deemed to be completed when the colours of the solution transitioned from orange to permanent red. The same procedure was conducted for the methanol samples and its titration curves are present in Appendix section B.

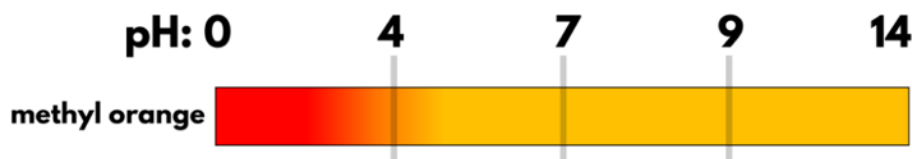


Figure 37 Methyl Orange operating pH range [64]

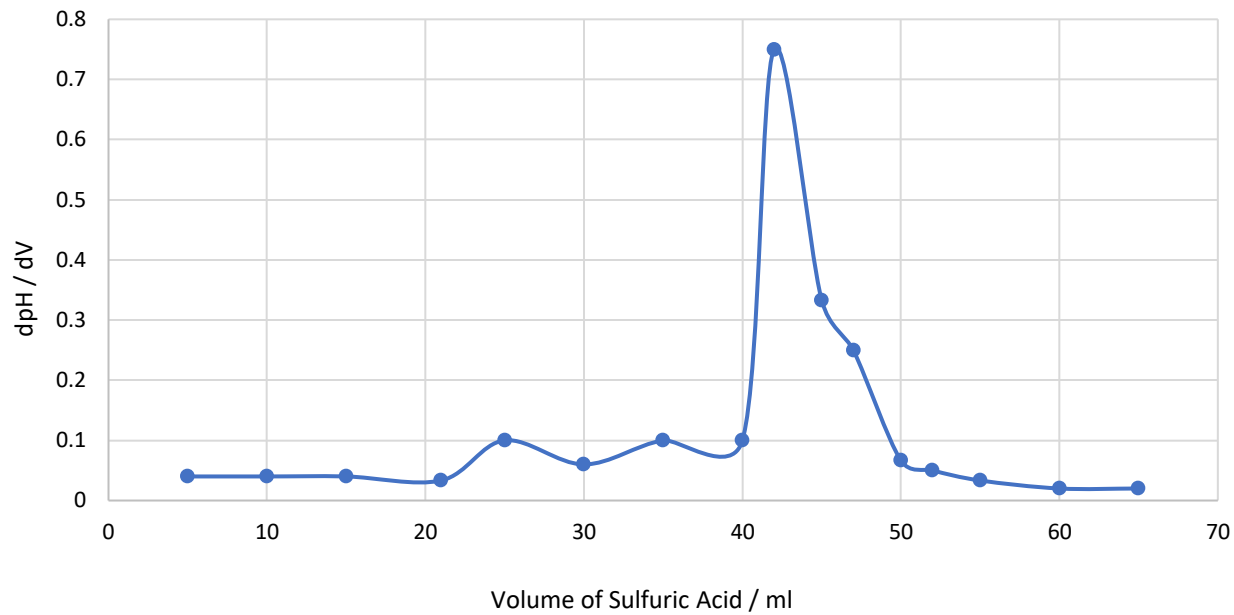


Figure 38 Computed Titration Curve for Ethanol / Ammonia

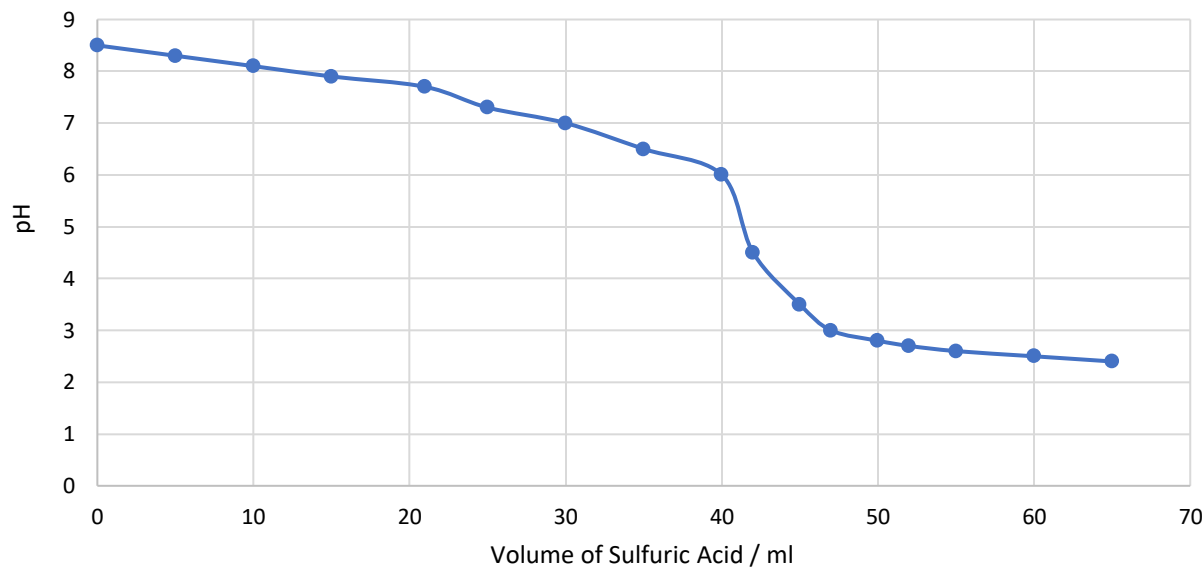


Figure 39 Equivalence point for Ethanol / Ammonia

In addition to the preliminary titration, Gas Chromatography–Mass Spectroscopy (GCMS) was conducted with Agilent Technologies 7890B GC in conjunction with 5977A MSD machines. A temperature program was developed to scan for ethanol and ammonia via trial and error. The GCMS machine was operated in spitless mode. The samples of interest were diluted to a ratio of 1:10 with dichloromethane as the solvent and the samples were injected via an autosampler. The column used is a Restek, 0.25 µm diameter and 30 m length with fused silica.

The results will be analysed qualitatively via Agilent Qualitative Mass Hunter software. The chromatogram will be processed via chromatogram deconvolution algorithms to reduce overlapping peaks which allows for more accurate identification and quantification of species. The Total Ion Chromatograms (TIC) are then searched with the NIST library which matches the ion peaks with databases and gives a list of potential species and the probability of a match. A calibration curve will be built to validate the method and allow for concentration determination via chromatogram peak areas.

Energy Content Analysis

A bomb calorimeter will be used to measure the heat of combustion and thus the energy content of the fuel under isochoric conditions. The start temperature was set at 22 °C and the machine computes the temperature increase of the water after igniting a cotton thread linked to the combustible sample by passing current through an ignition electrode and outputs the HHV. The machine used is the IKA C1 compact calorimeter connected to a water temperature chiller. Corrections are automatically applied to the Higher Heating value (HHV) to account for the presence of extraneous energy such as from the cotton thread, igniter and the acetobutyrate capsules into which the fuel samples were placed. The capsules had a gross calorific value of 18568 J/g. Calibration was conducted with benzoic acid tablets and a heat capacity of 4800 J/C° was chosen. 30 bars of oxygen were injected to ensure complete combustion of the sample.

Cross-validation was performed on the findings obtained from the chemical analysis procedures to check whether the ammonia fractions were accurate.

Combustion Characteristic Analysis

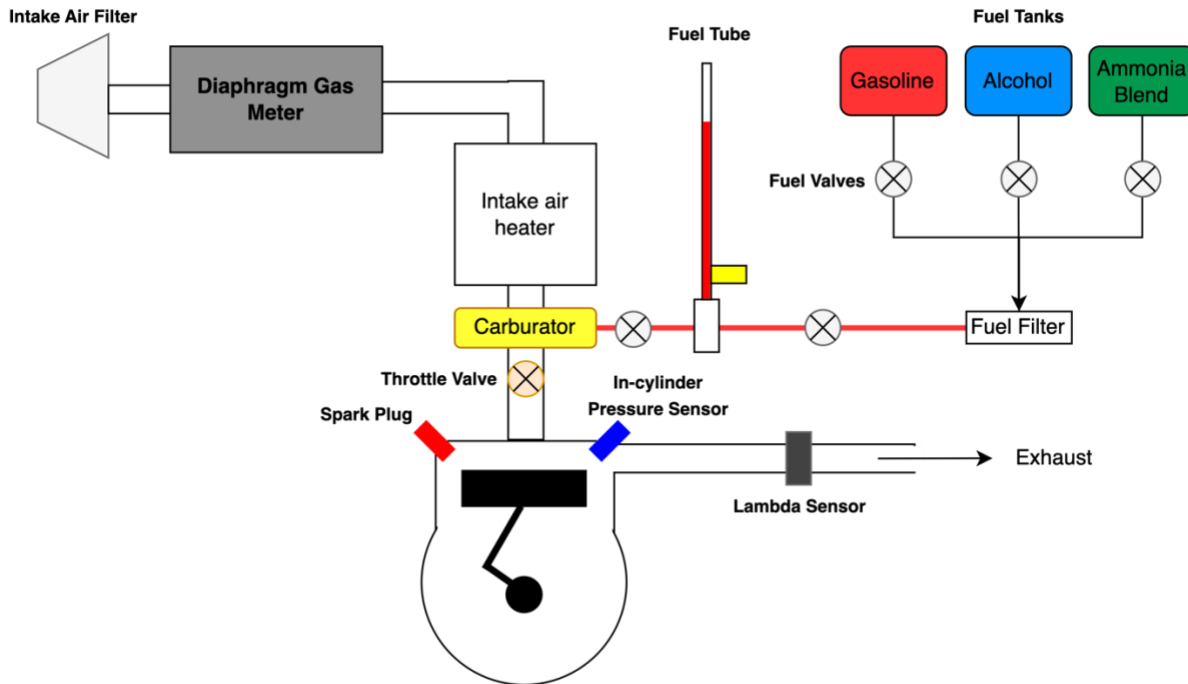


Figure 40 Engine Setup - Adopted from [65]

The engine used is a Ricardo E6 Engine variable compression engine which is illustrated in Figure 40. It was operated under spark ignition at 600 rpm. The engine is naturally aspirated and was set to the lowest possible compression ratio of 4.5. All the tests were conducted at the same test conditions of spark timing at 13 crank angle degrees before TDC, at the fuel mixtures stoichiometric air-fuel ratios (sample calculation present in the appendix section A) and wide-open throttle. Intake air pressure and temperature were kept at ambient conditions, the intake air heater was not used for the tests. The engine was warmed up with gasoline and left to rest for two minutes before samples were introduced. Each sample was run three times with two-minute rest intervals in between sampling to the engine cool. The fuel pipes were made sure to be cleaned by emptying and washing with the new sample in between runs to not interfere with the engine results. The in-cylinder pressure sensor was the main sensor used which allowed for the computation of in-cylinder pressure, filtered heat release rates, cumulative heat release rates, mass fraction burnt and knocking frequency.

A single cylinder was used because the fuel consumption would be low, allowing for the use of small sample volumes, the introduction of consistent fuel proportions into the combustion chamber, the absence of mixture variation [20], and most importantly, the elimination of inter-cylinder variation, which could result from mechanical variations in the form of compression ratios and lambdas.

Economic Feasibility

Aspen Simulation

To determine the cost drivers and thus the financial risk and viability of the alternative fuel in the markets an Aspen Plus simulation was conducted to see how competitive the alternative fuels price would compare to conventional fuels. Only one solvent was simulated for brevity purposes since they are both similar in price and affected by the same fundamental factors.

The simulation setup and technical results will be explained here but the economic results will be explained in economic results section. All the parameters were first optimized to get the required specifications and then further optimized to decrease operational duty requirements via built in the energy analysis function; some of the changes were the decrease in column length, larger pressure drop over the heat exchanger and optimizing the reflux and boil up ratios of the distillation column. The simulation method was based on Non-Random Two Liquid Redlich – Kwong (NRTL-RK) as recommended by the inbuilt methods assistant. Figure 41 shows the simulation flowchart with operating conditions, it consists of a mixer, a heat exchanger to make use of the excess duty from the wastewater streams and a distillation column to remove water from the final fuel stream. The simulation was conducted on the basis that the fuel reactants will all transported as one homogenous mixture. The mole purities and design specifications were determined by using the Vary Function. The distillation column was set up for calculating under equilibrium conditions with 70 stages. The boil-up ratio was computed to be 10 and the reflux rate was 500 kmol/hr both on a mole basis. The distillation column had a pressure drop of 2 bar with the condenser operating at 1 bar, the feed was introduced into the column at stage 36. The distillation columns' temperature, and pressure profiles alongside their distillation species profile are presented in Figures 42 and 43, respectively.

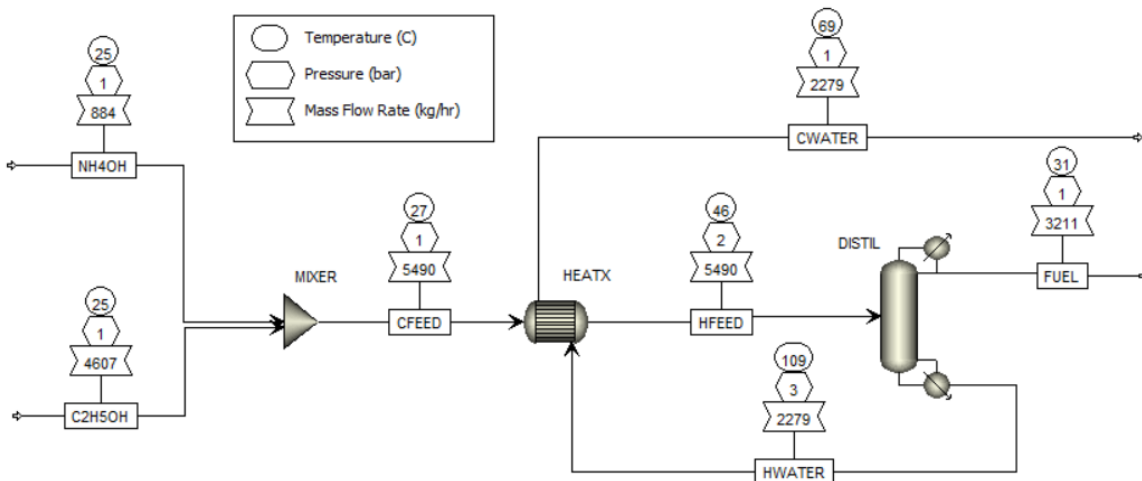


Figure 41 Simulation Flowsheet

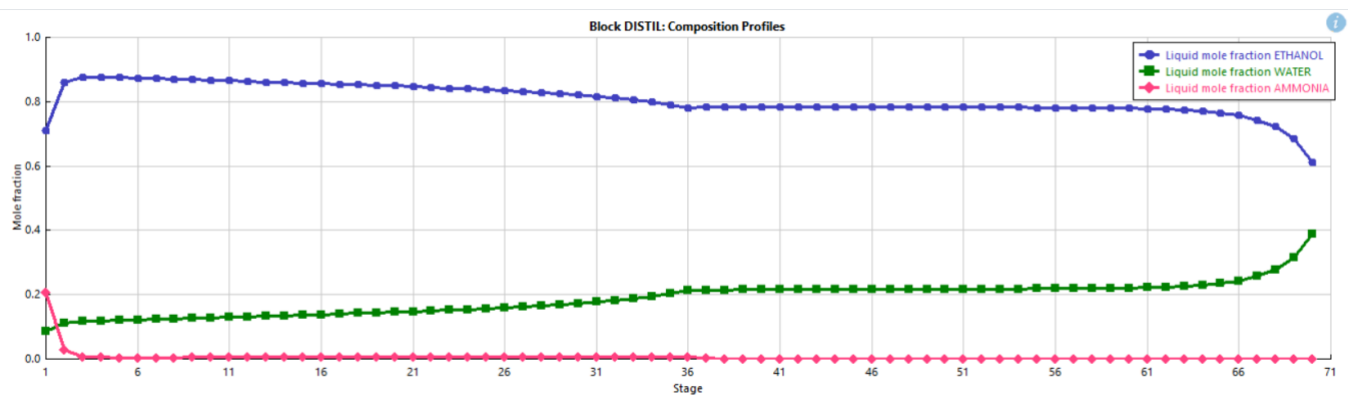


Figure 42 Distillation species profile

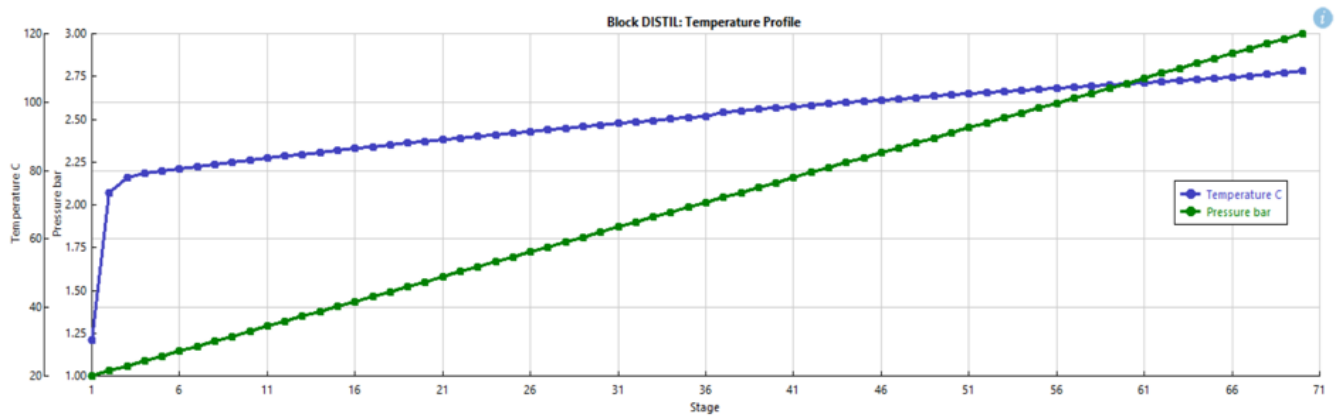


Figure 43 Distillation temperature, and pressure profiles

Time Series Forecasting

To further understand the viability of the fuel an Autoregressive Integrated Moving Average (ARIMA) model was used on sets of univariate time series with data taken from a Bloomberg terminal to look at the future viability from a financial perspective. The time series dataset was the Goldman Sachs Chicago Ethanol Index which was taken as weekly data points. The ARIMA model assumes the future value of an asset can be predicted by analysing past trends [66]. The ARIMA model analyses historical data and breakdowns it down into four aspects (Figure 44 & 46). The first aspect is the general trend over time e.g., increase in stock prices as companies grow and revenue. Next is seasonality; repetitive behaviours in the asset within the same period, e.g., ice cream sales increasing over the summer period. Closely related to seasonality is the cyclic behaviour, repetitive trends over unspecified time intervals, e.g., economic decline and recovery following financial crisis. Finally, noise is analysed, unpredictable and stochastic movements in the asset, e.g., such as stock price fluctuations every minute.

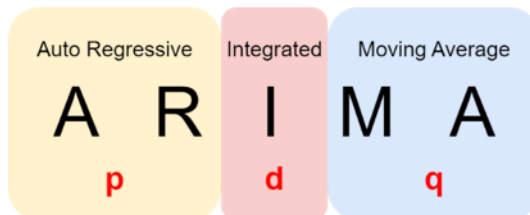


Figure 44 ARIMA model breakdown and terms

The ARIMA model works uses equation 3 and consists of two main terms, the Autoregressive term (AR) and Moving Average (MA) term with their respective coefficients as shown by Figure 44. The model was implemented with Python using readily available codes and statistical packages [67] [68] [69] [70] [71] [72]; the full code is available in appendix section C. The first aspect is stationarity, i.e., whether the data fluctuates around a constant mean value with constant variance over time [72]. The model only works if the data is stationary and thus was first analysed and manipulated to make it stationary, i.e., not exhibit a trend via first or second-order differencing. Next, the p, d and q terms which are illustrated in Figure 45 are estimated using correlation plots and the Akaike information criterion (AIC) (equation 4). Various combinations of p, d and q terms can be estimated leading to several different models. The AIC test can be used to select the best model which tests for how well the model fits the dataset and penalises models which are overly complicated, i.e., models which have large numbers of parameters [73].

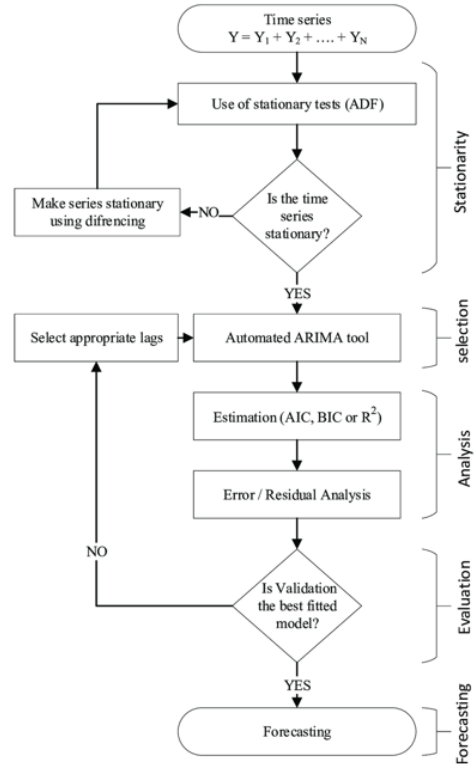


Figure 45 ARIMA model flowchart [74]

$$\text{Predicted Value} = \mu + \varphi_1 y_{t-1} + \cdots + \varphi_p y_{t-p} - \theta_1 e_{t-1} - \cdots - \theta_q e_{t-q} \quad \text{Equation (3) [75]}$$

where: $e = \text{error term}$, $c = \text{constant term}$, $y_t = \text{time series data}$,

$\varphi = \text{Autoregressive coefficient}$, $\theta_1 = \text{Moving Average coefficient}$

$$AIC = -2 \log(L) + 2(k) \quad \text{Equation (4) [73]}$$

where: $L = \text{likelihood}$, $k = \text{number of parameters}$

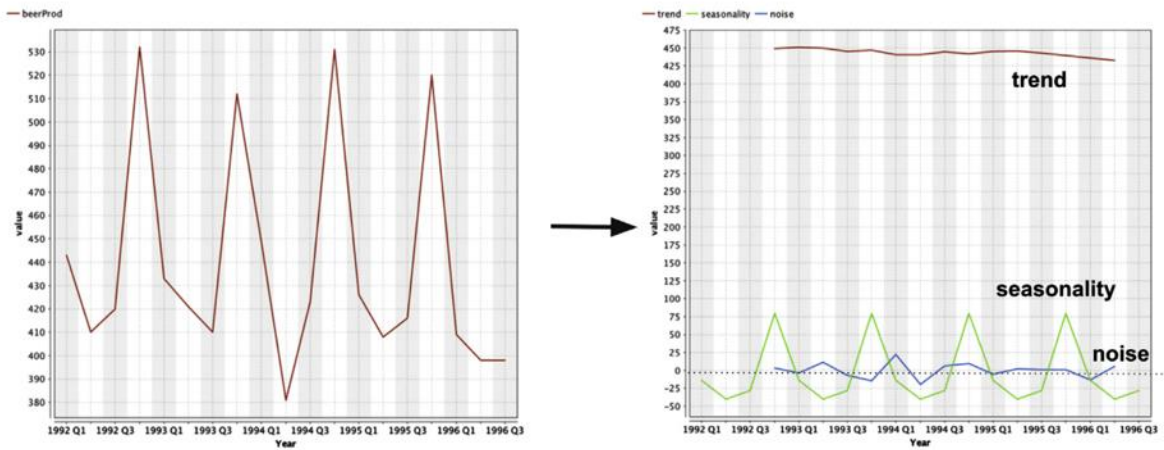


Figure 46 Time Series Decomposition, Historical data (Left), Time series characteristics (Right) [76]

Monte Carlo Simulations

A statistical methodology was employed to predict the forthcoming demand for fuel. Specifically, the main component of the fuel was simulated and analysed, as it is expected to exert the most significant influence on the overall fuel demand, thereby providing an estimation of future demand. The volatility of ethanol prices was assessed by calculating monthly price fluctuations. It was assumed that the volatilities of these prices would remain similar in the future, and a consistent upward trend was also assumed based on historical data, which indicates a general increase over time. To facilitate price forecasting, the most recent price from the dataset was acquired. Subsequently, a randomly selected monthly price change was factored in, and based on this, a random price path was calculated. The process is repeated numerous times, resulting in the generation of a considerable quantity of simulated future prices. To ensure the robustness of the simulation, it is very important to compute the number of iterations required for the cumulative mean price of the assets to converge and stabilise; this considers the law of large numbers.

Several assumptions were made to conduct the simulations. Initially, the assumption of constant variance and drift in the analysis was taken. This assumption implies that the size and direction of the asset's movement remain constant. The variance and drift were calculated based on the time series data's periodic daily returns, which were assumed to remain consistent in the future. One crucial assumption underlying this analysis is that the observed rise in the index price of assets primarily resulted from an increase in demand. This assumption is based on the historical stability of ethanol supply over the past few decades, as shown by the significantly low R squared value of 0.0068 depicted in Figure 47. There has been a noticeable trend observed in the year 2020, in which the supply of ethanol experienced a substantial decline. This downward trajectory in supply continued into 2021 and 2022. Notably, during this period, the ethanol price index exhibited a substantial increase, suggesting a potential correlation between the ethanol index price and demand. There is a strong likelihood that the index price is influenced by a range of additional factors, including weather patterns, supply chain constraints, investor sentiment, and market news. Nevertheless, regardless of these potential factors, the assumption facilitated the estimation of forthcoming demand, thereby carrying substantial importance for stakeholders and potential investors in making well-informed decisions. To enhance the robustness of the Monte Carlo Simulation, it is recommended in future to apply regression analysis to identify the exogenous variables that influence the index price.

The below equations [77] were utilized alongside Excel for the simulations:

$$\text{Periodic Daily Returns} = \ln\left(\frac{\text{Current Day's Price}}{\text{Previous Day's Price}}\right)$$

$$\text{Drift} = \text{Average Daily Return} - \frac{\text{Variance}}{2}$$

σ = Standard Deviation of periodic daily returns

$$\text{Random Value} = \sigma \times \text{NORM.S.INV(RAND)}$$

where NORM.S.INV = inverse normal cumulative distribution

$\text{RAND}()$ = random number which selects between range of periodic daily returns

$$\text{Forecasted Price} = \text{Current Price} \times e^{\text{Drift} + \text{Random Value}}$$

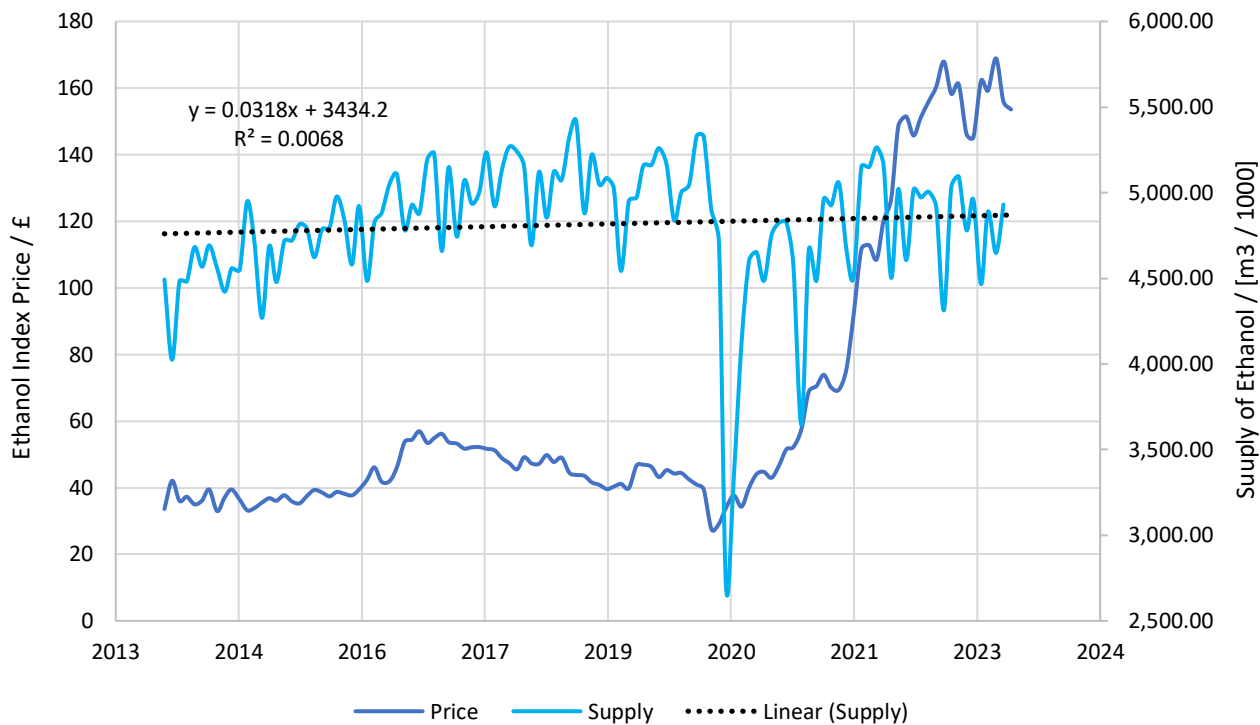


Figure 47 Supply of Ethanol in the United States and Goldman Sachs Chicago Ethanol Price Index [78] [79]

Experimental Results and Discussion

Calorimetry

Table 4 Calorimetry Results

| Ethanol J/g | Ethanol + NH ₃ / J/g | Methanol J/g | Methanol + NH ₃ J/g |
|-------------|---------------------------------|--------------|--------------------------------|
| 25,838 | 27,528 | 15,504 | 16,868 |
| 24,373 | 24,929 | 17,508 | 19,344 |
| 23,380 | 24,060 | 16,459 | 18,891 |
| 24,228 | 24,422 | 18,232 | 18,303 |
| 24,218 | 25,207 | 17,759 | 17,589 |
| 24,865 | 24,384 | 16,261 | 18,653 |

The difference in gross calorific value in the solvent/ammonia sample was assumed to be strictly due to the ammonia content. The results for the pure samples are lower than expected even after calibration and thus the values should not be looked at in absolute terms. The results also are not concordant, and outliers were removed to ensure a representative mean was taken. Nonetheless, the methodology only requires the difference between the samples to determine the ammonia content. The calorimetry data was analysed using the following methodology as shown below.

The results show an ammonia content of 2.7 wt% for the ethanol and 5.5 wt% for the methanol. The increase in ammonia content compared to ethanol is as expected, due to methanol's smaller carbon chain length which results in and thus increased ability to create hydrogen bonds with ammonia.

$$HHV_{mixture} = x_{NH_3}(HHV_{mixture}) + (1 - x_{NH_3})HHV_{solvent}$$

$$HHV_{mixture} - HHV_{solvent} = HHV_{Excess}$$

$$25,088 - 24,484 = \frac{605\text{ J}}{\text{g}}$$

$$\text{Ammonia Content \%} = \frac{HHV_{Excess}}{HHV_{ammonia}} * 100$$

$$\frac{\frac{605\text{ J}}{\text{g}}}{\frac{22,500\text{ J}}{\text{g}}} * 100 = 2.7\% \text{ NH}_3 \text{ Content}$$

Acid-Base Titrations

A sample calculation is provided below, accompanied by the average titres and the results, as indicated in Table 5. The findings indicate that the ethanol and methanol fuel mixture contain 3.4 wt% NH₃ and 6.3 wt% methanol respectively.

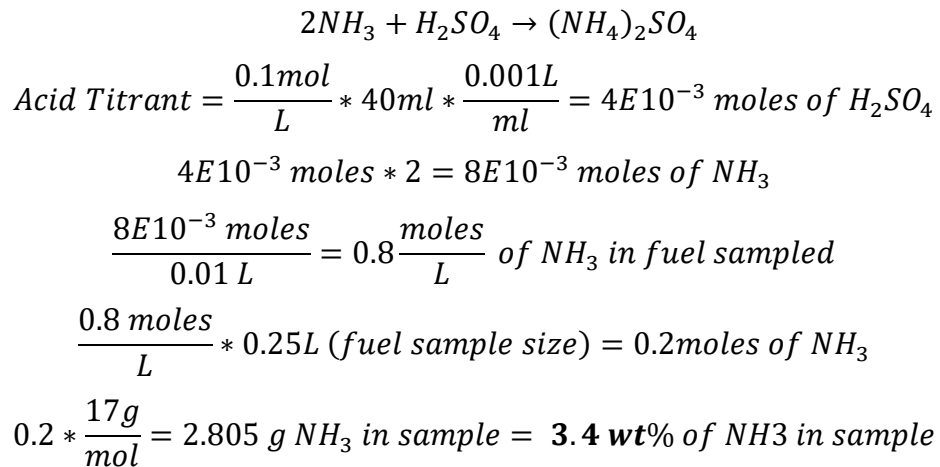


Table 5 Average Titres and corresponding ammonia content

| Sample | Average Titre/ ml | NH3 wt% |
|----------|-------------------|---------|
| Ethanol | 41 | 3.4 |
| Methanol | 62 | 6.3 |

The calorimetry and titration results do seem to be in good agreement with each other. The slight discrepancy between both sets of results could be down to measurement error but also to the fact that in the titrations the solvents are acting as weak bases and the addition of the pH indicator which is acidic may be leading to overestimation in the results. Nonetheless, we can be confident that roughly 3 wt% of ammonia is present in the ethanol sample and 6 wt% in the methanol sample. In the future perhaps a more robust way to carry out the titrations could be to fully neutralise the ammonia in the sample by adding an excess amount of acid and then conducting either a back titration which can identify the product of the stoichiometric equation 2 or by extracting and drying the ammonium sulphate salt and consequently conducting gravimetric analysis.

Although ammonia was identified in both samples, these are not the weight percent's (wt%) expected. Figure 48 depicts the theoretical solubility limits of ammonia in methanol and ethanol of which at ambient conditions should be 8 wt% NH₃ for ethanol and 13 wt% NH₃ for methanol. This shows the difficulty in keeping the ammonia retained in the solvents even after ensuring an excess amount of ammonia gas was injected relative to the solvent amount.

Ammonia has a distinct low solubility in ethanol, future studies could investigate increasing the solubility limit by mixing additives into the fuel blends. A computational study [80] used low-cost

alkali salt additives on 10 mol% aqueous water solutions, the results via Gibb's ensemble Monte Carlo simulations showed improvements in solubility. Figure 49 shows a clear increase in the concentration of ammonia content as the alkali metal salts are added across the temperature range. This phenomenon is further exemplified experimentally by the slower rate of ammonia vaporization when subjected to 50 °C with the addition of alkali salts compared to standard aqueous ammonia solutions, which shows a slower rate of evaporation (Figure 49). The researchers state an increase in Gibbs free energy upon the addition of the alkali salts; the solution is more thermodynamically stable; so, it would be beneficial to extend this research to ammonia alcohol systems. Cooling ammonia down can very easily be implemented by using existing infrastructure in the form of vapour recovery units present in most fuelling stations, future works could investigate the feasibility of replicating vapour recovery units inside vehicles to keep the fuel as a homogenous blend.

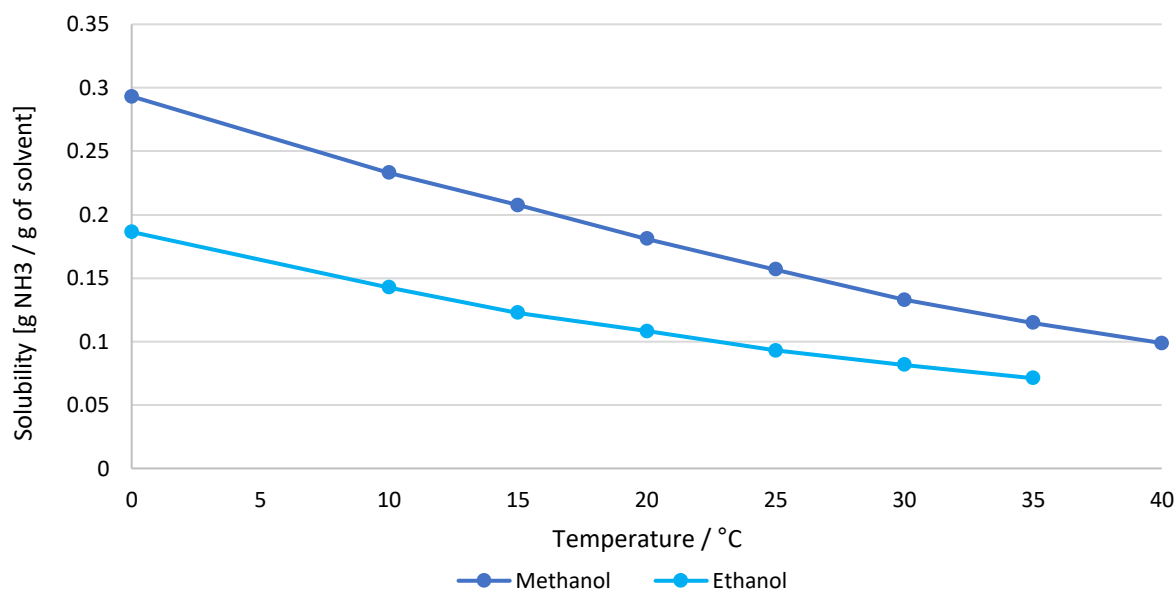


Figure 48 Theoretical ammonia solubility in solvents [81]

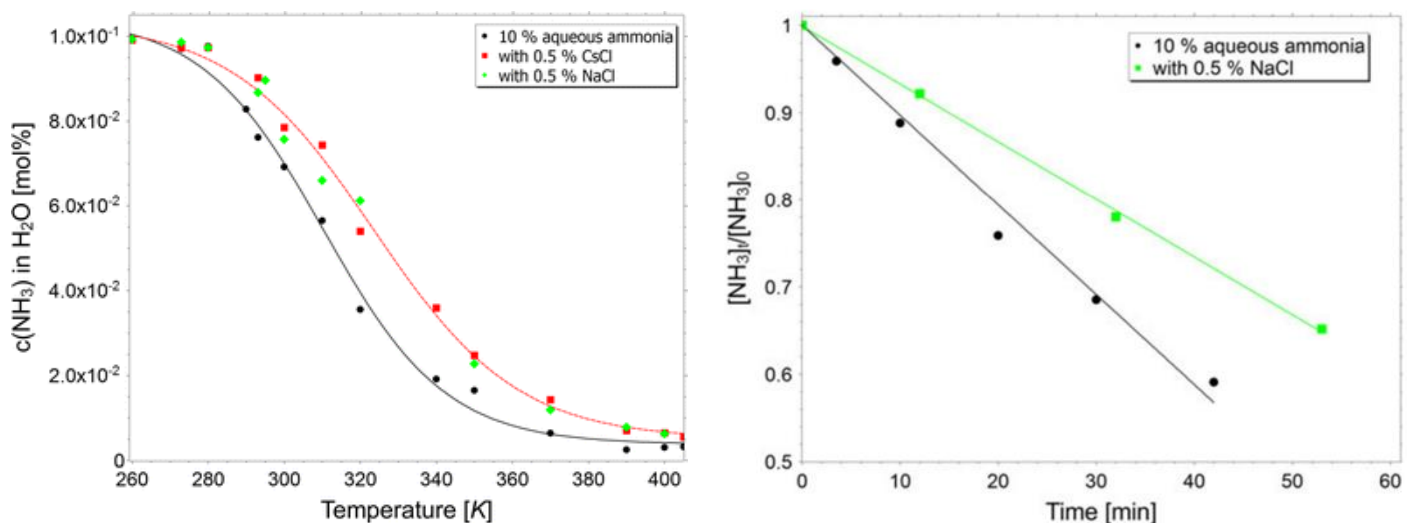


Figure 49 Simulated concentration of ammonia - effect of alkali addition (Left), experimental measurements of ammonia concentration from aqueous ammonia evaporation at 50 °C and 101 kPa (Right) [82]

Gas Chromatography Mass Spectroscopy Results and Discussion

An attempt was made with GCMS analysis, however due to technical constraints accurate results couldn't be obtained. As seen in Figure 50, the chromatogram isn't producing sharp peaks but is identifying the sample species in this case, ethanol which can be seen by the NIST search for compounds (Figure 51). An air-water check of the GCMS showed high levels of moisture, which changes the boiling point of the analytes and solvents and thus the retention time of the compounds inside the column. The high moisture content can be attributed to a low carrier gas level in the helium tank (the carrier gas) which tends to accumulate with water as the tank reaches low levels and the absence of a gas moisture filter. A solvent delay of 12 minutes with a heat ramp of 70 °C allowed for the detection of ethanol, and so future analysis and temperature program fine-tuning should start from these parameters. Nonetheless, titrations and calorimetric data was deemed sufficient to analyze the ammonia content.

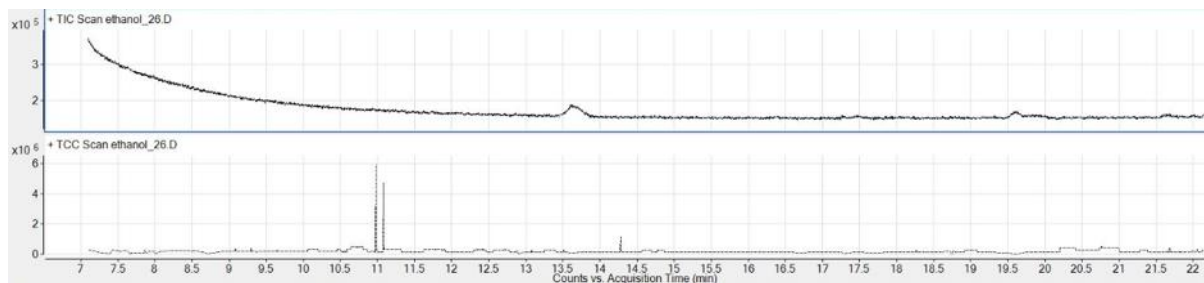


Figure 50 Initial Chromatogram for pure sample

| # | Lib. | Match | R.Match | Name |
|----|------|-------|---------|--|
| 1 | M | 907 | 955 | Ethanol |
| 2 | M | 748 | 753 | Acetic acid, ethoxyhydroxy-, ethyl ester |
| 3 | R | 737 | 742 | Diethyl carbonate |
| 4 | R | 731 | 742 | Ethanol, 2-nitro- |
| 5 | R | 729 | 738 | Ethyl formate |
| 6 | M | 726 | 802 | (1-Hydroxyethylidene)malonic acid diethyl e... |
| 7 | M | 714 | 723 | Hydrazine, methyl- |
| 8 | R | 711 | 720 | Acetic acid, hydroxy-, ethyl ester |
| 9 | R | 701 | 715 | 2-Butanol |
| 10 | R | 682 | 756 | Ethanol, 2-methoxy- |
| 11 | R | 675 | 685 | Ethyl ether |
| 12 | M | 666 | 674 | (S)-(+)-1,2-Propanediol |
| 13 | R | 655 | 664 | Propylene Glycol |
| 14 | M | 653 | 662 | Ethane, methoxy- |
| 15 | M | 646 | 653 | Carbonic acid, ethyl-, methyl ester |
| 16 | M | 643 | 648 | Ethanol, 2-bromo- |
| 17 | M | 642 | 650 | L-Lactic acid |
| 18 | R | 641 | 650 | Hydrazinecarboxylic acid, ethyl ester |
| 19 | R | 640 | 685 | Acetic acid, methoxy- |
| 20 | R | 637 | 644 | 2-Propanol, 1-chloro- |
| 21 | M | 636 | 646 | Ethanol, 2-(vinyloxy)- |
| 22 | M | 631 | 638 | (3-Methyl-oxiran-2-yl)-methanol |
| 23 | R | 630 | 664 | Ethane, 1-bromo-2-methoxy- |

Figure 51 NIST library search

Engine Testing

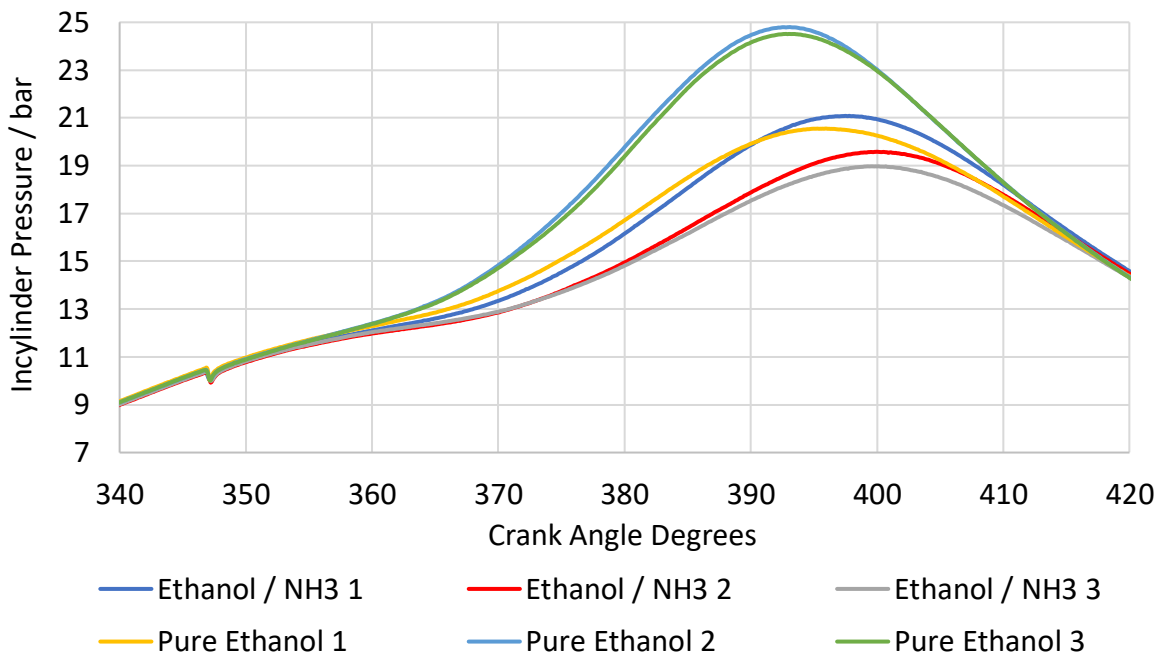


Figure 52 In-cylinder pressure of ethanol pure and blend samples

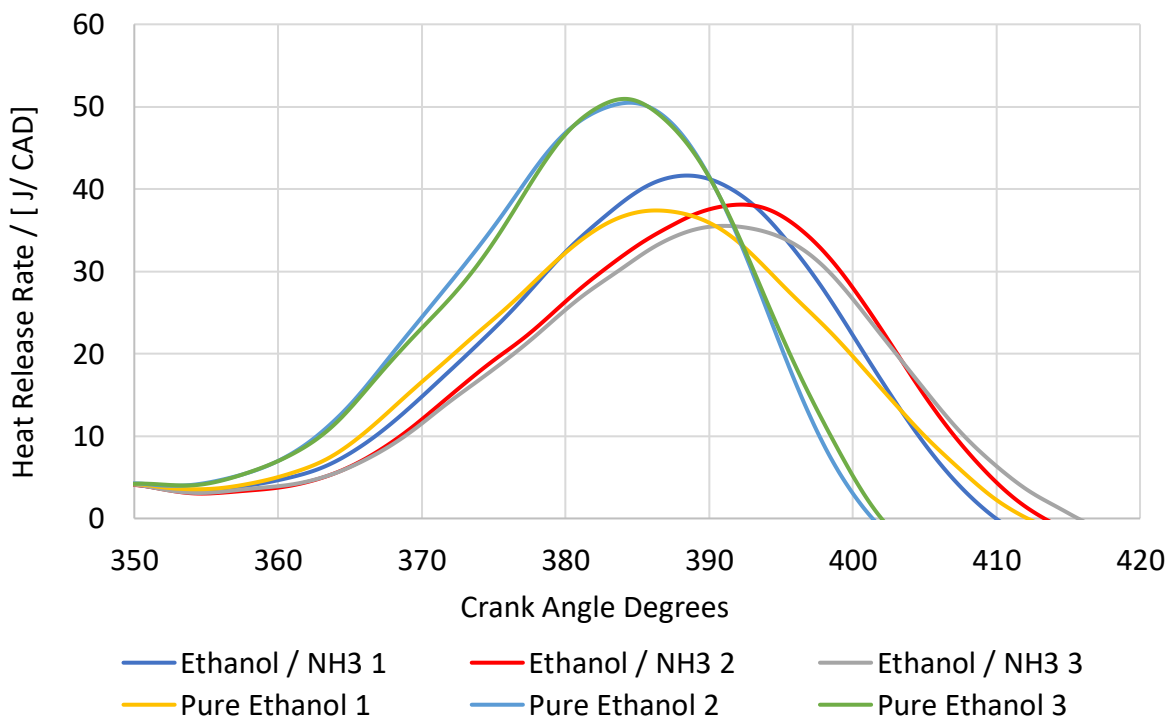


Figure 53 Filtered Heat Release Rates of ethanol pure and blend samples

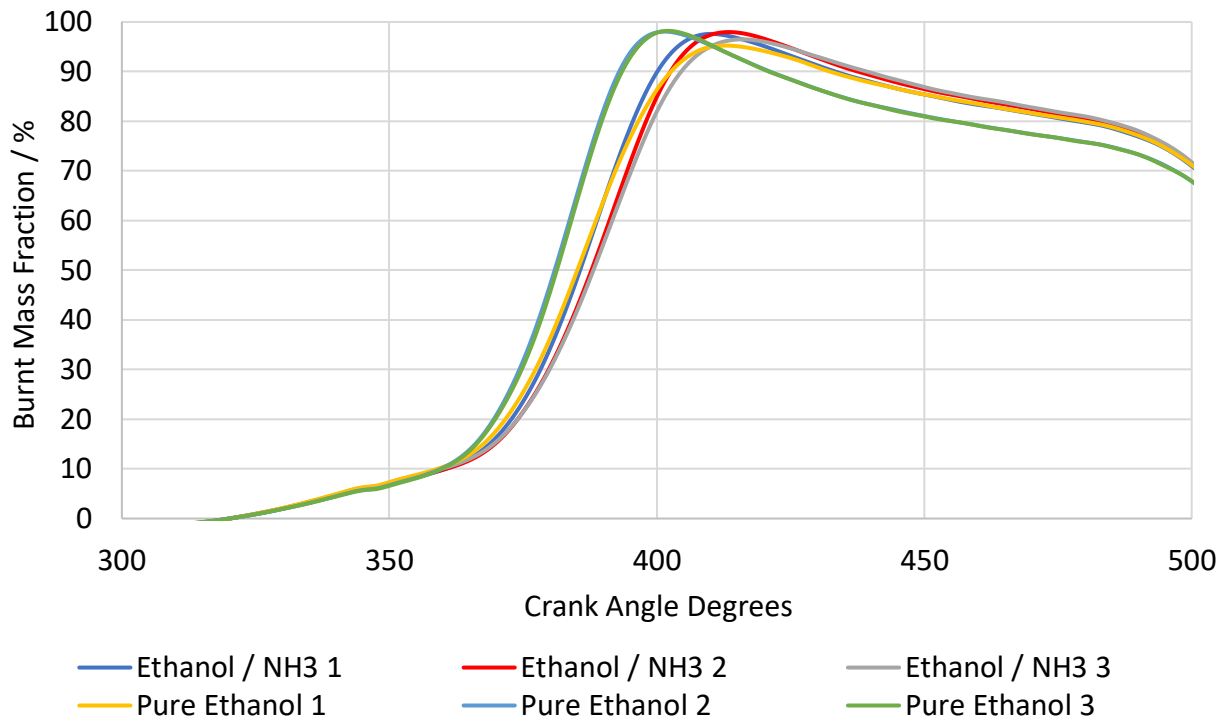


Figure 54 Mass Fraction Burnt of one sample.

There is a clear decrease in the in-cylinder pressure of the ammonia blended sample compared to pure ethanol as more samples are taken (Figures 52-54). This is as expected since the ammonia has a lower density relative to ethanol which means in the ammonia blended sample, a portion of the ethanol has been displaced by a relatively large amount of ammonia which has a lower calorific value, thus resulting in a lower mixture calorific value relative to pure ethanol. The adiabatic flame temperature of ammonia tends to be around 1800 °C [83] and ethanol's around 1965 °C [84], which again goes with expectations since ethanol has been displaced with a component with a lower adiabatic flame temperature component, which should directly relate to lower in-cylinder pressure.

The ammonia blend results in a slightly lower burnt mass fraction (BMF) and the whole combustion process finishes at later crank angle degrees relative to pure ethanol, which leads to decreased power output. The combustion process seems to be more complete for pure ethanol since the maximum peak BMF for the best pure ethanol sample is 98% whilst for the ammonia blended sample it is 97%, which means there is slightly improved combustion efficiency, but this is dependent on the timed run. Table 6 shows the BMF ranges which further extenuates the combustion behaviour between the blends for the last timed run of each type of blend. The lower BMF 90 – 10 confirms the whole combustion process is quicker in the pure ethanol sample. BMF 10 – Spark Ignition shows the flame kernel development time is the same in both pure and blended samples and is not quite affected by the introduction of ammonia which is beneficial. BMF 50 – 10 indicates a faster self-sustained flame propagation phase for the pure sample.

When comparing the BMF values to experimental data available in the literature [46] (Table 6) for similar intake pressures and ammonia contents, the BMFs for all ranges are lower for both pure and blended samples. This difference can be attributed to the type of fuel injection used in the literature study; direct injection at 120 bars which would result increased atomization and mixing with air of the fuel, leading to improved combustion.

Table 6 Burnt Mass Fraction Trends [46]

| Burnt Mass Fraction | Pure Ethanol / CAD | Ethanol + NH ₃ / CAD | Pure Ethanol Literature / CAD | Ethanol + NH ₃ Literature / CAD |
|---------------------|--------------------|---------------------------------|-------------------------------|--|
| BMF 90 - 10 | 33 | 44.7 | 14.7 | 23.7 |
| BMF 10 - SI | 13 | 13 | 13.8 | 23 |
| BMF 50 - 10 | 21 | 28 | 7 | 9.6 |

The heat release rate for the ammonia blend is slower and outputs a smaller heat release rate per crank angle degree. Literature [40] [42] suggests the LBV of the mixture should be slower with the addition of ammonia, which is confirmed by the significant reduction in the heat release rate after spark ignition in the blended samples. The later stage of the combustion process could be dominated by a turbulent flame front since the flame front is travelling through variations in fuel composition.

Literature studies [85] have investigated flame structures of methane with air and methane with ammonia and air, their findings could be extended to ammonia/alcohol systems. There is a clear change in the flame front structure between both mixtures as seen in Figure 55; the presence of turbulence induces the formation of wrinkles and expansion in the flame front, resulting in an enhanced turbulent flame speed in comparison to the laminar counterpart [85] [20]. This difference can lead to an increase in the preheating zone thickness [85] which would mean the unburnt gas is more likely to combust leading to improvements in flame propagation and combustion stability, this improvement can be seen in Figure 55 as there is less unburnt gas (grey area). Further studies could investigate at what operating conditions turbulent flames occur and their improvements in the flame speed, which should advance and create a narrower heat release rate.

All the trends observed through the ethanol samples are also seen in the methanol samples, the results are available at the end of this section (Figure 60 & 61).

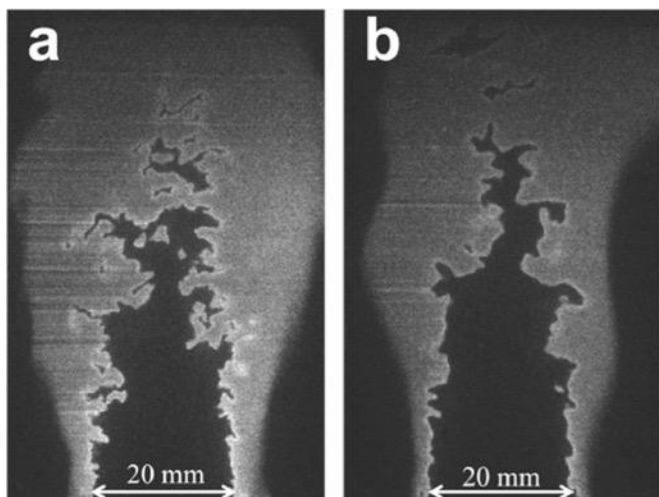


Figure 55 Planar Laser Induced Fluorescence images of turbulent flames at 0.5 MPa and mixture temperature of 298 K (a) methane - air flame; (b) methane-ammonia-air, same parameters, and conditions [85]

Table 7 Net Indicated Mean Effective Pressure and Combustion Stability for the last timed run of each sample

| Combustion Characteristic | Pure Ethanol | Ethanol + NH ₃ | Pure Methanol | Methanol + NH ₃ |
|---------------------------|--------------|---------------------------|---------------|----------------------------|
| Average NIMEP | 7.849 | 7.015 | 7.831 | 7.292 |
| Average GIMEP | 7.947 | 7.120 | 7.926 | 7.401 |
| COV NIMEP | 0.029 | 0.061 | 0.03 | 0.035 |
| COV GIMEP | 0.028 | 0.058 | 0.027 | 0.034 |

Table 7 presents the observed decrease in net indicated mean effective pressure (NIMEP) for both solvent blends relative to pure samples, along with enhanced combustion stability. Although the methanol blend exhibits a higher concentration of ammonia, there is no observed decrease in NIMEP relative to the ethanol blend, which means methanol has the advantage of increased power output and potentially decreased emissions reduction relative to ethanol blends.

The initial timed run of each sample demonstrated enhancements in power output and improved efficiency. However, as indicated in Figure 57, a subsequent decrease in NIMEP is observed with each additional timed run for the blended samples. The absence of this trend (as seen in Figure 56) in the pure solvent sample aligns with expectations since ethanol and methanol have high octane ratings and fast LBVs. The possibility of a decrease in engine power due to mechanical or sensor reading errors can be omitted since the reference samples combust as expected.

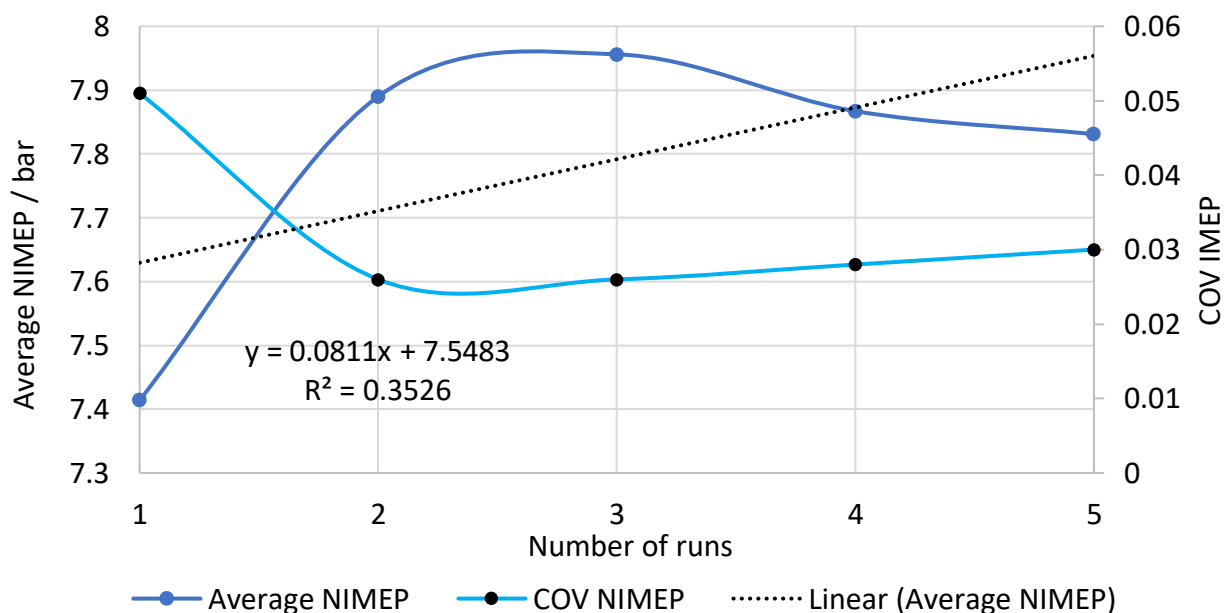


Figure 56 Pure Methanol NIMEP

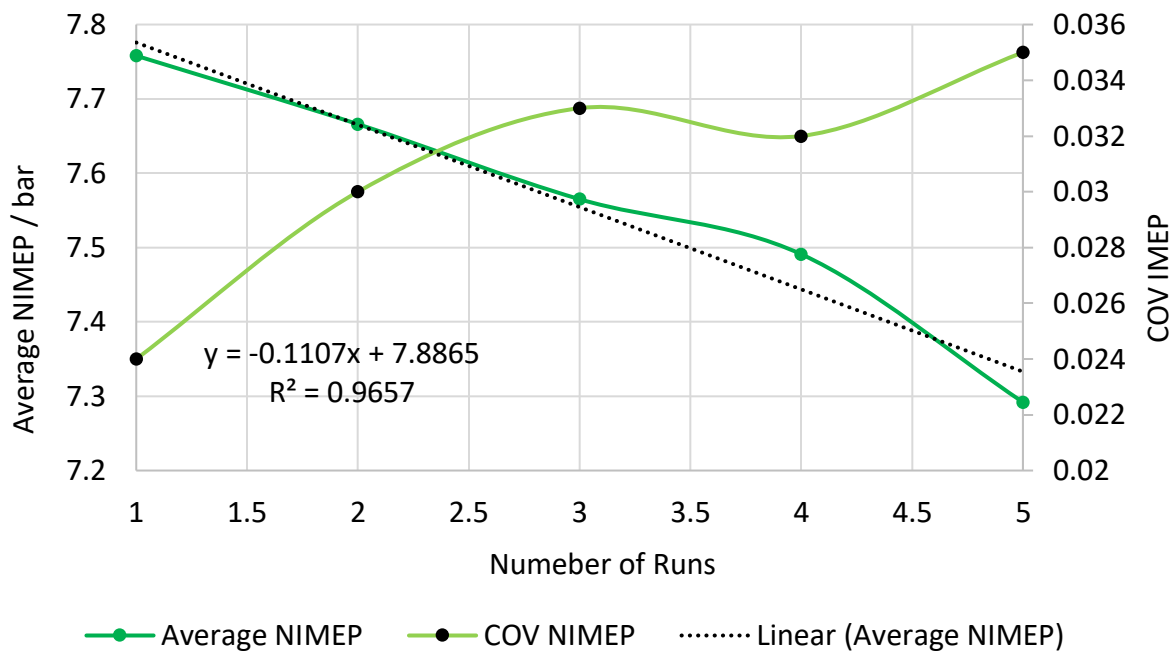


Figure 57 Methanol Blend NIMEP reduction

A decline in the level of combustion can be observed in which there is a consistent decrease as additional timed runs are carried out for the blended samples. The pattern of heat release is exhibiting a progressively delayed onset, resulting in reduced peak heat release rates, while the in-cylinder conditions are undergoing a significant decrease. There are two potential explanations for this phenomenon. Firstly, ammonia may be escaping before reaching the engine cylinder because of leaks or areas of high temperature in the fuel lines which can lead to the delayed introduction of ammonia. This scenario is not very feasible since the engine was allowed to cool down for two minutes between each run. Consequently, the temperatures of the engine components would either remain the same or decrease, indicating that the combustion process should not continue to decrease. However, it is recommended that future research should analyse temperatures such as coolant, oil, and actual fuel temperatures at various points along the fuel lines. Fuel stratification could be occurring, where the fuel blend undergoes separation based on differences in density, resulting in the mixture displaying a concentration gradient. This is illustrated in Figure 59 which shows the possible separation occurring and why the initial runs exhibit solvent-like characteristics and the later runs whilst engine testing are converging towards ammonia-like characteristics. Mixing the solution continuously may mitigate this issue, and further engine tests over extended time periods could be repeated to check if this phenomenon still occurs. Future research should conduct molecular dynamic simulations to understand the nature of bonding and the spatial distribution of the bonds within mixtures, this should be validated with spectroscopic techniques such as Planer Laser-Induced Fluorescence which can show concentration gradients.

Engine testing should be conducted at various equivalence ratios to see how the fuel blends would perform at differing loads which are needed in real-life conditions. Figure 58 shows how drastically the LBV of the ammonia changes across the equivalence range. HCCI operation would be the best-case scenario due to the possibility of ultra-low emissions but the ammonia's very low LBV in lean conditions means there is a possibility of incomplete combustion and knocking which could lead to increases in thermal NOx, spark time advancing could help mitigate this issue. Literature [46] has shown alcohol-ammonia fuel blends exhibit large changes in LBVs as the intake pressure is increased so it would be beneficial to investigate the flame propagation speeds induced by higher pressures which should lead to a higher collision frequency and whether in-cylinder fluid motions such as swirl and tumbling positively affect the ammonia-ethanol samples differently to pure samples due to the presence of varying composition as the flame front progresses.

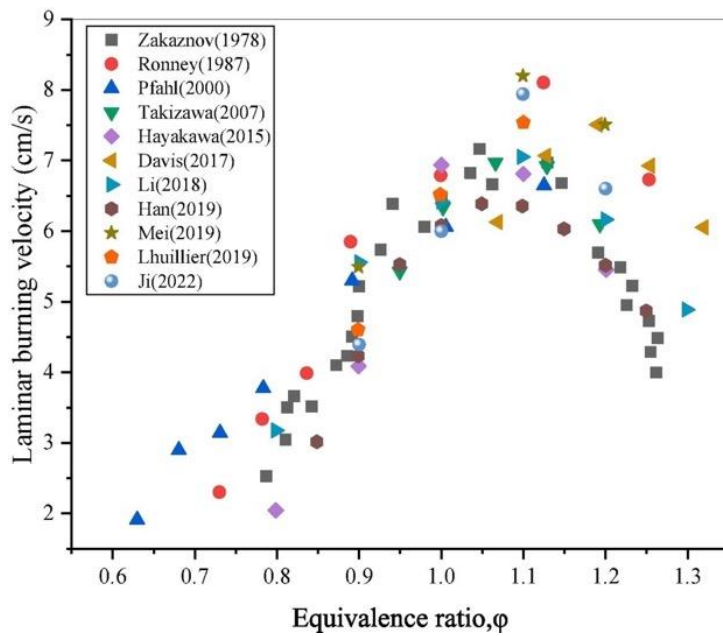


Figure 58 Laminar burning velocity at varying equivalence ratios [86]

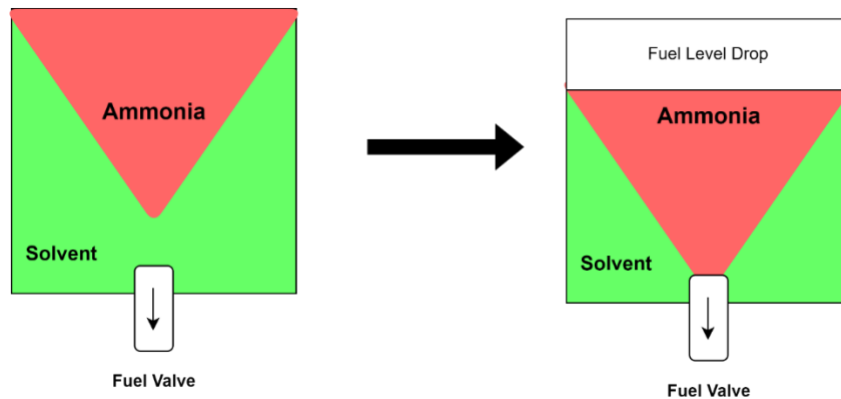


Figure 59 Proposed fuel stratification mechanism

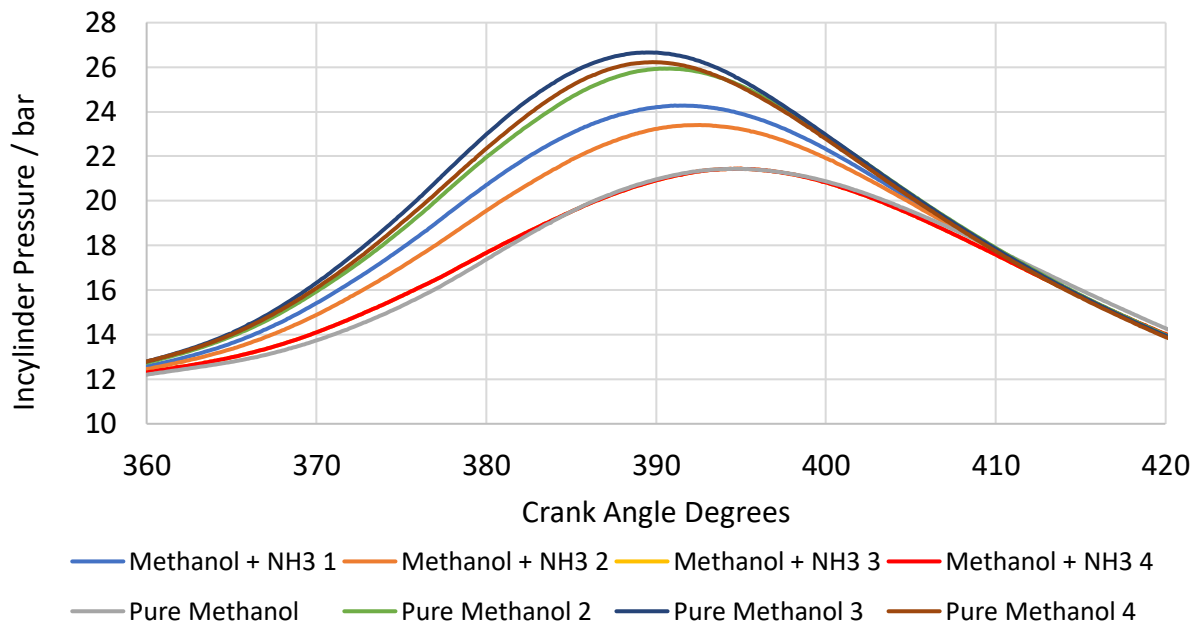


Figure 60 Methanol samples in cylinder pressures

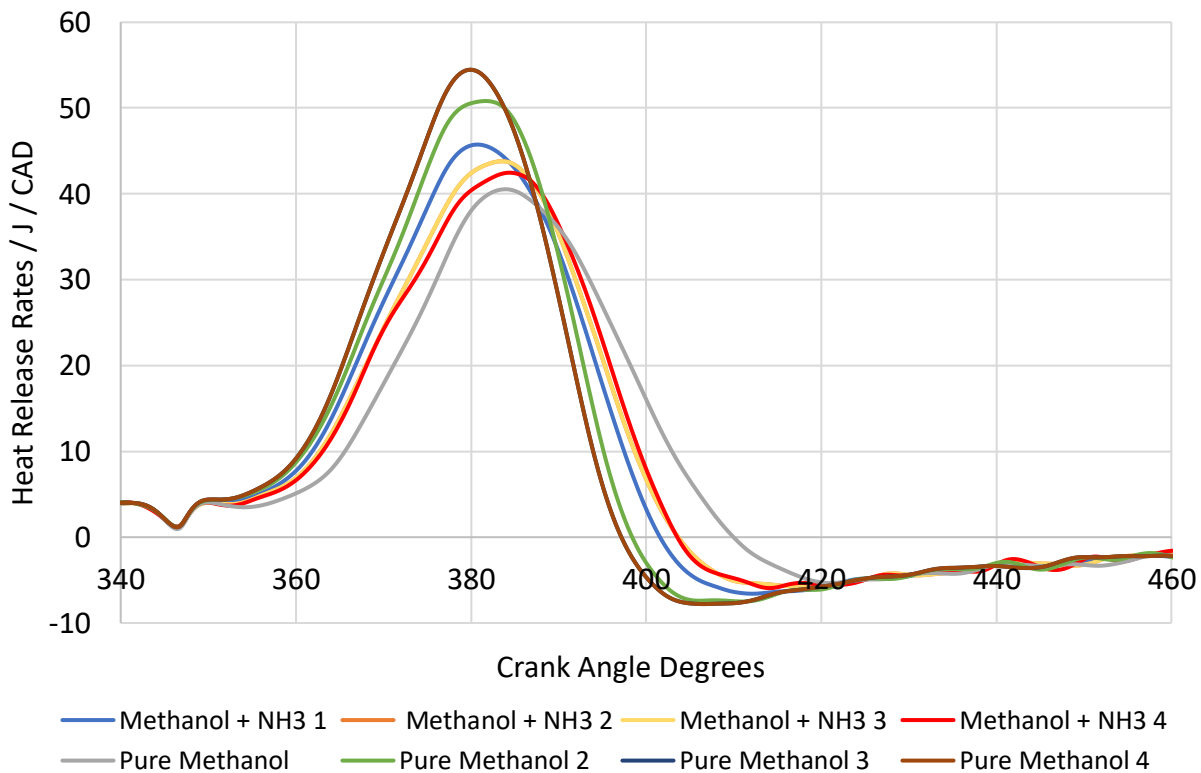


Figure 61 Methanol samples heat release rates

A visual difference between the samples was observed over one month. Figure 62 depicts the ethanol sample and figure 63 the methanol samples. A more drastic change is observed in the methanol samples which means there could be long-term storage issues if methanol is used as the solvent. It is hypothesised the colour change is due to thermal oxidation but accelerated ageing tests in conjunction with analytic methods such as GCMS could be utilized in future to understand which factors lead to degradation. To take this a step further for more robust findings, chemical markers in the form of isotopes or tracer molecules could be used to find which bonds are likely to break and thus deduce the degradation mechanism.



Figure 62 Ethanol / Ammonia Samples - Left - 1 month, Right - 1 day



Figure 63 Methanol / Ammonia Samples - Left - 1 month, Right - 1 day

Economic Analysis Results and Discussion

Aspen Simulation

Figure 64 shows the cost drivers to produce the alternative fuel, which was taken from the Aspen Economic Analyzer, the costs were converted from total yearly costs to costs per litre (Table 8) for ease of comparison. It is assumed the same infrastructure and transport techniques which are used for fossil fuels will be utilized for the ammonia blend and thus capital costs nor any costs of modification are considered. An important note is that the simulated price only considers the manufacturing phase, i.e., up to a maximum of 39.5% as seen by Figure 65, this means significant efforts in the form of implementing subsidies, carbon taxes, policy changes and improvements in process efficient need to be implemented to make the fuel cost effective.

Table 8 Simulated Price in comparison to conventional fuels spot price [87]

| Fuel | £ / L |
|---------------------------|-------|
| Ethanol / NH ₃ | 5.79 |
| Petrol | 1.55 |
| Diesel | 1.58 |

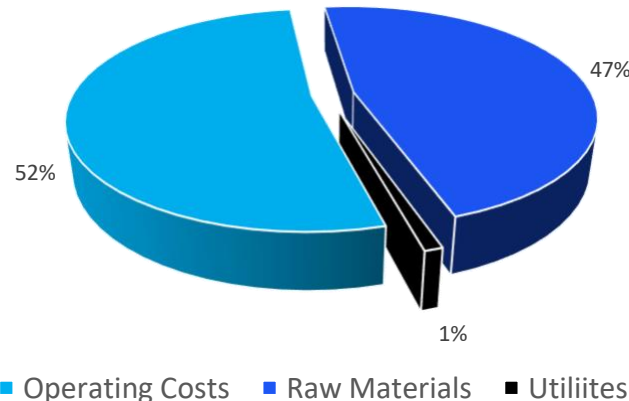


Figure 64 Fuel manufacturing costs £/L – Aspen Plus Simulation

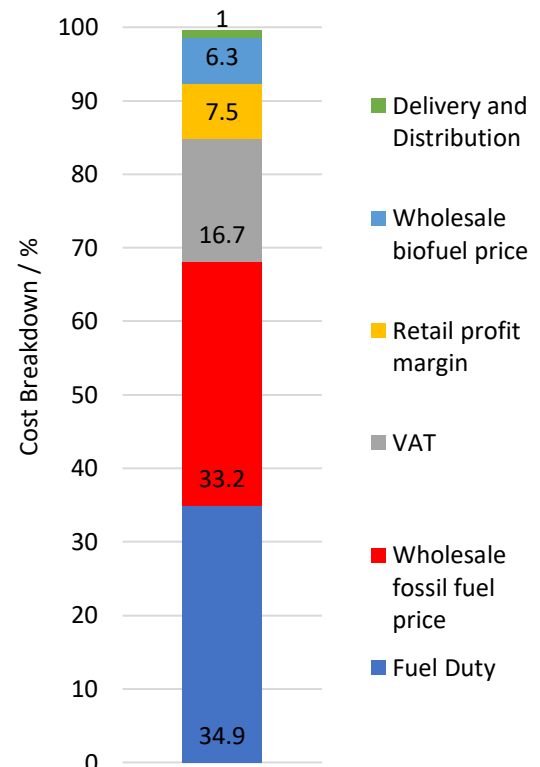


Figure 65 Cost Breakdown of petrol [88]

Operational costs are the main cost driver, with raw materials being a close second. Operational costs are relatively fixed and predictable, on the contrary, raw material costs can be highly volatile which can drastically impact consumers and businesses and it was decided to predict the demand of only the main raw material of the fuel, ethanol.

ARIMA model forecast

The Augmented Dickey-Fuller (ADF) test was conducted to determine the degree of stationarity in the time series data. The ADF test initially outputted a P value of 0.96 and an ADF value of 0.126 indicating strong non-stationarity and thus differencing was conducted to create a non-stationary data set. Figure 66 shows the results of first and second-order differencing. First-order differencing was deemed to be sufficient since Chart B in Figure 66 doesn't have any distinct trends and avoids any issues with over-differencing the data set [89], thus making the 'd' coefficient equal to 1. Since only the first lagged term is above the confidence interval (shaded blue area) and the rest of the lagged data points are within the shaded area; [90] as seen in image E in Figure 66, the 'p' factor to be chosen as 1.

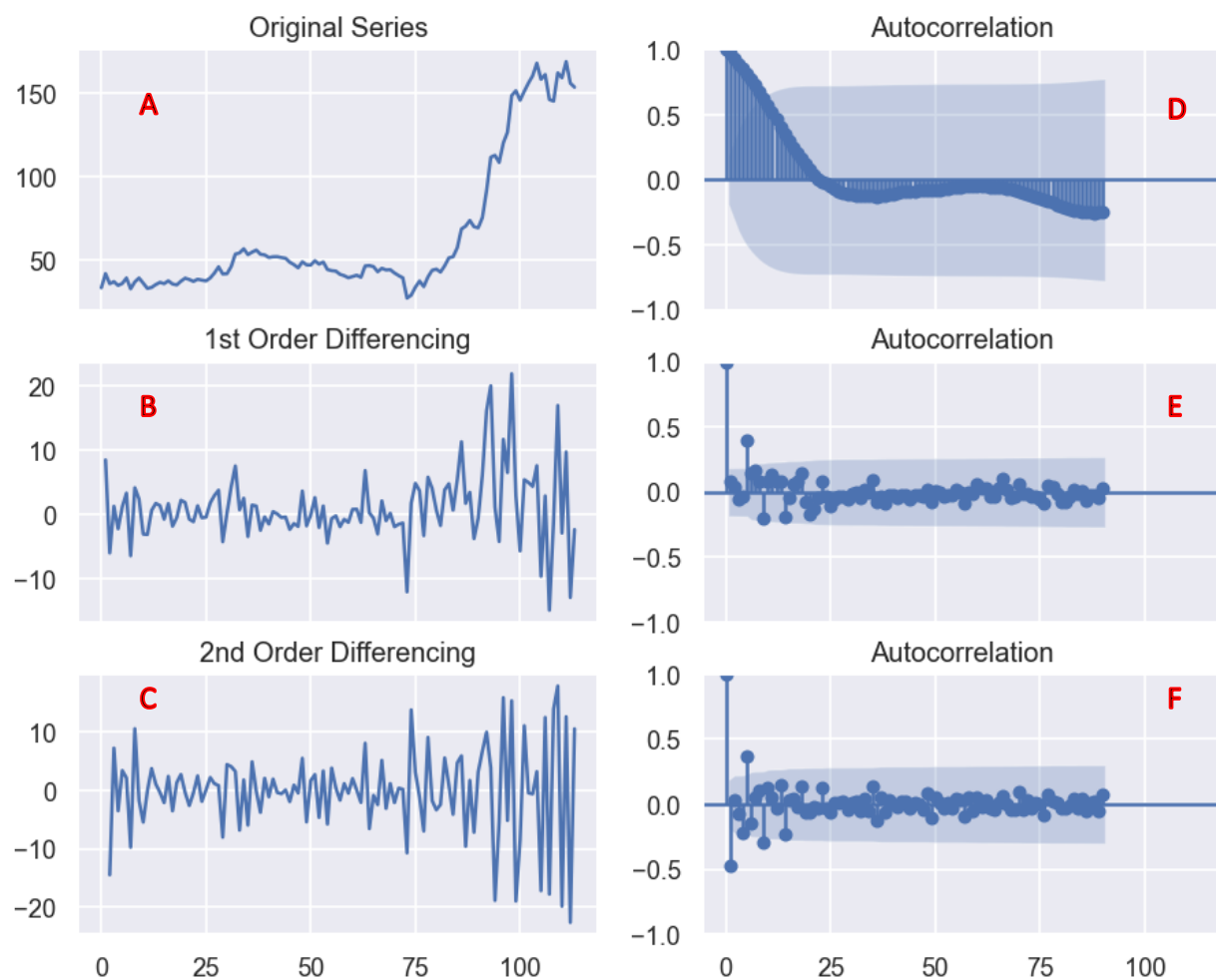


Figure 66 Ethanol differencing results

The order of the Auto Regressive term was selected based on the results from the Partial Auto Correlation Function graphs. The first two lags in the Partial Autocorrelation Function (PACF) plot (Figure 67) are above the confidence interval (blue shaded area) and thus the 'p' term was chosen

as 2. The d, p and q terms were further refined through trial and error and the combination which gave the lowest AIC value was chosen.

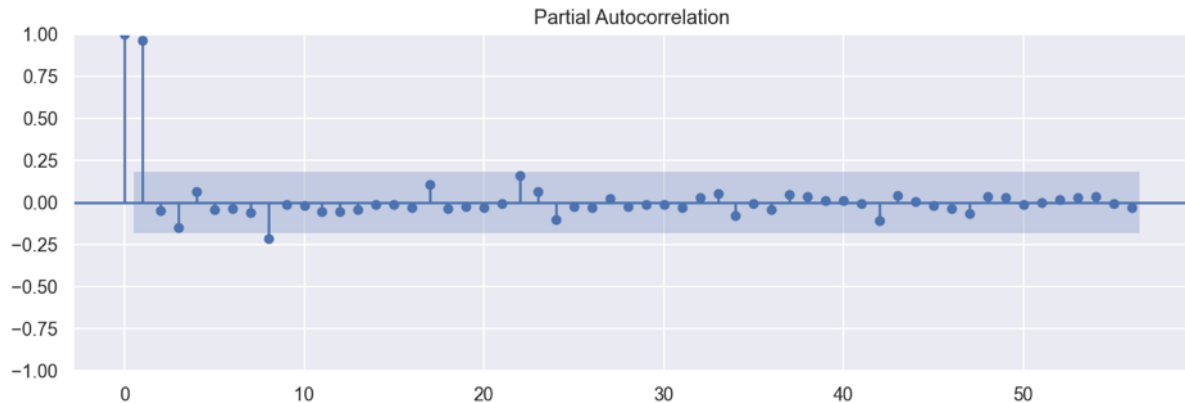


Figure 67 First iteration of parameter selection, PACF plots

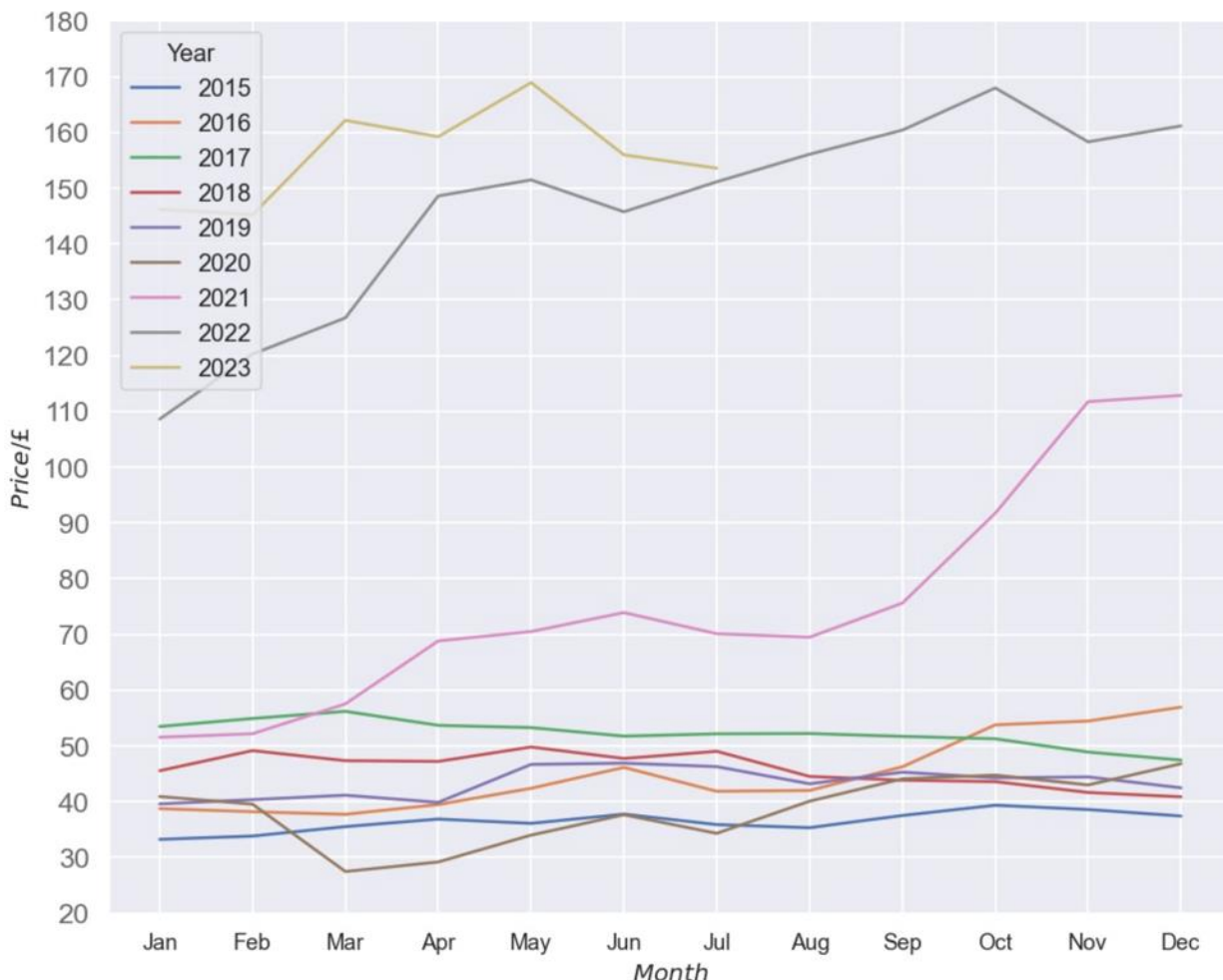


Figure 68 Seasonal Plot of Ethanol Cost

Next, the data was inspected for seasonality. Figure 68 depicts the time series data in years split into a monthly frequency to see if there are any seasonal patterns; there aren't any distinct patterns on a reoccurring monthly basis. Furthermore, figure 69 depicts seasonal (monthly) and normal differencing applied to the data and shows that normal differencing was sufficient to make the time series relatively stationary and thus the ARIMA model was not extended to a SARIMA model which incorporates seasonality. A few more quantitative tests were computed to validate the absence of seasonality since it has a large impact on the final forecast. The Kwiatkowski-Phillips-Schmidt-Shin (KPSS) test value was 0.97 and the PP (Phillips-Perron) test value was 1, these tests further indicate stationarity.

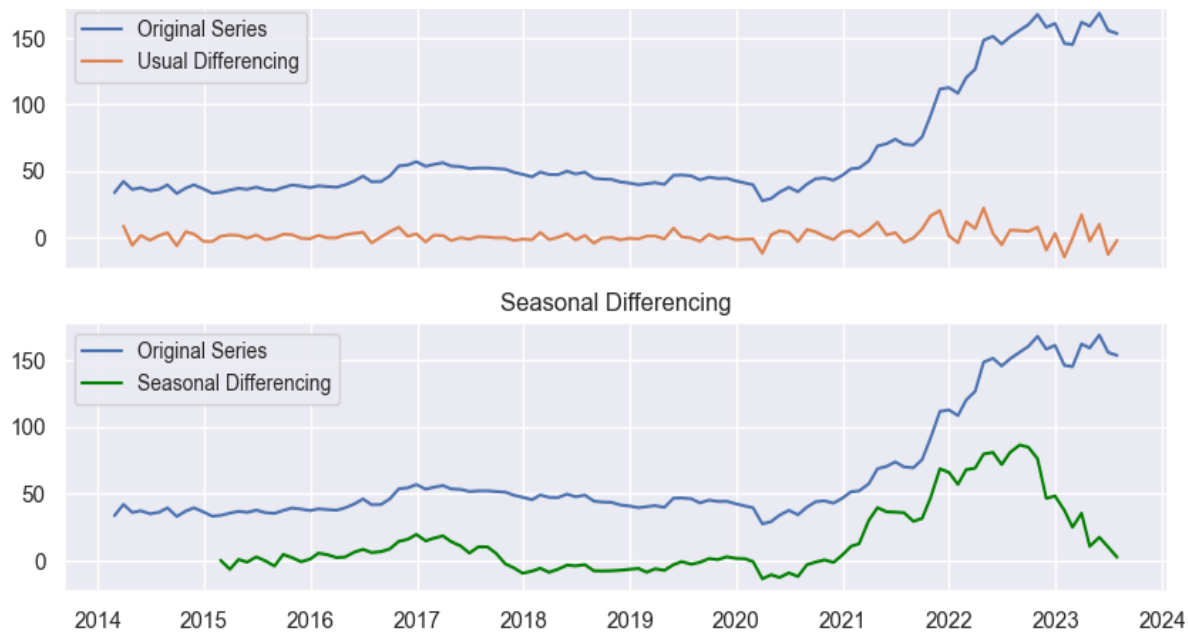


Figure 69 Effects of seasonal and normal differencing on Ethanol dataset

Table 9 Initial Statistical Test for Ethanol (pre-differencing)

| Statistical Test | Ethanol Dataset |
|------------------|-----------------|
| KPSS | 0.97 |
| PP | 1 |
| ADF | 0.12 |

The residuals of the dataset are next analysed to further validate the model and to detect further underlying patterns which the model may not be detected to ensure forecast reliability. Image A in Figure 70 shows the residuals fluctuating around zero showing a constant mean however the variance is increasing, which indicates a long-term temporal trend is present which the model

hasn't implemented. Image B in the same figure shows a narrow peak around zero showing an adequate level of constant variance. However, the Kernel Density Estimation (KDE) plot shows deviation from the expected normal distribution behaviour of the model. Additionally, this discrepancy can also be observed via the Normal Quantile – Quantile plot (Figure 70 Image C); the data points are not aligned on the red 45° line which means the residuals are not normally distributed [91].

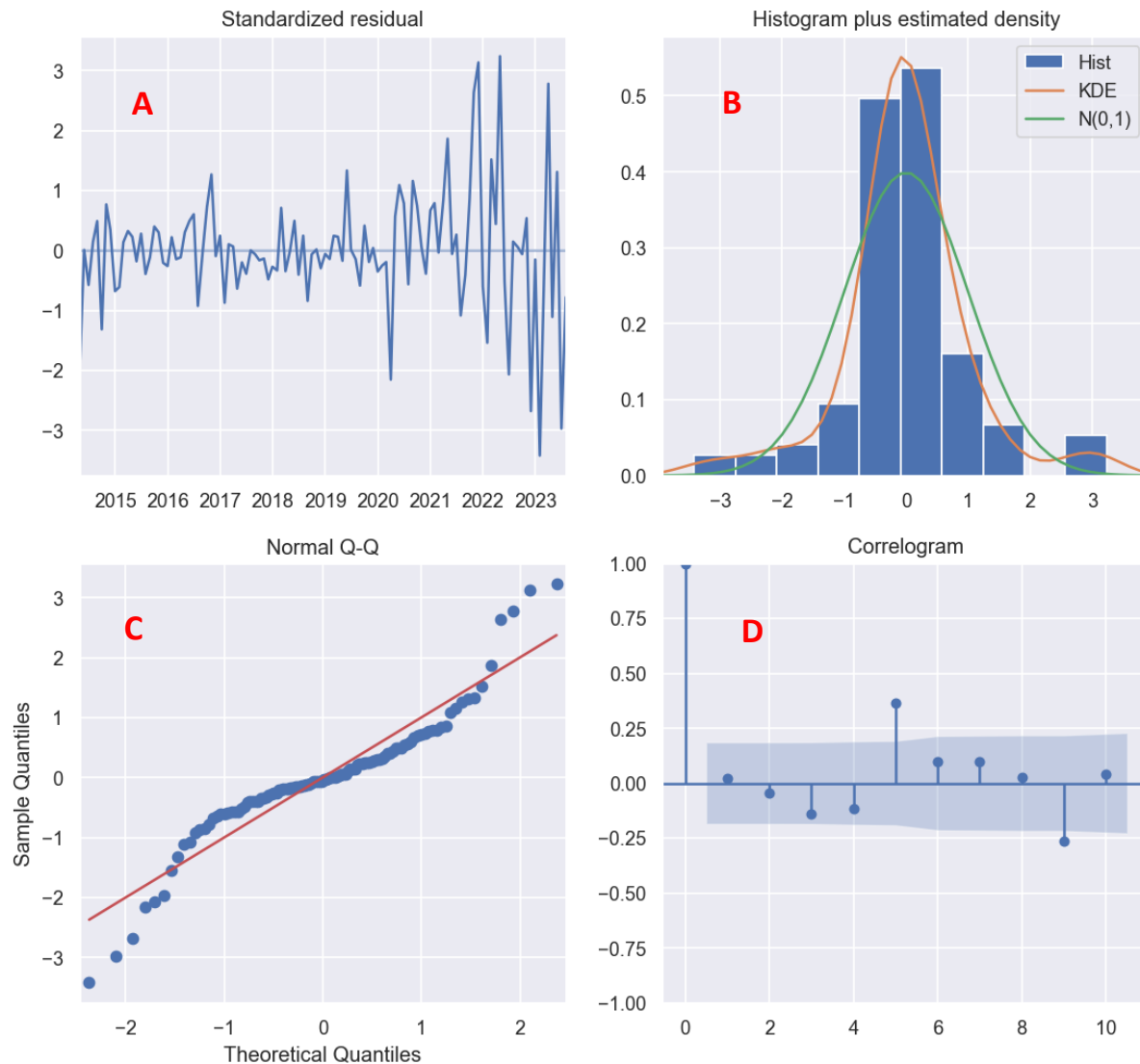


Figure 70 Residual Plots of ARIMA model. A - residual errors. B - Density plot, C- Quantile - Quantile Distribution D - ACF plot

Table 9 depicts the statistical results used to analyse how well the model fits the dataset. The metrics that are presented include a wide variety of different characteristics, and they shed light not only on the accuracy of the forecast but also on the nature of the variations that exist between the forecast and the actual values.

Table 10 Ethanol Statistical Results

| Model Fitness Stats | | Value |
|--|--|-------|
| Mean Absolute Percentage Error | | 0.14 |
| Mean Error | | 20.1 |
| Mean Absolute Error | | 22.5 |
| Mean Percentage Error | | 0.13 |
| Root Mean Squared Error | | 31.02 |
| Autocorrelation of First Residual | | 0.8 |
| Correlation | | 0.68 |
| Min – Max Score | | 0.11 |

Table 11 Ethanol Coefficient Selection Statistical Analysis

| ARIMA Term | coefficient | standard error | z value | P> z | [0.025 | 0.975] |
|-----------------|-------------|----------------|---------|-------|--------|--------|
| ma.L1 | -0.8827 | 0.040 | -21.896 | 0.000 | -0.962 | -0.804 |
| ma.S.L12 | -0.8123 | 0.087 | -9.328 | 0.000 | -0.983 | -0.642 |
| sigma2 | 32.9219 | 3.642 | 9.040 | 0.000 | 25.784 | 40.060 |

Table 12 Ethanol Residuals Analysis

| Statistic | Value |
|--------------------------------|-------|
| Ljung-Box (L1) (Q): | 0.41 |
| Prob(Q): | 0.52 |
| Heteroskedasticity (H): | 6.63 |
| Prob(H) (two-sided): | 0.00 |
| Jarque-Bera (JB): | 14.23 |
| Prob(JB): | 0.00 |
| Skew: | -0.08 |
| Kurtosis: | 4.84 |

ARIMA model discussion

The residual analysis of the ethanol dataset shows there are temporal or exogenous variables which the model isn't incorporating which does diminish the forecast reliability slightly since there is a possibility of significant fundamental factors being neglected. The autocorrelation of the first residual at 0.8 does show there is a short-term pattern, however the autocorrelation of the rest of the lagged residuals (Figure 71) are not significant which implies the model is considering these short-term patterns. Nonetheless, figure 71 shows that the predicted data points do match up to the historical time series well across a large time horizon, this is also observed by the mean absolute percentage error (MAPE) of 0.14, which means on average the models forecast deviates by 14% and in conjunction with a Mean Absolute Error (MAE) of 22.5 units which is acceptable. A correlation coefficient of 0.68 means there is a moderately linear relationship between the actual and predicted values. A well-fitted ARIMA model would exhibit a low root mean squared error (RMSE), the model developed in this thesis exhibits an RMSE of 31.02 which in absolute values seems high but relative to the commodities market is reasonably acceptable due to the inherent volatility present in the dataset.

In general, the ARIMA model exhibits a high level of agreement with the time series data. The escalating prices of ethanol projected in the forthcoming years indicates an expanding market that is evolving in response to a growing demand.

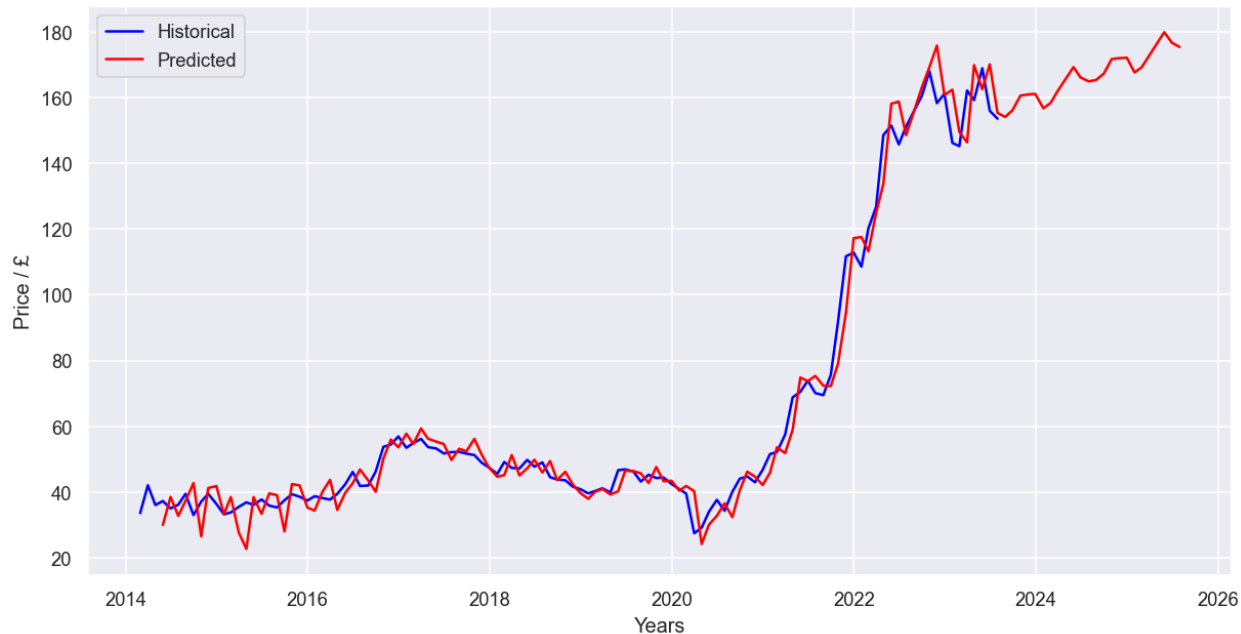


Figure 71 ARIMA model ethanol forecast

Monte Carlo Results

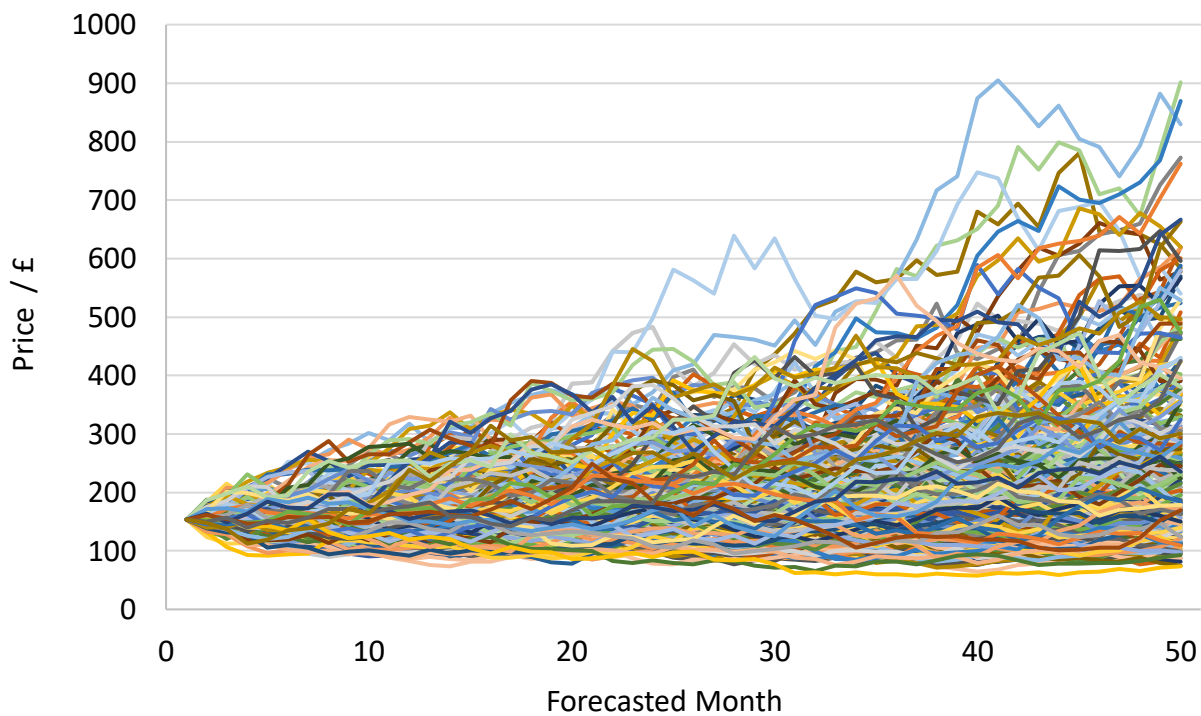


Figure 72 Monte Carlo simulation

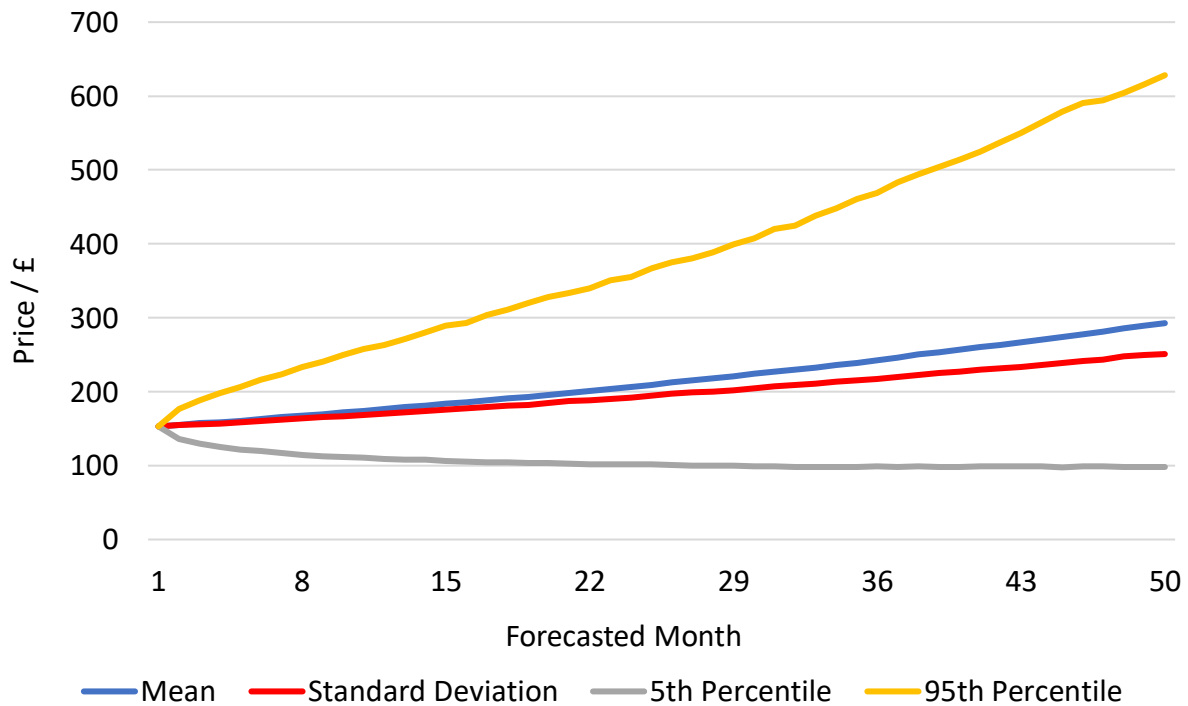


Figure 73 Statistical analysis of Monte Carlo simulation

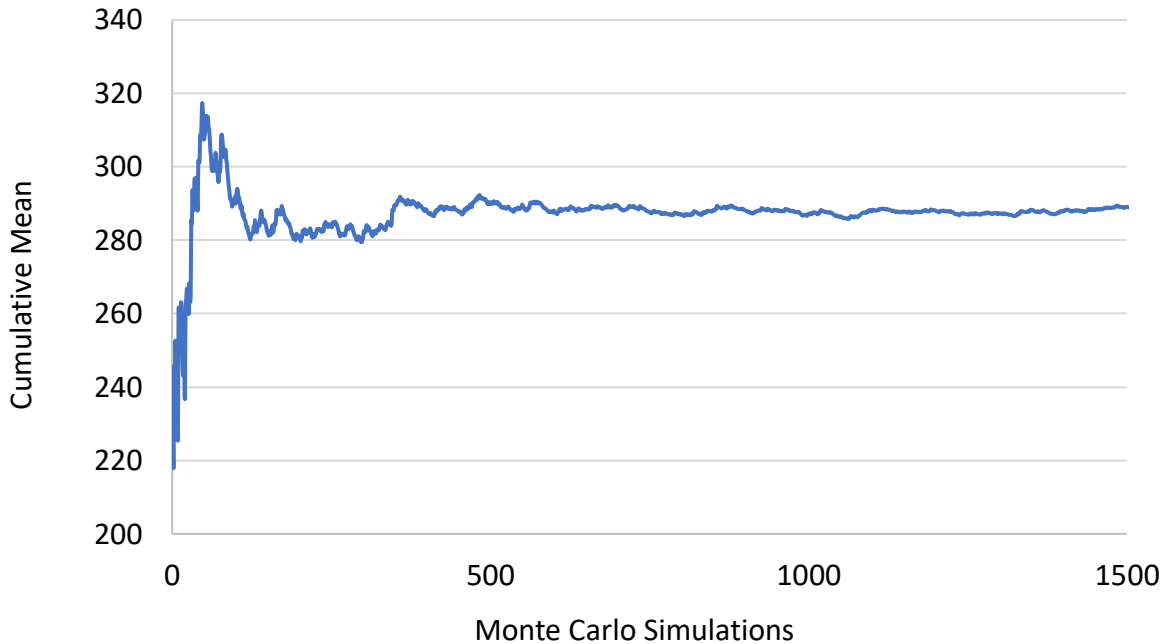


Figure 74 Convergence plot for Monte Carlo simulation

Monte Carlo Simulation Discussion

The Monte Carlo simulation results exhibit a consistent upward trajectory with minimal variability, which can be attributed to the inherent low variance observed in the original ethanol dataset. Figure 72 depicts all the iterations which were computed. To visualise and better understand the data, figure 73 can be used which shows a mean value amount of £300, within 50 months in the future, again showing an increase in demand is expected. The percentile range exhibits an upward trend as the forecasting horizon extends, indicating a heightened degree of uncertainty associated with long-term forecasts. Figure 74 demonstrates that conducting 1000 iterations of the simulations is enough, as the cumulative mean exhibit convergence after approximately 1000 iterations. This convergence ensures the robustness of the simulations and consequently provides a reliable representation of future prices.

One significant constraint associated with the Monte Carlo simulation is related to its inherent challenge in accurately forecasting significant unforeseen events that have the potential to cause substantial price fluctuations. Additionally, the model's failure to incorporate macroeconomic factors further limits its predictive capabilities. The simulation heavily relies on the efficient market hypothesis, which assumes that the current and future prices of assets can be solely determined by available data [92].

Conclusion

This thesis has developed a method to create and analyse alcohol-ammonia fuel blends. Aqueous ammonia is gently heated and bubbled through the solvent to create a homogenous mixture. The ammonia contents in both methanol and ethanol were not as expected even though excess ammonia was added to ensure the solubility limit was reached. This can be rectified by potentially implementing alkali metal salts which can create new bonds with the mixture and thus suppress ammonia vaporization, alternatively, the ammonia could be cooled down or pressurized to obtain more ammonia content within the solvents.

The combustion behaviour of the mixtures was as expected with the blended solutions exhibiting lower in-cylinder pressures, lower heat release rates and slower mass burnt fractions all of which means the combustion cycle for the blended samples was less thermally efficient and marginally less stable compared to the pure samples. Notable differences were observed between direct injection from literature and port fuel injection modes, the combustion characteristics are suitable for implementation in actual internal combustion engines but would benefit if the intake pressure is increased since the laminar burning velocity has the potential to also increase. Fuel stratification was hypothesised, this could explain the decrease in power and combustion performance as more timed runs were recorded. Although methanol contained more ammonia the combustion performance was better than ethanol which could be advantage in terms of emissions.

Aspen simulations have estimated the cost of fuel production if it were to be industrialised, the results show it is currently more expensive compared to conventional fuels at £5.79. However, Auto Regressive Moving Average and Monte Carlo models have predicted a rise in demand in the future given the supply of ethanol will remain the same. This shows there is potential for policy changes and subsidies to be implemented which could make the fuel more attractive.

Summary of future works:

- Investigate the efficacy of the addition of alkali salts in suppressing ammonia vaporisation
- Identify fuel stratification using PLIF and molecular dynamic simulations
- Conduct engine testing at varying equivalence ratios with strict control over water content and observe emissions and combustion performance
- Investigate the effects of forced induction and the behaviour of turbulent flames in the ammonia-ethanol mixtures
- Investigate fuel degradation mechanisms
- Feasibility of vapour recovery units inside vehicles to keep fuel blends homogenous
- Conduct regression analysis to see which variables affect demand and index price to improve Monte Carlo and ARIMA models

Bibliography

- [1] H. Ritchie, "Cars, planes, trains: where do CO₂ emissions from transport come from?," 06 10 2020. [Online]. Available: <https://ourworldindata.org/co2-emissions-from-transport>. [Accessed 12 07 2023].
- [2] E. A. B. Noah S. Diffenbaugh, "Data-driven predictions of the time remaining until critical global warming thresholds are reached," 30 01 2023. [Online]. Available: <https://www.pnas.org/doi/10.1073/pnas.2207183120>. [Accessed 02 07 2023].
- [3] Mckinsey & Company, "Global Energy Perspective 2022," April 2022. [Online]. Available: <https://www.mckinsey.com/industries/oil-and-gas/our-insights/global-energy-perspective-2022>. [Accessed 01 07 2023].
- [4] M. R. a. P. R. Hannah Ritchie, "Electricity Mix," ourworldindata, 2022. [Online]. Available: <https://ourworldindata.org/electricity-mix>. [Accessed 01 07 2023].
- [5] T. M. A. M.-G. a. O. R. Nathan Lash, "Charting the global energy landscape to 2050: Sustainable fuels," Mckinsey, 07 07 2022. [Online]. Available: <https://www.mckinsey.com/industries/oil-and-gas/our-insights/charting-the-global-energy-landscape-to-2050-sustainable-fuels>. [Accessed 18 07 2023].
- [6] S. Oğuz, "ELECTRIFICATIONLife Cycle Emissions: EVs vs. Combustion Engine Vehicles," 23 06 2023. [Online]. Available: <https://elements.visualcapitalist.com/life-cycle-emissions-of-electric-hybrid-and-combustion-engine-vehicles/>. [Accessed 26 06 2023].
- [7] L. Moore, "Greenhouse Gases: How Long Will They Last?," Enviromental Defense Fund, 26 02 2008. [Online]. Available: https://blogs.edf.org/climate411/2008/02/26/ghg_lifetimes/#:~:text=About%2050%25%20of%20a%20CO,lifetime%3A%2050%2D200%20years.. [Accessed 12 07 2023].
- [8] J. E. Jonson, "Impact of excess NO_x emissions from diesel cars on air quality, public health and eutrophication in Europe," Environmental Research Letters, 18 09 2017. [Online]. Available: https://www.researchgate.net/publication/319881480_Impact_of_excess_NO_x_emissions_from_diesel_cars_on_air_quality_public_health_and_eutrophication_in_Europe. [Accessed 22 08 2023].
- [9] International Coucil on Clean Transportation, "NEW STUDY QUANTIFIES GLOBAL HEALTH, ENVIRONMENTAL IMPACTS OF EXCESS NITROGEN OXIDE EMISSIONS FROM DIESEL VEHICLES," 15 05 2017. [Online]. Available: <https://theicct.org/new-study-quantifies-global-health-environmental-impacts-of-excess-nitrogen-oxide-emissions-from-diesel-vehicles/>. [Accessed 18 07 2023].
- [10] S. M. J. M. R. e. a. Anenberg, "Impacts and mitigation of excess diesel-related NO_x emissions in 11 major vehicle markets," nature, 15 05 2017. [Online]. Available: <https://www.nature.com/articles/nature22086#Fig4>. [Accessed 17 07 2023].
- [11] N. Morlanés, "A technological roadmap to the ammonia energy economy: Current state and missing technologies," Chemical Engineering Journal, 15 03 2021. [Online]. Available:

<https://www.sciencedirect.com/science/article/pii/S1385894720334343#f0005>. [Accessed 18 07 2023].

- [12] D. Erdemir, "A perspective on the use of ammonia as a clean fuel: Challenges and solutions," *Energy Research*, 25 11 2020. [Online]. Available: <https://onlinelibrary.wiley.com/doi/full/10.1002/er.6232>. [Accessed 21 07 2023].
- [13] D. J. W. M. J. T. R. Timothy J. Tse, "Production of Bioethanol—A Review of Factors Affecting Ethanol Yield," 18 11 2021. [Online]. Available: <https://www.mdpi.com/2311-5637/7/4/268#:~:text=Bioethanol%20is%20typically%20produced%20via,sugar%20cane%2C%20and%20sugar%20beets..> [Accessed 12 06 2023].
- [14] M.-V. T. ,. B. T. T. ,. G. S. ,. C. T. C. Chia Chun Lee, "A comprehensive review on the effects of additives on fundamental combustion characteristics and pollutant formation of biodiesel and ethanol," *Fuel*, 15 03 2021. [Online]. Available: <https://www.sciencedirect.com/science/article/pii/S0016236120327459#s0035>. [Accessed 02 07 2023].
- [15] J. G. ,. Z. C. H. C. ,. Y. Z. ,. Y. H. ,. Z. C. Xiaochen Wang, "Evaluation of hydrous ethanol as a fuel for internal combustion engines: A review," *Renewable Energy*, 07 2022. [Online]. Available: <https://www.sciencedirect.com/science/article/pii/S0960148122007832#sec1>. [Accessed 28 07 2023].
- [16] S. M. A. ,. R. W. D. J. Hunter Mack, "Demonstrating direct use of wet ethanol in a homogeneous charge compression ignition (HCCI) engine," *Energy*, 06 2009. [Online]. Available: <https://www.sciencedirect.com/science/article/pii/S0360544209000504>. [Accessed 01 07 2023].
- [17] J. H. Mack, "Demonstrating direct use of wet ethanol in a homogeneous charge compression ignition (HCCI) engine," *Energy*, 06 2009. [Online]. Available: <https://www.sciencedirect.com/science/article/pii/S0360544209000504>. [Accessed 23 07 2023].
- [18] H. K. Noh, "Effect of bioethanol on combustion and emissions in advanced CI engines: HCCI, PPC and GCI mode – A review," *Applied Energy*, 15 12 2017. [Online]. Available: <https://www.sciencedirect.com/science/article/pii/S0306261917313533#s0010>. [Accessed 13 08 2023].
- [19] X. Duan, "A review of controlling strategies of the ignition timing and combustion phase in homogeneous charge compression ignition (HCCI) engine," *Fuel*, 01 02 2021. [Online]. Available: <https://www.sciencedirect.com/science/article/pii/S0016236120321384>. [Accessed 16 08 2023].
- [20] R. Stone, *Introduction to Internal Combustion Engines*, London: MACMILLAN , 1999.
- [21] N. N. G. &. S. M. S. N. V. Petrukhin, "Ignition Delay Time – an Important Fuel Property," *Chemistry and Technology of Fuels and Oils* , 12 02 2016. [Online]. Available: [https://link.springer.com/article/10.1007/s10553-016-0642-0#:~:text=If%20the%20ignition%20delay%20time,preparation%20\(fragmentation%20and%20oxidation\)%20improves](https://link.springer.com/article/10.1007/s10553-016-0642-0#:~:text=If%20the%20ignition%20delay%20time,preparation%20(fragmentation%20and%20oxidation)%20improves). [Accessed 13 06 2023].

- [22] I. D. Dogan Erdemir, "A perspective on the use of ammonia as a clean fuel: Challenges and solutions," International Journal of Energy Research, 25 11 2020. [Online]. Available: <https://onlinelibrary.wiley.com/doi/full/10.1002/er.6232#er6232-bib-0013>. [Accessed 01 07 2023].
- [23] A. Valera-Medina, "Ammonia for power," Progress in Energy and Combustion Science, 11 2018. [Online]. Available: <https://www.sciencedirect.com/science/article/pii/S0360128517302320>. [Accessed 12 08 2023].
- [24] Engineering Toolbox, "Methanol - Thermophysical Properties vs. Temperature," 2008. [Online]. Available: https://www.engineeringtoolbox.com/methanol-properties-d_1209.html. [Accessed 17 08 2023].
- [25] Engineering Toolbox, "Ammonia - Thermophysical Properties," 2008. [Online]. Available: https://www.engineeringtoolbox.com/ammonia-d_1413.html. [Accessed 14 07 2023].
- [26] C. Tornatore, "Ammonia as Green Fuel in Internal Combustion Engines: State-of-the-Art and Future Perspectives," Insights in Engine and Automotive Engineering: 2021, 22 07 2022. [Online]. Available: <https://www.frontiersin.org/articles/10.3389/fmech.2022.944201/full>. [Accessed 01 09 2023].
- [27] Technology Collaboration Program on Advanced Motor Fuels, "Methanol," [Online]. Available: https://www.iea-amf.org/content/fuel_information/methanol.
- [28] liveaboutdotcom, "What You Should Know About the Diesel Fuel Cetane," 2023. [Online]. Available: <https://www.liveabout.com/what-is-cetane-85603>. [Accessed 12 08 2023].
- [29] R. Laursen, D. Barcarolo, H. Patel, M. Dowling, M. Penfold, J. Faber, J. Király, R. van der Ven and E. v. G. A. Pang, "Potential of Ammonia as Fuel in Shipping," EMSA, 16 09 2022. [Online]. Available: <https://www.emsa.europa.eu/newsroom/latest-news/download/7322/4833/23.html>. [Accessed 02 09 2023].
- [30] M. M. Caneon Kurien, "Review on the production and utilization of green ammonia as an alternate fuel in dual-fuel compression ignition engines," Energy Conversion and Management, 01 01 2022. [Online]. Available: <https://www.sciencedirect.com/science/article/pii/S0196890421011663#b0445>. [Accessed 04 07 2023].
- [31] J. N. Klüssmann, "Ammonia Application in IC Engines," Advanced Motor Fuels, 27 05 2020. [Online]. Available: <https://iea-amf.org/app/webroot/files/file/other%20publications/Ammonia%20Application%20in%20IC%20Engines.pdf>. [Accessed 12 07 2023].
- [32] L. M. P. S. M. D. J. Cinzia Tornatore, "Ammonia as Green Fuel in Internal Combustion Engines: State-of-the-Art and Future Perspectives," 22 07 2022. [Online]. Available: <https://www.frontiersin.org/articles/10.3389/fmech.2022.944201/full>. [Accessed 01 08 2023].
- [33] A. MOZAFARI-VARNUSFADRANI, "Predictions and measurements of spark-ignition engine characteristics using ammonia and other fuels," Predictions and measurements of spark-

- ignition engine characteristics using ammonia and other fuels, 1988. [Online]. Available: <https://qmro.qmul.ac.uk/xmlui/handle/123456789/1582>. [Accessed 14 07 2023].
- [34] T. C. a. D. Zhao, "Overview of Autoignition and Flame Propagation Properties for Ammonia Combustion," Aerospace Research Central, 08 05 2023. [Online]. Available: <https://arc.aiaa.org/doi/epdf/10.2514/1.J062764>. [Accessed 15 08 2023].
- [35] Q. Jing, "The flame propagation characteristics and detonation parameters of ammonia/oxygen in a large-scale horizontal tube: As a carbon-free fuel and hydrogen-energy carrier Author links open overlay panel," International Journal of Hydrogen Energy, 25 05 2021. [Online]. Available: <https://www.sciencedirect.com/science/article/pii/S0360319921008776#fig15>. [Accessed 12 08 2023].
- [36] F. P. B. Jorge Martins, "Alternative Fuels for Internal Combustion Engines," Energies, 20 05 2020. [Online]. Available: <https://www.mdpi.com/1996-1073/13/16/4086#B108-energies-13-04086>. [Accessed 19 07 2023].
- [37] J. G. Z. C. H. C. Y. Z. Y. H. Z. C. Xiaochen Wang, "Evaluation of hydrous ethanol as a fuel for internal combustion engines: A review," Renewable Energy, 07 2022. [Online]. Available: <https://www.sciencedirect.com/science/article/pii/S0960148122007832#sec1>. [Accessed 25 07 2023].
- [38] J. Martins, "Alternative Fuels for Internal Combustion Engines," energies, 06 08 2020. [Online]. Available: <https://www.mdpi.com/1996-1073/13/16/4086#B108-energies-13-04086..> [Accessed 12 07 2023].
- [39] S. M. M. P. M. R. R. G. M. S. J. R. A. N. B. Sangeeta, "Alternative fuels: An overview of current trends and scope for future," Renewable and Sustainable Energy Reviews, 04 04 2014. [Online]. Available: <https://www.sciencedirect.com/science/article/pii/S1364032114000343#bib56>. [Accessed 12 07 2023].
- [40] X. H. Y. H. R. Z. Y. Z. Z. Z. K. C. Zhihua Wang, "Experimental and kinetic study on the laminar burning velocities of NH₃ mixing with CH₃OH and C₂H₅OH in premixed flames," Combustion and Flame, 07 2021. [Online]. Available: <https://www.sciencedirect.com/science/article/pii/S0010218021001073?via%3Dihub>. [Accessed 19 07 2023].
- [41] a. B. S. Denghao Zhu, "Recent Progress on Combustion Characteristics of Ammonia-Based Fuel Blends and Their Potential in Internal Combustion Engines," scilight, 18 01 2023. [Online]. Available: <https://www.sciltp.com/journals/ijamm/issue13-paper207.html>. [Accessed 12 07 2023].
- [42] D. Zhu, "Recent Progress on Combustion Characteristics of Ammonia-Based Fuel Blends and Their Potential in Internal Combustion Engines," 18 01 2023. [Online]. Available: <https://www.sciltp.com/journals/ijamm/issue13-paper207.html>. [Accessed 13 06 2023].
- [43] Z. Wang, "Experimental and kinetic study on the laminar burning velocities of NH₃ mixing with CH₃OH and C₂H₅OH in premixed flames," Combustion and Flame, 07 2021. [Online]. Available:

<https://www.sciencedirect.com/science/article/pii/S0010218021001073?via%3Dihub>. [Accessed 21 07 2023].

- [44] M. Li, "Experimental and kinetic modeling study on auto-ignition properties of ammonia/ethanol blends at intermediate temperatures and high pressures," Proceedings of the Combustion Institute, 2023. [Online]. Available: <https://www.sciencedirect.com/science/article/pii/S1540748922001705?via%3Dihub>. [Accessed 18 08 2023].
- [45] R. P. P. B. J. B. C. Mounaïm-Rousselle, "Performances and pollutant emissions of spark ignition engine using direct injection for blends of ethanol/ammonia and pure ammonia," Sage Journals, 25 05 2023. [Online]. Available: <https://journals.sagepub.com/doi/full/10.1177/14680874231170661>. [Accessed 23 06 2023].
- [46] R. Pelé, "Performances and pollutant emissions of spark ignition engine using direct injection for blends of ethanol/ammonia and pure ammonia," Sage Journals , 25 05 2023. [Online]. Available: <https://journals.sagepub.com/doi/full/10.1177/14680874231170661>. [Accessed 15 07 2023].
- [47] M. C. Rehbein, "Mixtures of Ammonia and Organic Solvents as Alternative Fuel for Internal Combustion Engines," energy&fuels, 09 09 2019. [Online]. Available: https://pubs.acs.org/doi/full/10.1021/acs.energyfuels.9b01450?casa_token=2M9RNuwZOzMAAAAA:WDafUJS8a7dVivvubSOOTLHZQmtHPfalpo28g8KCNY2Bcpqdja9KcEfNyB6YodHQd0gdsK7eqWTNICQi. [Accessed 25 06 2023].
- [48] J. Clark, "Simple Reactions of Carboxylic Acids as Acids," Libretexts, [Online]. Available: https://chem.libretexts.org/Bookshelves/Organic_Chemistry/Supplemental_Modules_%28Organic_Chemistry%29/Carboxylic_Acids/Reactivity_of_Carboxylic_Acids/Simple_Reactions_of_Carboxylic_Acids_as_Acids. [Accessed 22 06 2023].
- [49] C. M. P. E. a. S. S. M. C. Rehbein, "Mixtures of Ammonia and Organic Solvents as Alternative Fuel for Internal Combustion Engines," energy & fuels, 09 09 2019. [Online]. Available: https://pubs.acs.org/doi/full/10.1021/acs.energyfuels.9b01450?casa_token=2M9RNuwZOzMAAAAA:WDafUJS8a7dVivvubSOOTLHZQmtHPfalpo28g8KCNY2Bcpqdja9KcEfNyB6YodHQd0gdsK7eqWTNICQi. [Accessed 12 08 2023].
- [50] J. K. Choongsik Bae, "Alternative fuels for internal combustion engines," Proceedings of the Combustion Institute, 2017. [Online]. Available: https://www.sciencedirect.com/science/article/pii/S1540748916304850?casa_token=zHxGb8cCffMAAAAA:J2dQ-Bjp7SSiFVQH-F-NLVhL_yHemROPxNTrNvRLkBArhRQ8qkvQK3G6tkXGFLdG1BxkAhl7IQ#bib0135. [Accessed 12 07 2023].
- [51] D. Saba, "Performance and Emission characteristics of Homogeneous charge compression ignition (HCCI) engine – A review," International Journal of Ambient Energy, 02 2016. [Online]. Available: https://www.researchgate.net/publication/295253790_Performance_and_Emission_characteristics_of_Homogeneous_charge_compression_ignition_HCCI_engine_-A_review. [Accessed 19 07 2023].

- [52] S.-Y. N. Hyun Kwon Noh, "Effect of bioethanol on combustion and emissions in advanced CI engines: HCCI, PPC and GCI mode – A review," *Applied Energy*, 15 12 2017. [Online]. Available: <https://www.sciencedirect.com/science/article/pii/S0306261917313533#s0010>. [Accessed 13 07 2023].
- [53] 2. ., H. P. M. 2. ., V. N. D. Thang Nguyen Minh 1, "A review of internal combustion engines powered by renewable energy based on ethanol fuel and HCCI technology," *AIMS Energy*, 2022 09 2022. [Online]. Available: <http://www.aimspress.com/article/doi/10.3934/energy.2022046>. [Accessed 12 07 2023].
- [54] T. N. Minh, "A review of internal combustion engines powered by renewable energy based on ethanol fuel and HCCI technology," *AIMS Energy*, 06 09 2022. [Online]. Available: <https://www.aimspress.com/article/doi/10.3934/energy.2022046>. [Accessed 14 08 2023].
- [55] S. M. A. ., R. W. D. J. Hunter Mack, "Demonstrating direct use of wet ethanol in a homogeneous charge compression ignition (HCCI) engine," *Energy*, 2009 06. [Online]. Available: <https://www.sciencedirect.com/science/article/pii/S0360544209000504#fig6>. [Accessed 11 07 2023].
- [56] S. S. Bhurat, "Technical barriers and their solutions for deployment of HCCI engine technologies – a review," *International Journal of Ambient Energy*, 16 05 2019. [Online]. Available: <https://www.tandfonline.com/doi/full/10.1080/01430750.2019.1611644?cookieSet=1>. [Accessed 16 07 2023].
- [57] Z. Zhang, "Effects of low-level water addition on spray, combustion and emission characteristics of a medium speed diesel engine fueled with biodiesel fuel," *Fuel*, 01 03 2019. [Online]. Available: <https://www.sciencedirect.com/science/article/pii/S0016236118319069>. [Accessed 11 07 2023].
- [58] R. M. F. P. A. S. Dmitrii V. Antonov, "Micro-Explosion Phenomenon: Conditions and Benefits," 03 11 2022. [Online]. Available: <https://www.mdpi.com/1996-1073/15/20/7670>. [Accessed 07 07 2023].
- [59] Z. Z. S. S. X. C. W. Y. Qi Zhang, "Chemical effect of water addition on the ammonia combustion reaction," 17 07 2023. [Online]. Available: <https://www.sciencedirect.com/science/article/pii/S2451904922001251>.
- [60] X. Z. J. W. Z. K. H. L. P. H. Muye Feng, "Ethanol oxidation with high water content: A reactive molecular dynamics," *Fuel*, 2019. [Online]. Available: <https://www.sciencedirect.com/science/article/pii/S0016236118314108?via%3Dihub>. [Accessed 23 07 2023].
- [61] pass my exams, "Addition Reaction of Alkenes with Hydrogen," [Online]. Available: <https://www.passmyexams.co.uk/GCSE/chemistry/alkenes-and-hydrogen-reaction.html>. [Accessed 12 07 2023].

- [62] StoliChem, “Gas-liquid mass transfer (kLa) in scalable flow chemistry. Scalable Agitated Baffle Reactor (SABRe),” 17 08 2021. [Online]. Available: <https://stoliche.com/gas-liquid-mass-transfer-kla-in-scalable-flow-chemistry-scalable-agitated-baffle-reactor-sabre/>. [Accessed 17 08 2023].
- [63] Y. Fu, “The influence of random packed column parameters on the liquid holdup and interfacial area,” AlChe Journal, 12 03 2022. [Online]. Available: <https://aiche.onlinelibrary.wiley.com/doi/full/10.1002/aic.17691>. [Accessed 12 06 2023].
- [64] chemnotcheem, “acids-bases-salts,” [Online]. Available: <https://chemnotcheem.com/acids-bases-salts/feed/>. [Accessed 12 07 2023].
- [65] P. H. ,. N. L. ,. M. T. ,. Z. K. Ahmad Almaleki, “Effects of fuel composition at varying air-fuel ratio on knock resistance during spark-ignition combustion,” Fuel, 15 07 2023. [Online]. Available: <https://www.sciencedirect.com/science/article/pii/S0016236123006282>. [Accessed 10 07 2023].
- [66] A. Hayes, “Autoregressive Integrated Moving Average (ARIMA) Prediction Model,” Investopedia, 18 12 2022. [Online]. Available: <https://www.investopedia.com/terms/a/autoregressive-integrated-moving-average-arima.asp>. [Accessed 13 08 2023].
- [67] S. Prabhakaran, “ARIMA Model – Complete Guide to Time Series Forecasting in Python,” machinelearningplus, [Online]. Available: https://www.machinelearningplus.com/time-series/arima-model-time-series-forecasting-python/?expand_article=1. [Accessed 03 08 2023].
- [68] S. Prabhakaran, “Time Series Analysis in Python – A Comprehensive Guide with Examples,” machinelearningplus, [Online]. Available: <https://www.machinelearningplus.com/time-series/time-series-analysis-python/>. [Accessed 01 08 2023].
- [69] Swetha, “Introduction to Time Series Forecasting — Part 2 (ARIMA Models),” towardsdatascience, 30 07 2021. [Online]. Available: <https://towardsdatascience.com/introduction-to-time-series-forecasting-part-2-arima-models-9f47bf0f476b>. [Accessed 02 08 2023].
- [70] S. Loukas, “Time-Series Forecasting: Predicting Stock Prices Using An ARIMA Model,” towardsdatascience, 23 07 2020. [Online]. Available: <https://towardsdatascience.com/time-series-forecasting-predicting-stock-prices-using-an-arima-model-2e3b3080bd70>. [Accessed 12 08 2023].
- [71] P. Pathak, “How to Create an ARIMA Model for Time Series Forecasting in Python,” Analytics Vidhya, 19 05 2023. [Online]. Available: <https://www.analyticsvidhya.com/blog/2020/10/how-to-create-an-arima-model-for-time-series-forecasting-in-python/>. [Accessed 05 08 2023].
- [72] B. Mather, Time Series with Python: How to implement time series analysis and forecasting with Python, 2020.
- [73] A. Zajic, “What Is Akaike Information Criterion (AIC)?,” builtin, 29 11 2022. [Online]. Available: <https://builtin.com/data-science/what-is-aic>. [Accessed 13 08 2023].

- [74] M. A. Musarat, "Kabul River Flow Prediction Using Automated ARIMA Forecasting: A Machine Learning Approach," ResearchGate, 07 2021. [Online]. Available: https://www.researchgate.net/publication/354860118_Kabul_River_Flow_Prediction_Using_Automated_ARIMA_Forecasting_A_Machine_Learning_Approach. [Accessed 07 08 2023].
- [75] R. Nau, "ARIMA models for time series forecasting," Fuqua School of Business Duke University, [Online]. Available: <https://people.duke.edu/~rnau/411arim.htm>. [Accessed 18 08 2023].
- [76] B. D. Vijay Kotu, "Chapter 12 - Time Series Forecasting," Data Science, 2019. [Online]. Available: <https://www.sciencedirect.com/science/article/pii/B9780128147610000125#s0015>. [Accessed 11 08 2023].
- [77] W. KENTON, "Monte Carlo Simulation: History, How it Works, and 4 Key Steps," Investopedia, 26 03 2023. [Online]. Available: <https://www.investopedia.com/terms/m/montecarlosimulation.asp>. [Accessed 12 08 2023].
- [78] Renewable Fuels Association, "Weekly Ethanol Production Review," [Online]. Available: <https://ethanolrfa.org/markets-and-statistics/weekly-and-monthly-ethanol-supply-and-demand>. [Accessed 14 07 2023].
- [79] Bloomberg Finance L.P., [Online]. [Accessed 22 06 2023].
- [80] P. J. & M. A. Stefan Salentinig, "A computational study of the suppression of ammonia volatility in aqueous systems using ionic additives," 13 04 2013. [Online]. Available: <https://link.springer.com/article/10.1007/s11224-013-0263-8#Fig6>. [Accessed 19 07 2023].
- [81] "Solubility of Ammonia in Alcohols," Americal Chemical Society, 1952. [Online]. Available: https://airgasspecialtyproducts.com/wp-content/uploads/2016/02/Solubility_of_Ammonia_in_Alcohols_.pdf. [Accessed 14 07 2023].
- [82] S. Salentinig, "A computational study of the suppression of ammonia volatility in aqueous systems using ionic additives," Structural Chemistry, 2014. [Online]. Available: <https://link.springer.com/article/10.1007/s11224-013-0263-8#Sec1>. [Accessed 04 07 2023].
- [83] G. D. C. C. F. H. Alka Karan, "High-pressure and temperature ammonia flame speeds," HAL open science, 02 03 2022. [Online]. Available: <https://hal.science/hal-03555362/document#:~:text=The%20adiabatic%20flame%20temperature%20and,to%20its%20anti%2Dknock%20characteristics..> [Accessed 01 09 2023].
- [84] T. E. ToolBox, "Adiabatic flame temperatures for hydrogen, methane, propane and octane - in Kelvin," The Engineering ToolBox, 2005. [Online]. Available: https://www.engineeringtoolbox.com/adiabatic-flame-temperature-d_996.html. [Accessed 01 09 2023].

- [85] H. Kobayashi, "Science and technology of ammonia combustion," Proceedings of the Combustion Institute, 2019. [Online]. Available: <https://www.sciencedirect.com/science/article/pii/S1540748918306345#sec0004>. [Accessed 01 09 2023].
- [86] L. Kang, "A review on ammonia blends combustion for industrial applications," Fuel, 15 01 2023. [Online]. Available: https://www.sciencedirect.com/science/article/pii/S001623612202974X?casa_token=pVcp2n6o7kAAAAA:KN_E3RrpYaAxgiY5xcOCS5DPjU_N4klpQNN4dXBfAlANgI0gSoi6lhOnRIfXzQT3gp4g6KbrqhU. [Accessed 12 07 2023].
- [87] RAC Drive, "Petrol and diesel prices," [Online]. Available: <https://www.rac.co.uk/drive/advice/fuel-watch/>. [Accessed 23 08 2023].
- [88] M. Armstrong, "UK Petrol: What Are You Paying For at the Pump?," statista, 21 03 2022. [Online]. Available: <https://www.statista.com/chart/27082/uk-petrol-price-breakdown-by-cost-component/>. [Accessed 19 08 2023].
- [89] S. Prabhakaran, "ARIMA Model – Complete Guide to Time Series Forecasting in Python," machinelearningplus, 01 08 2023. [Online]. Available: https://www.machinelearningplus.com/time-series/arima-model-time-series-forecasting-python/?expand_article=1. [Accessed 01 08 2023].
- [90] E. Lewinson, "A Step-by-Step Guide to Calculating Autocorrelation and Partial Autocorrelation," towardsdatascience, 30 01 2022. [Online]. Available: <https://towardsdatascience.com/a-step-by-step-guide-to-calculating-autocorrelation-and-partial-autocorrelation-8c4342b784e8>. [Accessed 01 08 2023].
- [91] C. Ford, "Understanding QQ Plots," University of Virginia Library, 26 08 2015. [Online]. Available: <https://library.virginia.edu/data/articles/understanding-q-q-plots#:~:text=The%20QQ%20plot%2C%20or%20quantile,as%20a%20normal%20or%20exponential..> [Accessed 12 08 2023].
- [92] L. Downey, "Efficient Market Hypothesis (EMH): Definition and Critique," Investopedia , 24 04 2023. [Online]. Available: <https://www.investopedia.com/terms/e/efficientmarkethypothesis.asp>. [Accessed 27 08 2023].
- [93] D. Bonderud, "Calculating Correlation in Excel: Your How-To Guide," HubSpot, 13 07 2022. [Online]. Available: <https://blog.hubspot.com/marketing/correlation-excel>. [Accessed 12 08 2023].
- [94] T. M. A. M.-G. a. O. R. Nathan Lash, "Charting the global energy landscape to 2050: Sustainable fuels," Mckinsey and Company, 07 07 2022. [Online]. Available: <https://www.mckinsey.com/industries/oil-and-gas/our-insights/charting-the-global-energy-landscape-to-2050-sustainable-fuels>. [Accessed 01 09 2023].
- [95] N. Morlanés, "A technological roadmap to the ammonia energy economy: Current state and missing technologies," Chemical Engineering Journal, 12 03 2021. [Online]. Available:

<https://www.sciencedirect.com/science/article/pii/S1385894720334343#f0005>.
[Accessed 1 08 2023].

- [96] S. H. Crolius, "Technology Advances for Blue Hydrogen and Blue Ammonia," 01 11 2019.
[Online]. Available: <https://www.ammoniaenergy.org/regions/switzerland/page/2/>.
[Accessed 02 09 2023].

Appendix

Section A - Air Fuel Ratio Calculation

6% NH₃ by weight fuel mixture:

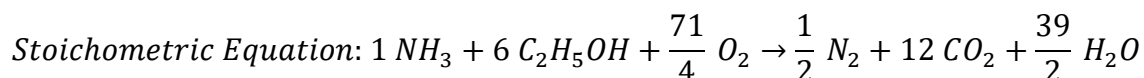
$$\frac{\frac{94g}{46.08g}}{mol} = 2.04 \text{ Moles of Ethanol}$$

$$\frac{\frac{6g}{17g}}{mol} = 0.3529 \text{ Moles of Ammonia}$$

How much Ethanol per 1 mole of NH₃ : Ethanol

$$\frac{0.3529}{0.3529} : \frac{2.0399}{0.3529}$$

1 : 6



$$\text{Air Fuel Ratio: } \frac{\text{Moles of O}_2 * \text{Molar Mass} * \frac{100}{\text{Proportion of Oxygen in Air}}}{\text{Total molar grams of fuel components}}$$

$$\text{Air Fuel Ratio} = \frac{\frac{71}{4} * \frac{32g}{mol} * \frac{100}{21}}{\left(6 * \frac{46.08g}{mol}\right) + \left(1 * \frac{17g}{mol}\right)} = \mathbf{9.216:1}$$

Section B – Titration Curves

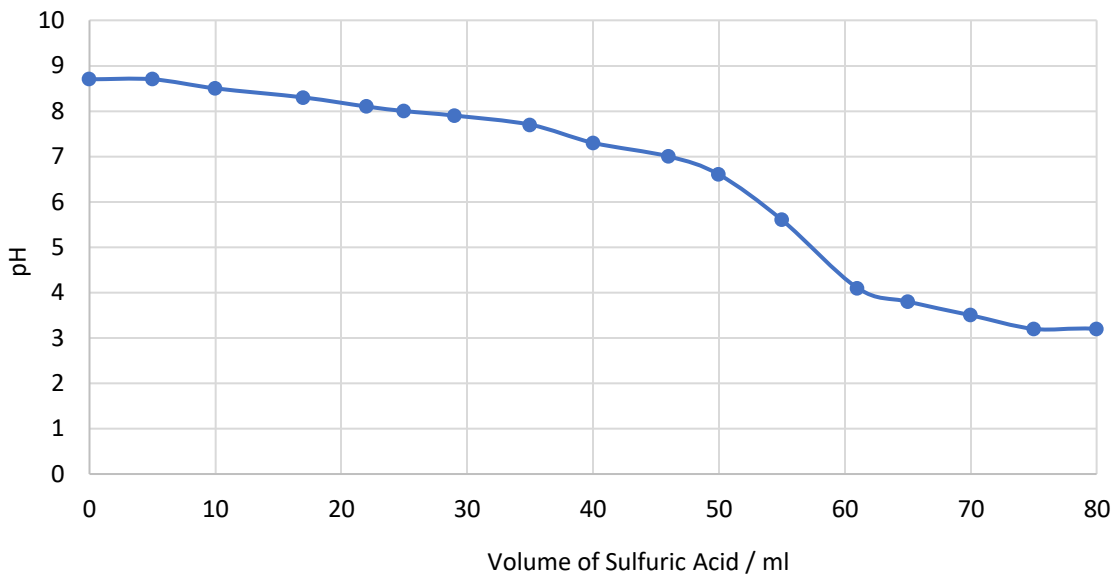


Figure 75 Titration Curve for fuel mixture / H_2SO_4 - Methanol

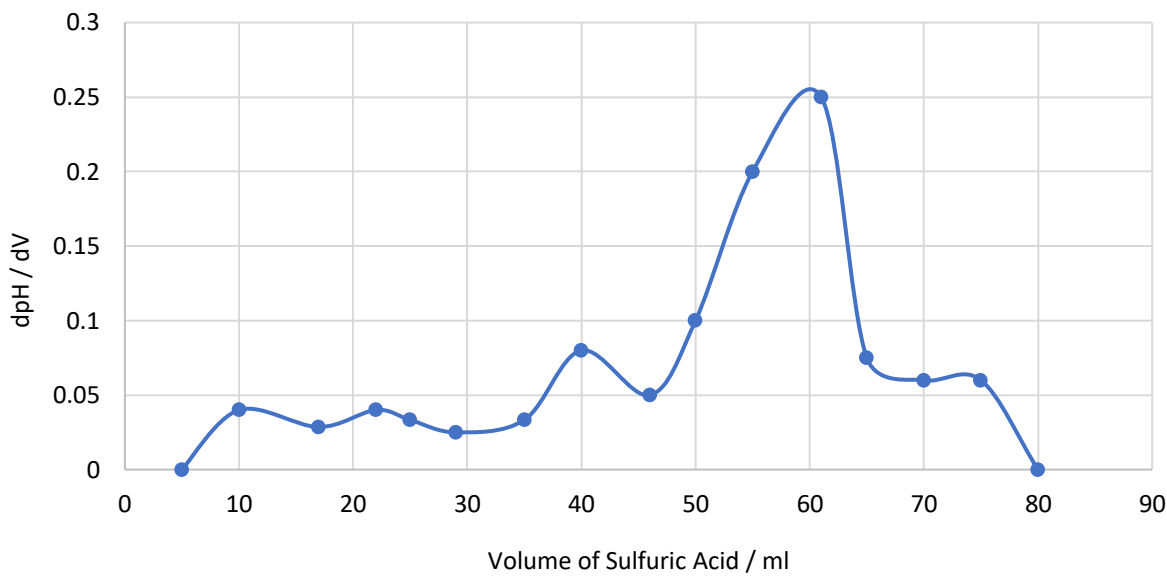


Figure 76 Titration Curve Equivalence point – Methanol

Section C – Arima Model Code

```
# importing all neccesary modules
import pandas as pd
import pmdarima as pm
from matplotlib import pylab as plt
import seaborn as sns
import statsmodels.api as sm
from matplotlib.pylab import rcParams

sns.set ()
rcParams ['figure.figsize'] = 15,6

# indexing the time series
data = pd.read_csv ('Ethanol.csv', index_col = 'Gold Man Sachs Ethanol Index',
                    parse_dates=True,
                    dayfirst=True,dtype='float')
data
```

Figure 77 ARIMA Code 1/13 [67] [68] [69] [70] [71] [72]

```
# plotting intial partial and autocorrelation graphs
ts = data.head(115)[ 'Price' ]
print(ts)
ts_acf = sm.tsa.stattools.acf (ts, nlags =56)
ts_acf

ts_pacf = sm.tsa.stattools.pacf (ts, nlags = 56, method = 'ols')
ts_pacf

fig = plt.figure(figsize = (12,8))
ax1 = fig.add_subplot(211)
fig = sm.graphics.tsa.plot_acf(ts, lags = 56, ax = ax1)
ax2 = fig.add_subplot (212)
fig = sm.graphics.tsa.plot_pacf(ts, lags = 56, ax = ax2)
```

Figure 78 ARIMA Code 2/13 [67] [68] [69] [70] [71] [72]

```
# differencing the time series
diff = ts-ts.shift ()
diff = diff.dropna ()

resDiff = sm.tsa.arma_order_select_ic (diff, ic = 'aic', trend = 'c')
resDiff

# creates the time series with chosen combination
ARIMA_MODEL = sm.tsa.ARIMA(ts,order = (0,1,2))
resultsARIMADiff = ARIMA_MODEL.fit()
resultsARIMADiff.summary()
```

Figure 79 ARIMA Code 3/13 [67] [68] [69] [70] [71] [72]

```

resid = ARIMA_MODEL.fit().resid

fig = plt.figure (figsize = (12,10))
ax1 = fig.add_subplot(211)
fig = sm.graphics.tsa.plot_acf(resid.values.squeeze(),lags=40,ax=ax1)
ax2= fig.add_subplot(212)
fig = sm.graphics.tsa.plot_pacf(resid, lags = 40 , ax=ax2)

```

Figure 80 ARIMA Code 4/13 [67] [68] [69] [70] [71] [72]

```

# visual differencing check
from statsmodels.graphics.tsaplots import plot_acf
import matplotlib.pyplot as plt
plt.rcParams.update({'figure.figsize':(9,7), 'figure.dpi':120})

# Import data
df = pd.read_csv('Ethanol.csv', names=['value'], header=0)

# Original Series
fig, axes = plt.subplots(3, 2, sharex=True)
axes[0, 0].plot(df.value); axes[0, 0].set_title('Original Series')
plot_acf(df.value, ax=axes[0, 1], lags=90)

# 1st order Differencing
axes[1, 0].plot(df.value.diff()); axes[1, 0].set_title('1st Order Differencing')
plot_acf(df.value.diff().dropna(), ax=axes[1, 1], lags=90) # y_n - y_n-1

# 2nd order Differencing
axes[2, 0].plot(df.value.diff().diff()); axes[2, 0].set_title('2nd Order Differencing')
plot_acf(df.value.diff().diff().dropna(), ax=axes[2, 1], lags=90) # y_n - y_n-2

plt.show()

```

Figure 81 ARIMA Code 5/13 [67] [68] [69] [70] [71] [72]

```

# statistical tests to check stationarity
from statsmodels.tsa.stattools import adfuller
result = adfuller(ts)
print('ADF Statistic: %f' % result[0])
print('p-value: %f' % result[1])

from pmdarima.arima.utils import ndiffs
df = pd.read_csv('Ethanol.csv',
| | | | | names=['value'], header=0)
y = df.value

## Adf Test
ndiffs(y, test='adf')

# KPSS test
ndiffs(y, test='kpss')

# PP test:
ndiffs(y, test='pp')

```

Figure 82 ARIMA Code 6/13 [67] [68] [69] [70] [71] [72]

```

sns.set ()
rcParams ['figure.figsize'] = 15,6

# Plot residual errors
residuals = pd.DataFrame(resid)
fig, ax = plt.subplots(1,2)
residuals.plot(title="Residuals", ax=ax[0], legend= False)
residuals.plot(kind='kde', title='Density', ax=ax[1], legend= False)
plt.show()

```

Figure 83 ARIMA Code 7/13 [67] [68] [69] [70] [71] [72]

```

## AIC minimisation order searching to check if trial and error combination matches

df = pd.read_csv('Ethanol.csv', names=['Price'], header=0)

model = pm.auto_arima(df['Price'], start_p=0, start_q=0,
                      test='adf',
                      max_p=5, max_q=5,
                      m=1,
                      d=None,
                      seasonal=True,
                      start_P=0,
                      D=0,
                      trace=True,
                      error_action='ignore',
                      suppress_warnings=True,
                      stepwise=True)

print(model.summary())

```

Figure 84 ARIMA Code 8/13 [67] [68] [69] [70] [71] [72]

```

# residual analysis
model.plot_diagnostics(figsize=(11,10))
plt.show()

#prediction
SARIMA = sm.tsa.SARIMAX (ts, order = (0,2,1), seasonal_order = (0,0,0,0)).fit()
print (SARIMA.summary())

resid = SARIMA.resid

fig = plt.figure (figsize = (12,10))
ax1 = fig.add_subplot(211)
fig = sm.graphics.tsa.plot_acf(resid.values.squeeze(),lags=26,ax=ax1)
ax2= fig.add_subplot(212)
fig = sm.graphics.tsa.plot_pacf(resid, lags = 25 , ax=ax2)

```

Figure 85 ARIMA Code 9/13 [67] [68] [69] [70] [71] [72]

```

# checking if seasonal terms are required
import pmdarima as pm

# Seasonal - fit stepwise auto-ARIMA
smodel = pm.auto_arima(data, start_p=1, start_q=1,
                       test='adf',
                       max_p=3, max_q=3, m=12,
                       start_P=0, seasonal=True,
                       d=None, D=1, trace=True,
                       error_action='ignore',
                       suppress_warnings=True,
                       stepwise=True)

smodel.summary()

```

Figure 86 ARIMA Code 10/13 [67] [68] [69] [70] [71] [72]

```

#forecast up to future date required
forecast = SARIMA.predict('30/05/2014', '28/07/2025')

plt.figure(figsize=(12, 6))
plt.plot(ts, label='Historical', color ='blue')
plt.plot(forecast, label='Predicted', color='red')
plt.xlabel('Years')
plt.ylabel('Price / £')
plt.legend()
plt.show()

```

Figure 87 ARIMA Code 11/13 [67] [68] [69] [70] [71] [72]

```

# Import
data = pd.read_csv('Ethanol.csv', index_col='Gold Man Sachs Ethanol Index',
                   parse_dates=True,
                   dayfirst=True, dtype='float')

# Plot
fig, axes = plt.subplots(2, 1, figsize=(10,5), dpi=100, sharex=True)

# Usual Differencing
axes[0].plot(data[:,], label='Original Series')
axes[0].plot(data[:,].diff(1), label='Usual Differencing')
axes[0].set_title('Usual Differencing')
axes[0].legend(loc='upper left', fontsize=10)

# Seasonal Differencing
axes[1].plot(data[:,], label='Original Series')
axes[1].plot(data[:,].diff(3), label='Seasonal Differencing', color='green')
axes[1].set_title('Seasonal Differencing')
plt.legend(loc='upper left', fontsize=10)
plt.suptitle('Ethanol Price', fontsize=16)
plt.show()

```

Figure 88 ARIMA Code 12/13 [67] [68] [69] [70] [71] [72]

```

# visual check of seasonality
import pandas as pd
import matplotlib.pyplot as plt

# Import Data
df = pd.read_csv('Ethanol.csv', parse_dates=['Gold Man Sachs Ethanol Index'], dayfirst=True)
df.rename(columns={'Gold Man Sachs Ethanol Index': 'date', 'Price': 'value'}, inplace=True)

# Prepare data
df['year'] = [d.year for d in df.date]
df['month'] = [d.strftime('%b') for d in df.date]
years = df['year'].unique()

# Draw Plot
plt.figure(figsize=(10, 8), dpi=120)
for i, y in enumerate(years):
    if i > 0:
        plt.plot('month', 'value', data=df.loc[df.year==y, :], label=y)

plt.gca().set(ylabel='$Price / £$', xlabel='$Month$')
plt.yticks(fontsize=14, alpha=.7, ticks=range(20, 190, 10))

# Add legend
plt.legend(title='Year', fontsize=12, title_fontsize=12, loc='upper left')

plt.show()

```

Figure 89 ARIMA Code 13/13 [67] [68] [69] [70] [71] [72]

Section D – In cylinder Volume Engine

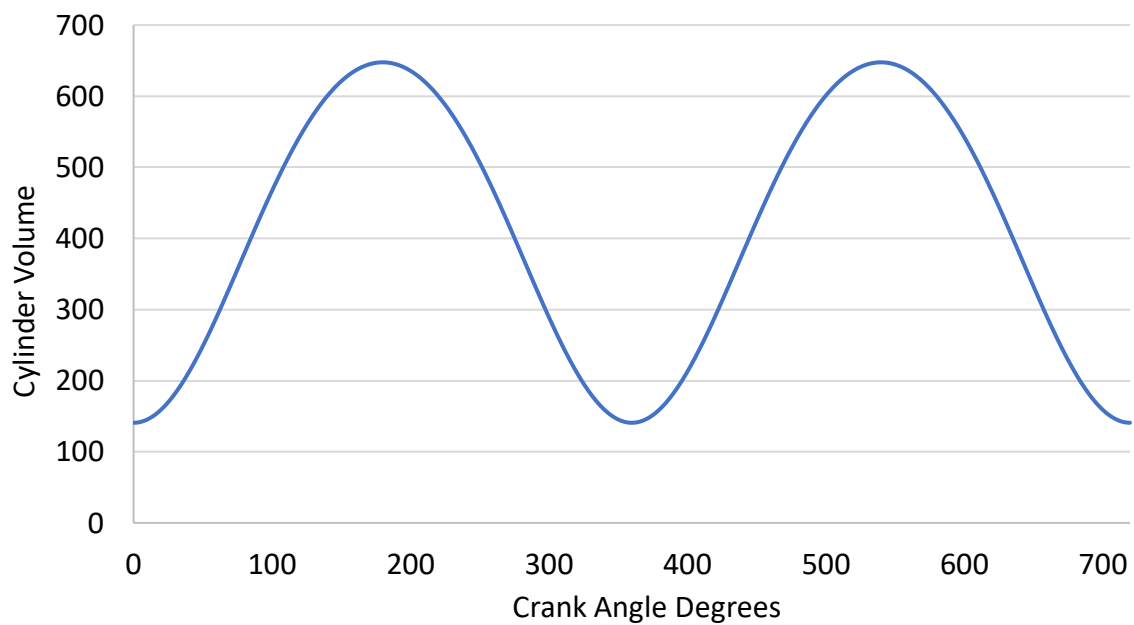


Figure 90 In cylinder volume of test engine